AEDC-TR-76-149

A MAGNETIC-GUIDEWAY/GUIDED-PROJECTILE SYSTEM CONCEPT FOR AEROBALLISTIC RANGES

VON KÁRMÁN GAS DYNAMICS FACILITY
ARNOLD ENGINEERING DEVELOPMENT CENTER
AIR FORCE SYSTEMS COMMAND
ARNOLD AIR FORCE STATION, TENNESSEE 37389

February 1977

Final Report for Period July 1973 – February 1976

Prepared for

DIRECTORATE OF TECHNOLOGY (DY)
ARNOLD ENGINEERING DEVELOPMENT CENTER
ARNOLD AIR FORCE STATION, TENNESSEE 37389

NOTICES

When U. S. Government drawings specifications, or other data are used for any purpose other than a definitely related Government procurement operation, the Government thereby incurs no responsibility nor any obligation whatsoever, and the fact that the Government may have formulated, furnished, or in any way supplied the said drawings, specifications, or other data, is not to be regarded by implication or otherwise, or in any manner licensing the holder or any other person or corporation, or conveying any rights or permission to manufacture, use, or sell any patented invention that may in any way be related thereto.

Qualified users may obtain copies of this report from the Defense Documentation Center.

References to named commercial products in this report are not to be considered in any sense as an endorsement of the product by the United States Air Force or the Government.

This report has been reviewed by the Information Office (OI) and is releasable to the National Technical Information Service (NTIS). At NTIS, it will be available to the general public, including foreign nations.

APPROVAL STATEMENT

This technical report has been reviewed and is approved for publication.

FOR THE COMMANDER

William E Cole

WILLIAM E. COLE
Captain, USAF
Requirements Planning Division
Directorate of Technology

Robert O Dietz

ROBERT O. DIETZ
Director of Technology

REPORT DOCUMENTATION PAGE		READ INSTRUCTIONS BEFORE COMPLETING FORM
1 REPORT NUMBER AEDC-TR-76-149	2 GOVT ACCESSION NO	3 RECIPIENT'S CATALOG NUMBER
4 TITLE (and Subtitle) A MAGNETIC-GUIDEWAY/GUIDED-PROJECTILE SYSTEM CONCEPT FOR AEROBALLISTIC RANGES		5 TYPE OF REPORT & PERIOD COVERED Final Report - July 1973-February 1976 6 PERFORMING ORG REPORT NUMBER
7 AUTHOR(s) George D. Arney, Jr. and Charles W. Pender, Jr., ARO, Inc.		8 CONTRACT OR GRANT NUMBER(s)
9 PERFORMING ORGANIZATION NAME AND ADDRESS Arnold Engineering Development Center (DY) Air Force Systems Command Arnold Air Force Station, Tennessee 37389		10 PROGRAM ELEMENT, PROJECT, TASK AREA & WORK UNIT NUMBERS Program Element 65807F
11 CONTROLLING OFFICE NAME AND ADDRESS Arnold Engineering Development Center (DYFS) Arnold Air Force Station, Tennessee 37389		12 REPORT DATE February 1977 13 NUMBER OF PAGES 102
14 MONITORING AGENCY NAME & ADDRESS(if different from Controlling Office)		15 SECURITY CLASS (of this report) UNCLASSIFIED 15a DECLASSIFICATION/DOWNGRADING SCHEDULE N/A

16 DISTRIBUTION STATEMENT (of this Report)

Approved for public release; distribution unlimited.

17 DISTRIBUTION STATEMENT (of the abstract entered in Block 20, if different from Report)

18 SUPPLEMENTARY NOTES

Available in DDC

19 KEY WORDS (Continue on reverse side if necessary and identify by block number)

magnetic guidance	interactions
guided missiles	deployment
ranges (aeroballistic)	currents
electrodynamic	force (aerodynamic)

20 ABSTRACT (Continue on reverse side if necessary and identify by block number)

A system concept for the incorporation of magnetic projectile guidance into aeroballistic ranges is presented and analyzed. Basis of the concept is motion-induced, electrodynamic interaction between conductive material in the projectile's forebody and a guideway of field source currents. Theory is developed for deployment of the currents such that on the one hand the forebody will be repulsed toward the guideway centerline as a function of

DD FORM 1 JAN 73 1473 EDITION OF 1 NOV 65 IS OBSOLETE

20. ABSTRACT (Continued)

error in lateral position whereas, on the other hand, there will be damping of resulting lateral motion. Expressions are subsequently derived which interrelate the magnitude of forces to the magnitude of guideway currents, and generalized equations of motion for the projectile are developed with both electrodynamic and aerodynamic forces being considered. A design example is included wherein the developed theory is correlated to an existing aeroballistic range (AEDC/VKF Range G) where projectiles with base diameters on the order of 0.05 m are launched at velocities of 4,000 to 6,000 m/sec. Results are gratifying in that computed flight paths for varying conditions indicate that stable guided flight can be achieved with guideway currents of reasonable magnitude. Practical means of providing these are discussed.

AFSC
Arnold AFS Tenn

PREFACE

The research reported herein was sponsored and conducted by the Arnold Engineering Development Center (AEDC), Air Force Systems Command (AFSC), under Program Element 65807F. The results presented were obtained by ARO, Inc. (a subsidiary of The Sverdrup Corporation), contract operator of AEDC, AFSC, Arnold Air Force Station, Tennessee. The work was done under ARO Projects No. VF444-11GA, V31S-35A, and V31S-04A. The authors of this report were G. D. Arney, Jr. and C. W. Pender, Jr., ARO, Inc. The manuscript (ARO Control No. ARO-VKF-TR-76-24) was submitted for publication on March 4, 1976.

During the course of the research the authors received suggestions from Drs. Max Kinslow and J. T. Miller, Jr. of the von Kármán Gas Dynamics Facility (VKF) and from Dr. H. J. Fink of the University of California at Davis, all of which have been of considerable value and are hereby acknowledged. Thanks is also due Mr. P. M. Dyer of the VKF for assemblage of some of the earlier computer programs.

CONTENTS

ILLUSTRATIONS

Figure

1.0 INTRODUCTION

The purpose of this report is to present a concept along with supporting theory for a magnetic-guideway/guided-projectile system that has been devised for the AEDC/VKF Aeroballistic Range G (Ref. 1). The concept has evolved out of a somewhat broader effort to provide alternate, or "backup" technology to that presently under development wherein the launch sabot is retained during flight and serves as a shoe for mechanical containment of the projectile between guide rails. The objective of either approach is to provide a guided hypervelocity vehicle that will better enable study of the ablative and erosive environments that high-speed missiles and space vehicles often must survive. To adequately perform such studies in aeroballistic ranges it is required that the flightpath be predetermined to enhance data from wayside photography, etc., and to provide for flight into deceleration devices where the projectile can be retrieved for postflight measurements. Potential advantages to be gained by use of the magnetic method include:

1. Elimination of sliding surface contact and associated wear, erosion, and gouging of the shoe and guideway,
2. Elimination or reduction of problems associated with shock interaction between projectile and guideway,
3. Less critical alignment and smoothness requirements for the guideway, and
4. Periods of essentially free flight with no track or other obstructions to interfere with wayside photography.

As will be seen, the concept is closely related to presently accepted notions for repulsive magnetic levitation and guidance of ground transport vehicles and rocket sleds (Refs. 2, 3, 4, and 5). In these cases, the dominant scheme consists of attaching high-intensity, superconducting magnets to the vehicle and providing roadways/guideways of aluminum or other normally conductive materials. By virture of vehicular motion, the fields of the magnets induce and react against eddy currents in the roadway/guideway with the resulting forces experienced by the magnets being used for levitation and guidance.

The present concept is similarly based on motion-induced electrodynamic interaction but with reversal in location of the key elements; i.e., the guideway provides a range-length inducing field and conductive material is integrated into the projectile with the forces it experiences being utilized for guidance. Resort to this approach has been necessitated in the present situation because of launch considerations; i.e., projectile velocities of interest for abalation and erosion tests are 4,000 to 6,000 m/sec and to achieve such in the VKF Range G a projectile must withstand accelerations up to 2×10^5 g's in a staged powder-hydrogen gun. As reported in Ref. 6, superconducting magnets are not strong enough structurally to withstand this. The alternative of permanent magnets would not provide a field of sufficient intensity and normal electromagnets would require a power supply which makes them unsuited for incorporation into the projectile. An electromagnetic guideway with only normally conductive material in the projectile as proposed is technically feasible, however, and its practicability for the case of Range G is strongly suggested by the nearby Tunnel F power supply (Ref. 7). From this flywheel/inductor stored energy source, power pulses can be made available at currents up to 10^6 amp for energization of the guideway during a projectile's flight.

2.0 SYSTEM DESCRIPTION

As previously stated, the system concept is based on motion-induced electrodynamic interaction between conductive material that is to be deployed in projectiles and a stationary electromagnetic guideway that is to be provided around the desired flightpath. More specifically, the conductive material is to be in the form of a shell around the projectile's forebody and the guideway is to be such that as a projectile moves off course it will be exposed to increasing magnetic field intensity and as it moves downrange it will be exposed to spacewise modulations in this intensity. Because of high-frequency shielding effects, the forebody will appear diamagnetic to the modulations and experience forces such that its preferred position of equilibrium will be the guideway axis where the field is zero. These "positional" forces are to modify the projectile's angle of attack so as to enlist aerodynamic forces that are capable of maintaining flight along the guideway axis. Flight stabilization is achievable by virtue of the fact that lateral motion of the conductive shell will be through field nonuniformities such that attendant eddy current losses will tend to dampen or retard such motion.

As initially envisioned, and as can be envisioned for present analytical purposes, the guideway field is to be generated by two superimposed sets of four currents that are symmetrically oriented about the range centerline or z axis as shown in Fig. 1. As indicated, one set is composed of range-length line currents of magnitude I_D while the other is composed of transposed line current segments of magnitude I_P and length Δ. Also, as indicated, there are two go and two return currents in each set with those of like direction being diagonally opposite each other. The magnetic field of the I_D currents is independent of distance downrange as indicated in Fig. 2 whereas that of the I_P currents is of opposite polarity in adjoining segments as indicated in Fig. 3.

In both cases, as should be expected from the Biot-Savart law, a so-called null-flux field is produced whose intensity is strong near the currents and decreases to a zero or null value at their axis of symmetry. Anticipating that the I_D field will be stronger than the I_P field, the combined results of I_D and I_P will be a null-flux field whose intensity is modulated with respect to z. Later analysis, however, will consider the two independently with the I_D field being treated as the means for generation of lateral damping forces and I_P being treated as the means for generation of lateral positional forces.

Insofar as the projectile itself is concerned, the shape and structure shown in Fig. 4 have been adopted for investigation of theoretical system feasibility herein. Whereas, as will be discussed, prospects exist for improvements from other viewpoints, this configuration yields an agreeable analytical model. This is primarily because the shell on the forebody is in the form of a cylinder and thus lends itself well to electrodynamic analysis. It is also to be appreciated that the projectile's overall outer surface is in the form of a flared cylinder (with optional nose) which lends itself to aerodynamic stability and, when in aerodynamic flight, develops side forces as a function of angle of attack. Moreover, by being a relatively standard aerodynamic shape, much data is available from which to predict flight behavior. The fact is that, in the past, use of projectiles with this general overall shape has been common in ballistic range work. Through use of strippable sabots this shape adapts well to present launch techniques and, as is seen, is quite flexible insofar as the type of nose test article it can carry.

3.0 ANALYTICAL DEVELOPMENT

3.1 GUIDEWAY AND SHELL INTERACTIONS

For the purpose of developing theoretical aspects of the system electrodynamics to the point where guideway and shell parameters can be chosen, an idealized, two-dimensional mathematical model will be utilized; i.e., the cylinder is of infinite length in the z-direction, conditions do not change with respect to z, etc. The concept being pursued is compatible with such a model if the following conditions can be met:

1. All guideway current elements that lie in the z direction are long compared to the radial dimension of the guideway. Despite the use of long current elements, the needed high-frequency effects will be created if projectile velocity is sufficient.
2. The shell axis remains approximately parallel to the z axis at all times. This is possible if in actual flight only slight deviations from such conditions is required to develop needed aerodynamic forces for maintenance of course.
3. All eddy currents in the cylindrical shell (except for those in the end surfaces which are to be ignored) flow approximately in streamlines parallel to the z axis. This will be reasonably true when:
   (a) the vector potential of their inducing field, i.e., the field of the guideway currents, lies in this direction (see condition (1) above);
   (b) the shell has a large length-to-diameter ratio; and
   (c) the end walls are made thick for decreased opposition to current flow across them.

Later application of two-dimensional analytical results to design of an actual system will demonstrate that compliance with these conditions is quite feasible.

3.1.1 Conditions for Diamagnetic and Damping Behavior

The diamagnetic and damping effects that are to be employed are both dependent upon eddy currents being induced in the conductive

shell as a result of its motion through the guideway field. Diamagnetic behavior is synonymous with the shielding of the shell's interior which is achievable via such currents and is related to the inductive (or reactive) energy in their magnetic fields; i.e., the induced eddy current field required to completely nullify or cancel an inducing field within a body is identical to that field which would be required if cancellation were by induced diamagnetic polarizations. In both cases, positional forces exist on the body that are proportional to the change in induced field energy with respect to position. For the case of the shell, damping, or retardation of motion, is related to the rate at which such energy is dissipated in the shell as joulean heat.

Quite obviously, only positional and damping forces that act in the lateral direction are useful for guidance purposes. The fact is, however, that to achieve radial positional forces by the scheme being pursued it is not possible to avoid altogether the development of both positional and damping forces that act in the axial direction. Nor is it possible to develop the desired radial damping forces without creating some level of undesired positional forces. Fortunately, the axial positional force acts first in one direction and then the other as the projectile passes through the transposed guideway so as to have insignificant net effect. Moreover, as will be seen, it is possible to choose guideway and shell parameters such that desired radial forces will dominate those that are not desired.

With its radius and length being a and h, respectively, visualize for the present that the cylindrical shell lies concentric with the z axis of a cylindrical coordinate system where points in space are defined by r, θ, and z as shown in Fig. 5. Visualize further that from external sources there exists an inducing field whose magnetic vector potential, $\overline{A}_i$, is parallel to the axis and whose magnitude is varying with respect to time. Because the shell is conductive, eddy currents will flow whose magnetic vector potential can be represented by $\overline{A}'$. The total induced electric field, $\overline{E}$, is then composed of that due to the original inducing field plus the reactive contribution of the eddy currents. From the laws of induction by Faraday and Lenz it can be expressed as

$$\text{Total induced } \overline{E} = -\frac{\partial}{\partial t}\left(\overline{A}_i + \overline{A}'\right) \tag{1}$$

where t is time. Current must then flow along the surface in accordance with Ohm's law which can be written as

$$\overline{E} = \text{[illegible]} \tag{2}$$

where $\bar{i}$ is the current density along the surface and ς is the area resistivity. Finally, in absence of displacement currents the vector potential and current density must be interrelated through Ampere's law for all points in space. With μ_o being the permeability of free space and the shell, this relationship can be expressed as

$$\nabla^2\bar{A}' = \mu_o\bar{i} \tag{3a}$$

For points in space that are not part of the surface there can be no current flow so that for these points the relationship reduces to

$$\nabla^2\bar{A}' = 0 \tag{3b}$$

Equations (3a) and (3b) will be recognized as those of Poisson and Laplace, respectively.

Recall now that in Section 3.0 the ratio of the shell's length to diameter has been postulated as being large so that two-dimensional solutions for the conditions of Eqs. (1), (2), and (3) are adequate. Fortunately, the two-dimensional situation has been treated at some length by Smythe for the case of a timewise - sinusoidal inducing field (Ref. 8, p. 400). The treatment expands the vector potential of both the inducing field and an assumed eddy current field into a series of circular harmonics. For polar positions of $r \leq a$ that series obtained for the inducing field is

$$\bar{A}_i(r,\theta,t) = \hat{k} \sum_{n=1}^{\infty} C_n r^n a^{-n} \cos(n\theta + \delta_n) \cos\omega t \tag{4}$$

where $\hat{k}$ is a unit vector in the z direction, n is the degree of the harmonic, C_n is the coefficient of the n^{th} harmonic, δn is the phase angle for the n^{th} harmonic, and ω is the angular frequency. Proceeding to match boundary conditions under the assumption that each harmonic decays independently and exponentially, several pertinent solutions that were obtained in the treatment are as follows:

1. Area density of eddy currents

$$\bar{i}(a,\theta,t) = -\frac{\hat{k}2}{\mu_o a} \sum_{n=1}^{\infty} n\, C_n \cos(n\theta + \delta_n) \cos\epsilon_n \cos(\omega t - \epsilon_n) \tag{5}$$

where ϵ_n represents a phase lag between $\bar{A}_i$ and $\bar{A}'$ and is given by

$$\epsilon_n = \tan^{-1}\left[\frac{-2n\varsigma}{\omega\mu_o a}\right] \tag{6}$$

2. Vector potential of the eddy currents at $r \leq a$

$$\bar{A}'(r,\theta,t) = -\hat{k}\sum_{n=1}^{\infty} C_n r^n a^{-n} \cos\epsilon_n \cos(n\theta + \delta_n)\cos(\omega t - \epsilon_n) \tag{7}$$

3. Ratio for the n^{th} harmonic of the vector potential of the eddy currents to that of the inducing field at $r = a$

$$\frac{|\bar{A}'(r,\theta,t)|}{|\bar{A}_i(r,\theta,t)|} = \cos\epsilon_n \tag{8}$$

4. Total vector potential at $r \leq a$

$$\bar{A}_i(r,\theta,t) + \bar{A}'(r,\theta,t) = -\hat{k}\sum_{n=1}^{\infty} C_n r^n a^{-n} \sin\epsilon_n \cos(n\theta + \delta_n)\sin(\omega t - \epsilon_n) \tag{9}$$

5. Shielding effect of shell; i.e., ratio of n^{th} term of the vector potential inside the shell as opposed to that with the shell removed.

$$\delta_n = \frac{|\bar{A}_{in}(r,\theta,t) + \bar{A}'_n(r,\theta,t)|}{|\bar{A}_{in}(r,\theta,t)|} = \sin\epsilon_n \tag{10}$$

6. Time averaged real power per unit length; i.e., time averaged rate of energy dissipated per unit shell length

$$P_{real} = 2\pi\varsigma(\mu_o^2 a)^{-1}\sum_{n=1}^{\infty} n^2 C_n^2 \cos^2\epsilon_n \tag{11}$$

Now, in addition to real power, it is instructive to think in terms of reactive (imaginary) and total apparent power. From Eqs. (1) and (3) it is clear that the portion of induced electic field attributable to reactance of the eddy currents is

$$\text{Reactive } E_z(a,\theta,t) = -\frac{\partial A'_z(a,\theta,t)}{\partial t} \tag{12}$$

A time average reactive (or imaginary) power per unit shell length can then be defined as

$$P_{imag} = \frac{1}{2} a \int_{o}^{2\pi} \frac{\partial[A'_z(a,\theta,t)]}{\partial t} i_z(a,\theta,t) d\theta \tag{13}$$

Combining Eqs. (5), (7), (12), and (13) yields

$$P_{imag} = \frac{\pi\omega}{\mu_o} \sum_{n=1}^{\infty} n C_n^2 \cos^2 \epsilon_n \tag{14}$$

Combining Eqs. (11) and (14)

$$\frac{P_{n\ real}}{P_{n\ imag}} = \frac{2\varsigma n}{\mu_o a\omega} = -\tan \epsilon_n \tag{15}$$

The total apparent power per unit shell length for each harmonic would then be

$$P_{n\ total} = \sqrt{P^2_{n\ real} + P^2_{n\ imag}} \tag{16}$$

Finally, combining Eqs. (15) and (16)

$$\frac{P_{n\ real}}{P_{n\ total}} = \frac{1}{\sqrt{1 + \dfrac{\mu_o^2\omega^2 a^2}{4\varsigma^2 n^2}}} = \frac{1}{\sqrt{1 + \cot^2 \epsilon_n}}$$

$$= \sin \epsilon_n = \delta_n \text{ (see Eq. (10))} \tag{17}$$

and

$$\frac{P_{n\ imag}}{P_{n\ total}} = \frac{1}{\sqrt{1 + \dfrac{4\varsigma^2 n^2}{\mu_o^2 a^2 \omega^2}}} = \frac{1}{\sqrt{1 + \tan^2 \epsilon_n}}$$

$$= \cos \epsilon_n = |\bar{A}'|/|\bar{A}_i| \text{ (see Eq. (8))} \tag{18}$$

The ratios $P_{n\ real}/P_{n\ total}$, $P_{n\ imag}/P_{n\ total}$, $|\bar{A}'_n|/|\bar{A}_{ni}|$ and δ_n are plotted in Fig. 6 as functions of the parameter $\mu_o a\omega(2n\varsigma)^{-1}$, i.e., $-\cot \epsilon_n$. It should be noted that as this correlation parameter approaches zero, power becomes totally real; i.e., magnetic energy

of the eddy currents is dissipated as joulean heat at the same rate it is generated. At this extreme it can also be seen that the vector potential of the eddy currents becomes small as compared to that of the inducing field. Unfortunately, this implies correspondingly low values of eddy currents so that to dissipate significant energy for damping of motion the inducing field will need to be strong.

It should also be noted from Fig. 6 that as the correlation parameter becomes large the power becomes essentially totally reactive and there is almost perfect shielding of the shell's interior. It should be understood that such reactive power represents energy transfer to and from the magnetic field of the eddy currents. From Lenz' Law, the flux of this field is in direct opposition to and tends to cancel that of its inducing field within the shell, hence the shielding or artificially diamagnetic effect.

Fortunately, again from Fig. 6, it should be noted that as the correlation parameter is increased by a factor of approximately 25, i.e., from a value of 0.2 to 5, the eddy current power moves from approximately 98-percent real* to 98-percent reactive.* Note also that for a given n all quantities in the correlation parameter except angular frequency are fixed when a cylindrical shell is specified. Advantage is to be taken of these facts in the guideway design. On the one hand, the interval between guideway transpositions as shown in Fig. 1 will be established such that high-frequency eddy currents will be induced that are $\geq$98-percent reactive, and shielding or diamagnetic effects are large. In this way, needed lateral positional forces can be generated with minimum retardation of axial motion. On the other hand, the flightpath will be tailored so that excursions across the guideway centerline will result in lower frequency eddy currents that are $\geq$98-percent real where damping effects dominate. This will allow needed lateral damping forces to be generated with minimal extraneous positional forces.

3.1.2 Diamagnetic Force Relationships

Through use of the principle of superposition, it is possible to relate the conductive shell and the guideway field modulations produced by the I_P current segments of Fig. 1 independently of the basic field generated by the I_D currents, and vice versa. Therefore, considering only effects of the transposed field, one can visualize that as high-speed projectiles move downrange they are exposed to a null-flux

*Intended to imply magnitudes that are 98 percent of the apparent power.

field of first one polarity, then another, etc. So that the shell will appear diamagnetic, the frequency components of this effectively alternating field are to be such that the interior of the shell, if appropriately designed, will be shielded (see Fig. 6).

Now, as will be seen, the length, Δ, of the line current segments is to be quite large as compared to their individual distance b from the range centerline (see Figs. 1 and 3). Therefore, during flight, the conductive shell spends most of its time between transpositions where a null-flux field exists whose strength is for all practical purposes equivalent to that which would exist if the current segments were of infinite length. This can be seen through application of the Biot-Savart law to a simple set of segments of alternate polarity which lie on a straight line.

Consider the situation shown in Fig. 7 where such a set lies on a z' axis parallel to the z axis. Let r' be the normal distance from the z' axis to a point of interest and n stand for the n^{th} segment downrange. From the differential form of the Biot-Savart law (Ref. 9) the magnetic induction at (r', z') attributable to the n^{th} segment is

$$\bar{B}_{n^{th}}(r', z') = \frac{\mu_o}{4\pi} \frac{\bar{I} \times \hat{r}'}{} \int_{(n-1)\Delta}^{n\Delta} \frac{dz'}{[(z_1' - z')^2 + (r')^2]^{3/2}} \tag{19}$$

where $\bar{I}$ is the magnitude of the current segments. Allowing for reversals in current from segment to segment, the induction produced by all transposed segments then is

$$\bar{B}_{TRP}(r', z) = \frac{\mu_o \bar{I} \times \hat{r}'}{4\pi} \sum_{n=1}^{\infty} (-1)^{n+1} \int_{(n-1)\Delta}^{n\Delta} \frac{dz'}{[(z_1' - z')^2 + (r')^2]^{3/2}} \tag{20}$$

which upon integration yields

$$B_{TRP}(r', z') = \frac{\mu_o \bar{I} \times \hat{r}'}{4\pi r'} \sum_{n=1}^{\infty} (-1)^{n+1} \left\{ \frac{z_1' - n\Delta}{\sqrt{(z_1' - n\Delta)^2 + (r')^2}} - \frac{z_1' - (n-1)\Delta}{\sqrt{[z_1' - (n-1)\Delta]^2 + (r')^2}} \right\} \tag{21}$$

In the limiting case of an infinite line current, i.e., n = 1, z = $\Delta/2$, and $\Delta \to \infty$, the summation reduces to a quantity of 2 so that, as it should per Ref. 10,

$$\bar{B}_{INF}(r', z') = \frac{\mu_o \bar{I} \times \hat{r}'}{2\pi r'} \tag{22}$$

The ratio of transposed magnitude to nontransposed magnitude then is

$$\left|\frac{B_{TRP}(r', z_1')}{B_{INF}(r', z_1')}\right| = \frac{1}{2}\sum_{n=1}^{\infty}(-1)^{n+1}\left\{\frac{(z_1 - n\Delta)}{\sqrt{(z_1 - n\Delta)^2 + (r')^2}} - \frac{z_1 - (n-1)\Delta}{\sqrt{[z_1 - (n-1)\Delta]^2 + (r')^2}}\right\} \quad (23)$$

A plot of this ratio truncated at n = 9 has been obtained through use of a digital computer* and is shown for several values of Δ/r' in Fig. 8. From this it should be clear that if Δ/b is 15 to 20, as it will be, then a traveling projectile will see the current segments as essentially infinite in length 80 percent of the time. The remainder of the time is spent near transpositions where the radial and axial fields of the angular current segments become effective. Again, the shell sees alternating polarities of these at relatively high frequencies and therefore experiences a system of diamagnetic forces that on the average act repulsively toward the guideway centerline.

In view of the above arguments, a reasonable approximation is that the conductive shell experiences the same forces as if it were traveling through the null-flux field of four infinite line currents but was diamagnetic to a degree corresponding to the currents (and fields) being segmented and transposed. Fortuitously, again, a treatment by Smythe (Ref. 8, p. 309) relative to the placement of a cylinder of magnetic material with permeability μ adjacent and parallel to a single such current I is applicable. With the radius of the cylinder being a and the distance from its axis to the line current being $r = r_1$, as shown in Fig. 9a, the significant results are:

1. The magnetic vector potential in the region outside the cylinder due to its presence is the same as if the cylinder were replaced by a parallel "image" current I′ located between I and the axis at a distance a^2/r_1 from the latter, plus a current of -I′ along the axis as shown in Fig. 9b. The magnitude of the image currents is given by

$$I' = \frac{1 - \mu_o/\mu}{1 + \mu_o/\mu} I \quad (24)$$

*See Appendix A for a listing of Fortran programs.

2. The vector potential inside the cylinder is the same as if the cylinder were removed and I were replaced by I'', where

$$I'' = \frac{2}{1 + \mu_o/\mu} I \tag{25}$$

The latter result is directly comparable to the shielding effect of a conductive, cylindrical shell by virtue of the fact that, within its interior, the vector potential of an exterior line current I lying parallel to its axis is the same as if the shell were removed and I were replaced by I'' where

$$I'' = \delta I \tag{26}$$

From Eqs. (25) and (26) there then is the equivalence that

$$\delta = \frac{2}{1 + \mu_o/\mu} \tag{27}$$

Upon solving this for μ_o/μ in terms of δ and substituting in Eq. (24) there results the fact that when there is effective shielding the vector potential outside the conductive shell due to parallel line currents is the same as if the shell were replaced by image line currents I' and $-I'$ as shown in Fig. 9b where

$$I' = (\delta - 1) I \tag{28}$$

The force per unit length, $\bar{F}$, on the cylinder is then the same as the sum of that which would be exerted on the two image currents by the field of the original current, i.e.,

$$\bar{F} = -\bar{I}' \times \bar{B}_I(0, 0) + \bar{I}' \times \bar{B}_I(a^2/r_1, 0) \tag{29}$$

From Eq. (22), with $\bar{r}'$ being appropriately replaced, the magnetic induction of I at the points of interest are

$$\bar{B}_1(0, 0) = -\frac{\mu_o \bar{I} \times \hat{r}}{2\pi r_1} \tag{30}$$

and

$$\overline{B}_1(a^2/r_1, 0) = -\frac{\mu_0 \overline{I} \times \hat{r}}{2\pi}\left\{\frac{r_1}{r_1^2 - a^2}\right\} \tag{31}$$

In conjunction with appropriate vector identities combination of Eqs. (28) through (30) yields finally, for the force per unit length on the cylinder

$$\overline{F} = \frac{\mu_0 I^2 a^2 (\delta - 1)\hat{r}}{2\pi r_1 (r_1^2 - a^2)} \tag{32}$$

Because δ is relatively near zero for the diamagnetic case, it is seen that the force is directed opposite to $\hat{r}$, i.e., away from the original current I. A plot of $\overline{F}$ versus r_1 is given in Fig. 10.

For the situation of interest herein, i.e., four line currents of equal magnitude surrounding the cylinder, the image currents are as shown in Fig. 11. Note that, because of equal magnitude Ip and equal quantities of go and return currents, there is complete cancellation of images located on the cylinder axis. However, for each line current I_n at distance r_n from the axis there is a corresponding image I'_n that, as before, lies a distance a^2/r_n away from the axis toward I_n. With radial and angular position of the cylinder axis being denoted by $\mathcal{R}$ and β, respectively, cartesian coordinates x_n and y_n of the line currents have been taken to be

$$\begin{aligned} x_1 &= b & y_1 &= 0 \\ x_2 &= 0 & y_2 &= b \\ x_3 &= -b & y_3 &= 0 \\ x_4 &= 0 & y_4 &= -b \end{aligned} \tag{33}$$

By triangulation, coordinates of the images then become

$$\begin{aligned} x_1' &= \mathcal{R}\cos\beta + \frac{a^2(b - \mathcal{R}\cos\beta)}{\mathcal{R}^2 + b^2 - 2\mathcal{R}b\cos\beta} & y_1' &= \mathcal{R}\sin\beta - \frac{a^2\mathcal{R}\sin\beta}{\mathcal{R}^2 + b^2 - 2\mathcal{R}b\cos\beta} \\ x_2' &= \mathcal{R}\cos\beta - \frac{a^2\mathcal{R}\cos\beta}{\mathcal{R}^2 + b^2 - 2\mathcal{R}b\sin\beta} & y_2' &= \mathcal{R}\sin\beta + \frac{a^2(b - \mathcal{R}\sin\beta)}{\mathcal{R}^2 + b^2 - 2\mathcal{R}b\sin\beta} \\ x_3' &= \mathcal{R}\cos\beta - \frac{a^2(b + \mathcal{R}\cos\beta)}{\mathcal{R}^2 + b^2 + 2\mathcal{R}b\cos\beta} & y_3' &= \mathcal{R}\sin\beta - \frac{a^2\mathcal{R}\sin\beta}{\mathcal{R}^2 + b^2 + 2\mathcal{R}b\cos\beta} \end{aligned} \tag{34}$$

$$x_{4'} = \Re \cos\beta - \frac{a^2 \Re \cos\beta}{\Re^2 + b^2 + 2\Re b \sin\beta} \qquad y_{4'} = \Re \sin\beta - \frac{a^2(b + \Re \sin\beta)}{\Re^2 + b^2 + 2\Re b \sin\beta} \tag{34}$$

The magnetic force per unit length experienced by the cylinder is the same as that which would be experienced by the four image currents in the combined fields of the original line currents and can be written as

$$\bar{F}_M = \sum_{n'=1}^{4} (-1)^{n'} \bar{I}_P \times \bar{B}_i(x_{n'}, y_{n'}) \tag{35}$$

Now from Ref. 11

$$\bar{B}_i(x_{n'}, y_{n'}) = \bar{\nabla} \times \bar{A}_i(x, y)\big|_{x_{n'}, y_{n'}} \tag{36}$$

and

$$\bar{A}_i(x, y) = \frac{\mu_o \bar{I}_P}{2\pi} \sum_{n=1}^{4} (-1)^n \ln \varkappa_n \tag{37}$$

where

$$\varkappa_n = \sqrt{(x - x_n)^2 + (y - y_n)^2} \tag{38}$$

Also, for this two-dimensional case with $\hat{i}$ and $\hat{j}$ being unit vectors in the x and y direction, respectively,

$$\bar{\nabla} \times \bar{A}(x, y) = \frac{\partial A_z}{\partial y} \hat{i} - \frac{\partial A_z}{\partial x} \hat{j} \tag{39}$$

so that

$$\bar{B}_i(x_{n'}, y_{n'}) = \frac{\mu_o I_P}{2\pi} \sum_{n=1}^{4} (-1)^n \left\{ \frac{y_{n'} - y_n}{(x_{n'} - x_n)^2 + (y_{n'} - y_n)^2} \hat{i} - \frac{x_{n'} - x_n}{(x_{n'} - x_n)^2 + (y_{n'} - y_n)^2} \hat{j} \right\} \tag{40}$$

Through combination of this result with Eqs. (28) and (35) there results for force per unit length on the cylinder

$$\bar{F}_M = \frac{\mu_o I_P^2}{2\pi}(\delta - 1) \sum_{n'=1}^{4}(-1)^{n'} \sum_{n=1}^{4}(-1)^n \left\{ \frac{y_{n'} - y_n}{(x_{n'} - x_n)^2 + (y_{n'} - y_n)^2}\,\hat{i} - \frac{x_{n'} - x_n}{(x_{n'} - x_n)^2 + (y_{n'} - y_n)^2}\,\hat{j} \right\} \quad (41)$$

This can be resolved into radial and angular components by taking dot products with unit vectors so directed, i.e.,

$$F_{M\mathcal{R}} = \bar{F}_M \cdot \hat{\mathcal{R}} \quad (42)$$

and

$$F_{M\beta} = \bar{F}_M \cdot \hat{\beta} \quad (43)$$

where

$$\hat{\mathcal{R}} = \hat{i}\cos\beta + \hat{j}\sin\beta \quad (44)$$

and

$$\hat{\beta} = \hat{i}\sin\beta - \hat{j}\cos\beta \quad (45)$$

The resulting components are

$$F_{M\mathcal{R}} = \frac{\mu_o I_P^2}{2\pi}(\delta - 1) \sum_{n'=1}^{4}(-1)^{n'} \sum_{n=1}^{4}(-1)^n \left\{ \frac{(y_{n'} - y_n)\cos\beta - (x_{n'} - x_n)\sin\beta}{(x_{n'} - x_n)^2 + (y_{n'} - y_n)^2} \right\} \quad (46)$$

and

$$F_{M\beta} = \frac{\mu_o I_P^2}{2\pi}(\delta - 1) \sum_{n'=1}^{4}(-1)^{n'} \sum_{n=1}^{4}(-1)^n \left\{ \frac{(y_{n'} - y_n)\sin\beta - (x_{n'} - x_n)\cos\beta}{(x_{n'} - x_n)^2 + (y_{n'} - y_n)^2} \right\} \quad (47)$$

These equations, in conjunction with Eqs. (33) and (34), have been normalized with respect to b and solved at varying positions using a digital computer.* The results for various values of a/b are shown in Fig. 12 for radial forces and Fig. 13 for angular forces.

*A listing of the Fortran program is included in Appendix A.

It should be noted from Fig. 12 that for $a/b \leq 0.2$ the radial forces for all β can be approximated by a single straight line if $\Re/b \leq 0.3$. It is also to be noted from Fig. 13 that for this condition the angular forces remain zero for all practical purposes. Therefore, for this condition the positional forces are purely radial and it is possible to define, for later use in development of flight equations, a linear positional force coefficient K_M such that

$$K_M = \frac{F_M \Re^h}{\Re} \tag{48}$$

where h denotes the length of the conductive shell. When using the slope of the straight line approximation on the normalized curves this becomes

$$K_M = \frac{l_p^2 h(\delta - 1)}{b^2} \times \text{slope} \tag{49}$$

In summary, the slope of these normalized values is shown in Fig. 14 as a function of the ratio a/b. Use of these results is, of course, strictly valid only when the position of the projectile is such that the ratio $\Re/b$ is ≤ 0.3 and the ratio a/b is ≤ 0.2. With discretion, use beyond these limits can obviously be permitted.

An alternative which would be advantageous in this regard would be to gradually spiral the field modulation currents of Fig. 1 in lieu of making sudden transpositions. One complete spiral each 4_a would give the needed fundamental frequency for effecting diamagnetic behavior. Such spiral would be so gradual that for any z the currents and their field would again, for all practical purposes, be two-dimensional. To a traveling projectile, the radial forces experienced would tend to be an average of radial forces for β varying from 0 to 2π. This would result in the radial forces being approximated by a single straight line for larger values of $\Re/b$ than would be the case for the previous transposed system. For example, in the case depicted in Fig. 12a the straight line approximation for the spiraled field should be valid at least for $\Re/b = 0.4$.

3.1.3 Damping Force Relationships

Consider now the interactions which occur between the conductive shell and the field of the nontransposed currents of Fig. 2. First of all it is to be noted that if the shell's motion is strictly parallel to

the z axis it will sense no changes in the magnetic field to which it is exposed. Hence, once equilibrium penetration is established, no eddy currents will be induced and there will be no interactions. However, it is clear that lateral motion or rotation will result in the shell being nonuniformly exposed to changing amounts of flux so that eddy currents will be induced. These are to be utilized for the purpose of damping oscillatory flight excursions across the range centerline.* In this case, as stated earlier, tailored flight is required so that eddy current power will be essentially real ($\geq$98 percent real, see Fig. 6). Otherwise, shielding will occur and randomly orientated positional forces will be introduced.

As the first step toward relating damping forces to other parameters, the distribution of eddy currents in a cylindrical shell arising out of relative motion with respect to a single parallel line current I_D will be found. Superposition will then be used to obtain the solution for the case of four such line currents in the null-flux arrangement of interest. From this, the power to joulean heating of the shell will be obtained and finally related to retardation or damping of its radial and angular motion.

Now consider the position of a streamline on the surface of the cylinder to be specified by polar coordinates a, ϕ and the position of the line current to be specified by r_1, θ_1, both as shown in Fig. 15. Also, consider the end surface of the cylinder to be highly conductive so that each is isopotential at $\Phi_1(t)$ and $\Phi_2(t)$, respectively, as shown. Next, insofar as surface conditions are concerned, it is to be recalled from Fig. 6 that for power $\geq$ 98-percent real the magnetic vector potential of the eddy currents is relatively small in comparison to that of the inducing field. Moreover, the phase angle ϵ between the inducing field $\bar{A}_i$, and the field $\bar{A}'$ of the eddy currents is such that their vector sum differs little in magnitude from that of the inducing field $\bar{A}_i$ alone. Hence, for the situation of interest, only the latter need be considered insofar as solving for eddy current magnitudes and distribution is concerned.

Returning to Fig. 15, the total electric field along any z-directed streamline of the cylinder's surface is that induced along this line plus that caused by charge accumulations and can be written for the two dimensional case as

*As would result from positioned forces alone.

$$\bar{E}(a, \phi, t) = - \frac{\partial \bar{A}_D(a, \phi, t)}{\partial t} + [\Phi_2(t) - \Phi_1(t)] \frac{\hat{k}}{h} \tag{50}$$

so that from Ohm's Law the current density is

$$\bar{i}(a, \phi, t) = \frac{1}{\varsigma} \left\{ - \frac{\partial \bar{A}_D(a,\phi,t)}{\partial t} + [\Phi_2(t) - \Phi_1(t)] \frac{\hat{k}}{h} \right\} \tag{51}$$

where ς is area resistivity, h is the cylinder length, and $\bar{A}_D$ is the magnetic vector potential of I_D. From Ref. 12, the vector potential can be expressed as

$$\bar{A}_D(a, \phi, t) = \frac{\mu_o \bar{I}_D}{2\pi} \ln \sqrt{r_1^2 + a^2 - 2ar_1 \cos(\phi - \theta_i)} + C_1 \tag{52}$$

with the argument of ln being the distance from the streamline of interest to the line current and with C_1 being an arbitrarily large constant. Upon substitution of this into Eq. (51) and differentiation with respect to time there results

$$\bar{i}(a, \phi, t) = \frac{\mu_o \bar{I}_D}{2\pi\varsigma} \left\{ \frac{[r_1 - a \cos(\phi - \theta_1)] dr_1/dt - ar_1 \sin(\phi - \theta_1) d\theta_1/dt}{a^2 + r_1^2 - 2ar_1 \cos(\phi - \theta_1)} \right\} + \frac{\Phi_2(t) - \Phi_1(t)}{\varsigma h} \tag{53}$$

In conjunction with the fact that $\bar{i}$ has only z conponents, an obvious boundary condition is that there can be no net flow of current past the cylinder ends, i.e.,

$$a \int_0^{2\pi} \bar{i}(a, \phi, t) d\phi = 0 \tag{54}$$

After substituting for $\bar{i}$ (a, ϕ, t) from Eq. (53), integration of Eq. (54) leads to the result that

$$\frac{\Phi_2(t) - \Phi_1(t)}{h} = - \frac{\mu_o I_D}{2\pi r_1} \frac{dr_1}{dt} \tag{55}$$

Upon returning this result to Eq. (53) and manipulating, the distribution of eddy currents attributable to one line current becomes

$$\bar{i}(a, \phi, t) = \frac{\mu_o \bar{I}_D}{2\pi\varsigma} \left\{ \frac{ar_1 \cos(\phi - \theta_1) - a^2}{r_1[a^2 + r_1^2 - 2ar_1 \cos(\phi - \theta_1)]} \frac{dr_1}{dt} - \frac{ar_1 \sin(\phi - \theta_1)}{a^2 + r_1^2 - 2ar_1 \cos(\phi - \theta)} \frac{d\theta_1}{dt} \right\} \tag{56}$$

In generalized form for the n^{th} of several line currents this becomes

$$\bar{i}_n(a, \phi, t) = \frac{\mu_o \bar{I}_D}{2\pi\varsigma} \left\{ \frac{ar_n \cos(\phi - \theta_n) - a^2}{r_n[a^2 + r_n^2 - 2ar_n \cos(\phi - \theta_n)]} \frac{dr_n}{dt} - \frac{ar_n \sin(\phi - \theta_n)}{a^2 + r_n^2 - 2ar_n \cos(\phi - \theta_n)} \frac{d\theta_n}{dt} \right\} \tag{57}$$

For the situation of interest which is four line currents of equal magnitudes and alternate directions as shown in Fig. 16, the total current density can then be written as

$$\bar{i}_T(a, \phi, t) = \frac{\mu_o I_D}{2\pi\varsigma} \sum_{n=1}^{4} (-1)^{n-1} \left\{ \frac{ar_n \cos(\phi - \theta_n) - a^2}{r_n[a^2 + r_n^2 - 2ar_n \cos(\phi - \theta_n)]} \frac{dr_n}{dt} - \frac{ar_n \sin(\phi - \theta_n)}{a^2 + r_n^2 - 2ar_n \cos(\phi - \theta_n)} \frac{d\theta_n}{dt} \right\} \tag{58}$$

Again, as indicated, the Cartesian coordinates of the line currents are taken to be (b, 0), (0, b), (-b, 0), and (0, -b). With the cylinder's radial and angular positions being $\mathcal{R}$ and β, there then exists in addition to Eq. (58) the generalized geometric relationships that

$$r_n = \sqrt{b^2 + \mathcal{R}^2 - 2\mathcal{R}b \cos\left(\frac{n-1}{2}\pi - \beta\right)} \tag{59}$$

and

$$\theta_n = \frac{n-1}{2}\pi + \sin^{-1}\left[\frac{\mathcal{R}}{r_n} \sin\left(\frac{n-1}{2}\pi - \beta\right)\right] \tag{60}$$

Differentiation of these with respect to time leads to the further generalized relationships that

$$\frac{dr_n}{dt} = \left[\frac{\mathcal{R} - b \cos\left(\frac{n-1}{2}\pi - \beta\right)}{r_n}\right] \frac{d\mathcal{R}}{dt} - \left[\frac{\mathcal{R}b \sin\left(\frac{n-1}{2}\pi - \beta\right)}{r_n}\right] \frac{d\beta}{dt} \tag{61}$$

and

$$\frac{d\theta_n}{dt} = \left[\frac{r_n^2 \sin\left(\frac{n-1}{2}\pi - \beta\right) - \Re \sin\left(\frac{n-1}{2}\pi - \beta\right)\left[\Re - b\cos\left(\frac{n-1}{2}\pi - \beta\right)\right]}{r_n^2\sqrt{r_n^2 - \Re^2 \sin^2\left(\frac{n-1}{2}\pi - \beta\right)}}\right]\frac{d\Re}{dt}$$

$$- \left[\frac{\Re\, r_n^2 \cos\left(\frac{n-1}{2}\pi - \beta\right) - \Re^2 b \sin^2\left(\frac{n-1}{2}\pi - \beta\right)}{r_n^2\sqrt{r_n^2 - \Re^2 \sin^2\left(\frac{n-1}{2}\pi - \beta\right)}}\right]\frac{d\beta}{dt} \tag{62}$$

Now recall that the radial and angular components of the shell's velocity are

$$V_\Re = \frac{d\Re}{dt} \tag{63}$$

and

$$V_\beta = \Re \frac{d\beta}{dt} \tag{64}$$

Upon substituting these into Eqs. (61) and (62), the results into Eq. (58), and regrouping, the total eddy current distribution resulting from the four currents becomes

$$\bar{\iota}_T(a, \phi, t) = \frac{\mu_o \bar{I}_D}{2\pi\zeta} \sum_{n=1}^{4} (-1)^{n-1}[\mathcal{F}_n(a, b, r, \Re, \beta, \phi, \theta) V_\Re + \mathcal{G}(a, b, r, \Re, \beta, \phi, \theta) V_\beta] \tag{65}$$

where

$$\mathcal{F}_n = \frac{[ar_n \cos(\phi - \theta_n) - a^2][\Re - b\cos(\frac{n-1}{2}\pi - \beta)]}{r_n^2[r_n^2 + a^2 - 2ar_n\cos(\phi - \theta_n)]}$$

$$- \frac{ar_n \sin(\phi - \theta_n)\sin(\frac{n-1}{2}\pi - \beta)}{[r_n^2 + a^2 - 2ar_n\cos(\phi - \theta_n)][r_n^2 - \Re^2\sin^2(\frac{n-1}{2}\pi - \beta)]^{1/2}}$$

$$+ \frac{\Re a \sin(\phi - \theta_n)\sin(\frac{n-1}{2}\pi - \beta)[\Re - b\cos(\frac{n-1}{2}\pi - \beta)]}{r_n[r_n^2 + a^2 - 2ar_n\cos(\phi - \theta_n)][r_n^2 - \Re^2\sin^2(\frac{n-1}{2}\pi - \beta)]^{1/2}} \tag{66}$$

and

$$\mathcal{G}_n = \frac{[ar_n \cos(\phi - \theta_n) - a^2][-b \sin(\frac{n-1}{2}\pi - \beta)]}{r_n^2[r_n^2 + a^2 - 2ar_n \cos(\phi - \theta_n)]}$$

$$\mp \frac{[ar_n \sin(\phi - \theta_n)]\cos(\frac{n-1}{2}\pi - \beta)}{[r_n^2 + a^2 - 2ar_n \cos(\phi - \theta_n)][r_n^2 - \mathcal{R}^2 \sin^2(\frac{n-1}{2}\pi - \beta)]^{1/2}}$$

$$- \frac{\mathcal{R}ab \sin(\phi - \theta_n) \sin^2(\frac{n-1}{2}\pi - \beta)}{r_n[r_n^2 + a^2 - 2ar_n \cos(\phi - \theta_n)][r_n^2 - \mathcal{R}^2 \sin^2(\frac{n-1}{2}\pi - \beta)]^{1/2}} \tag{67}$$

Now the power dissipated as joulean heat per unit cylinder length is

$$P = a\varsigma \int_0^{2\pi} [\bar{\iota}_T(a, \phi, t)]^2 d\phi \tag{68}$$

If V_β is zero, that power per unit length attributable to $V_\mathcal{R}$ becomes

$$P_{\mathcal{R}V} = \frac{a\mu_o^2 I_D^2}{4\pi^2 \varsigma} \int_0^{2\pi} [\sum_{n=1}^{4} (-1)^{n-1} \mathcal{F}_n(a, b, r, \mathcal{R}, \beta, \phi, \theta) V_\mathcal{R}]^2 d\phi \tag{69}$$

But this power is derived from mechanical motion where the incremental work per unit length is

$$dW_{\mathcal{R}V} = F_{\mathcal{R}M} d\mathcal{R} = -F_\mathcal{R} V_\mathcal{R} \tag{70}$$

with $F_{\mathcal{R}M}$ being the implied mechanical force acting radially per unit length against a retarding or damping force $F_\mathcal{R}$. The instantaneous power or rate of doing mechanical work per unit length is then

$$P_{\mathcal{R}V} = \frac{dW}{dt} = -F_\mathcal{R} \frac{d\mathcal{R}}{dt} = -F_\mathcal{R} V_\mathcal{R} \tag{71}$$

Now, for later convience, radial and angular magnetic damping coefficients are defined such that

$$K_{MD\mathcal{R}} = F_\mathcal{R} h V_\mathcal{R}^{-1} \tag{72}$$

and

$$K_{MD\beta} = F_\beta\, h\, V_\beta^{-1} \tag{73}$$

Equating Eqs. (69) and (71) and combining with Eq. (72) results finally in

$$K_{MD\Re} = -\frac{ah\,\mu_o^2\, I_D^2}{4\pi^2 \varsigma} \int_o^{2\pi} \left[\sum_{n=1}^{4} (-1)^{n-1}\, \mathcal{F}_n(a, b, r, \Re, \beta, \phi, \theta)\right]^2 d\phi \tag{74}$$

By setting $V_\Re$ equal to zero, the angular damping constant is obtained in a similar way with the result that

$$K_{MD\beta} = -\frac{ah\,\mu_o^2\, I_D^2}{4\pi^2 \varsigma} \int_o^{2\pi} \left[\sum_{n=1}^{4} (-1)^{n-1}\, \mathcal{G}_n(a, b, r, \Re, \beta, \phi, \theta)\right]^2 d\phi \tag{75}$$

These equations have been normalized with respect to "b" and solved with a digital computer* for the same positions as before in the treatment of diamagnetic forces. Surprisingly, for any given position, $K_{MD\Re}$ and $K_{MD\beta}$ are equal. Normalized results for both are shown in Fig. 17. It is to be noted that within the previous limits established for linearization of positioned forces, i.e., $a/b \leq 0.2$ and $\Re/b \leq 0.3$, the damping coefficients are essentially constants that are independent of β as required for a linear damping term in the equations of motion to be developed later. In either the positional or damping situations a choice of larger limits would not be unrealistic. In summary, their normalized value is plotted versus the ratio a/b in Fig. 18.

3.2 FLIGHT DYNAMICS

For simplicity, the following development will assume flight to be confined to a y-z plane of symmetry which passes through both the projectile axis and the guideway centerline (z axis). This assumption is justified on the basis that the projectile is to be a body of rotation and the guideway design is to be such that magnetic positional forces are almost totally radial. Any angular components are sufficiently small that their effect on dispersion of the projectile from the guideway centerline should be negligible. A means of visualizing their effect is to imagine relatively slow rotation of the plane of symmetry about the z axis.

*A listing of the Fortran program is included in Appendix A.

Within the plane of symmetry γ will be used to denote the angle between the z axis and the velocity vector $\overline{V}$ of the projectile's c_g (center of gravity), α will denote the projectile's angle of attack with respect to $\overline{V}$, and y will denote the dispersion of the c_g from the z axis (all shown in Fig. 19). Still within this plane, the aerodynamic lift and drag forces will be considered to act through an assumed center of aerodynamic pressure c_p a distance ℓ aft of c_g, and the magnetic positional and damping forces will be considered to act through an assumed center of magnetic pressure c_M a distance ℓ_M forward of c_g.

Recall also from Figs. 12, 13, and 17 that the design can be such that the magnetic positional forces will be a linear function of distance from the z axis with the magnetic damping forces being a linear function of the rate this distance changes. Additionally, the allowable angles of attack are to be small so that aerodynamic lift and damping can be assumed linear functions thereof with drag an independent linear function of velocity alone. Then at fixed velocity within the anticipated operating conditions the equations of motion can be assumed to be linear and will be so treated.

3.2.1 Equations of Motion

Referring again to Fig. 19, the sum of y forces acting on the projectile must be zero so that for small α and γ one can write

$$M\frac{d^2y}{dt^2} - qS_bC_{L\alpha}\alpha - K_M[y + \ell_M(\alpha + \gamma)] + qS_bC_{DO}\gamma - K_{MD}[(dy/dt) + \ell_M(d\alpha/dt)] = 0 \quad (76)$$

where previously unmentioned parameters M and S_b are projectile mass and base area respectively, q is dynamic pressure ($\frac{1}{2}\rho V^2$ with ρ being density of the working gas), and $C_{L\alpha}$ and C_{DO} are the aerodynamic lift and drag coefficients, respectively.

Additionally, the sum of moments about c_g must be zero so that one can also write

$$J\frac{d^2(\alpha + \gamma)}{dt^2} + qS_b\ell(C_{L\alpha} + C_{DO})\alpha - 2qS_br_b^2C_{m\dot{\alpha}}V^{-1}\frac{d\alpha}{dt}$$

$$- K_M\ell_M[y + \ell_M(\alpha + \gamma)] - K_{MD}\ell_M[(dy/dt) + \ell_M(d\alpha/dt)] = 0 \quad (77)$$

where J and r_b are projectile moment of inertia and base radius, respectively, and $C_{m\dot{\alpha}}$ is the aerodynamic damping coefficient.

The angle γ and its derivative can be eliminated from Eqs. (76) and (77) by the approximation for small angles that

$$\gamma = V^{-1} \frac{d\psi}{dt} \tag{78}$$

Upon doing this, the Laplace transformation of the resulting equations has made it possible to combine and solve algebraically for both ψ and α in terms of the complex quantity s with the result that

$$\psi(s) = \frac{\begin{array}{l}[(D_6 + V)\psi_o]\,s^3 + [(D_5V - D_2 + D_8)\psi_o + (D_6 + V)\dot{\psi}_o]s^2 \\ - [(D_2D_5 - D_4 + D_1D_6)\psi_o - D_6V\alpha_o - D_8 V\alpha_o + D_2\dot{\psi}_o - D_6\ddot{\psi}_o - D_8\dot{\psi}_o]s \\ + [(D_4D_5 - D_1D_8)\psi_o - (D_4D_6 + D_2D_8)\alpha_o + (D_4\dot{\psi}_o + D_8\ddot{\psi}_o + D_8V\dot{\alpha}_o)]\end{array}}{\begin{array}{l}[(D_6 + V)s^4 + [D_8 + D_5V - D_2]s^3 + [(D_4 - D_2D_5 - D_7V - D_1D_6]\,s^2 \\ + [D_4D_5 + D_2D_7 - D_3D_6 - D_1D_8]s - [D_3D_8 + D_4D_7]\end{array}} \tag{79}$$

and

$$\alpha(s) = \frac{\begin{array}{l}[(D_6 + V)\alpha_o]s^3 + [\ddot{\psi}_o - D_2\alpha_o + V\dot{\alpha}_o + D_5\dot{\psi}_o + D_5V\alpha_o - D_7\psi_o]\,s^2 \\ + [(D_1\dot{\psi}_o - D_1D_6\alpha_o + D_3\psi_o + D_5\ddot{\psi}_o - D_2D_5\alpha_o + D_5V\dot{\alpha}_o - D_7\dot{\psi}_o - D_7V\alpha_o]\,s \\ - [D_3D_6\alpha_o - D_1D_7\psi_o - D_3\dot{\psi}_o - D_3D_5\psi_o + D_7\ddot{\psi}_o - D_2D_7\alpha_o + D_7V\alpha_o]\end{array}}{\begin{array}{l}[(D_6 + V)]s^4 + [D_8 + D_5V - D_2]s^3 + [(D_4 - D_2D_5 - D_7V - D_1D_6]s^2 \\ + [D_4D_5 + D_2D_7 - D_3D_6 - D_1D_8]s - [D_3D_8 + D_4D_7]\end{array}} \tag{80}$$

where the subscript "o" denotes the initial condition, the superscripts $\cdot$ and $\cdot\cdot$ denote, respectively, the first and second derivatives with respect to time and

$$\begin{aligned} D_1 &= [K_M\ell_M^2 + K_{MD}\ell_M V]\,J^{-1} & D_5 &= [qS_bC_{DO} - K_M\ell_M - K_{MD}V]\,M^{-1}V^{-1} \\ D_2 &= [2qS_br_b^2C_{m\dot{\alpha}} + K_{MD}\ell_M^2 V]J^{-1} & D_6 &= K_{MD}\ell_M M^{-1} \\ D_3 &= K_M\ell_M^2 V\,J^{-1} & D_7 &= K_M M^{-1} \\ D_4 &= V[qS_b\ell(C_{L\alpha} + C_{DO}) - K_M\ell_M^2]\,J^{-1} & D_8 &= [qS_bC_{L\alpha} + K_M\ell_M]M^{-1} \end{aligned} \tag{81}$$

Note that the denominators of Eqs. (79) and (80) are identical quartics and that the numerators are cubics whose difference lies in the coefficients of the powers of s. Letting the roots of the quartic be R_1, R_2, R_3, and R_4, a general expression for Eqs. (79) or (80) is

$$f(s) = \frac{as^3 + \ell s^2 + cs + d}{\mathcal{I}(s - R_1)(s - R_2)(s - R_3)(s - R_4)} \tag{82}$$

where, for brevity, a, ℓ, c, d, and $\mathcal{I}$ are used in place of the coefficients. Upon application of Heaviside's Expansion Theorem (Ref. 13) an equivalent expression in terms of partial fractions is

$$f(s) = \frac{K_1}{s - R_1} + \frac{K_2}{s - R_2} + \frac{K_3}{s - R_3} + \frac{K_4}{s - R_4} \tag{83}$$

where

$$K_n = [(s - R_n) f(s)]_{s=R_n} \tag{84}$$

i.e.,

$$K_n = \left. \frac{(s - R_n)(a R_n^3 + \ell R_n^2 + c R_n + d)}{\mathcal{I}(s - R_1)(s - R_2)(s - R_3)(s - R_4)} \right|_{s=R_n} \tag{85}$$

An inverse transformation of Eq. (83) yields finally that in the time domain

$$f(t) = \sum_{n=1}^{4} K_n \exp(R_n t) \tag{86}$$

Recall that this is a general solution which is applicable to solving Eqs. (79) or (80) for $\mathcal{I}(t)$ or $\alpha(t)$.

Unfortunately, the solution does not yield a general expression for the roots of the quartic. It has been necessary therefore to resort to numerical techniques and the digital computer as a means of obtaining their value for each set of chosen parameters. At the same time the computer has also been used to determine the values of K_1, K_2, K_3, K_4, and finally to yield a timewise solution for both $\mathcal{I}$ and α. A listing of the Fortran program is included in Appendix A.

3.2.2 Discussion of Roots

In general, as might be expected from the physics of the problem, the four roots have been found to consist generally of two pairs of complex conjugates. One pair represents an oscillation that exists primarily because of aerodynamic forces. The second pair, whose value is also influenced greatly by aerodynamics, arises when magnetic guidance is added which, to a certain extent, modifies the first pair. The interrelation is involved and a clear separation has not been made.

A design methodology which would allow direct determination of unknown parameters from initially specified roots might possibly be developed in the future. The means of achieving this would be through use of the roots to form a quartic as in the denominator of Eqs. (79) and (80). The methodology would consist of a systematic means of adjusting parameters to yield equivalent coefficients for all powers of s.

4.0 RANGE "G" CORRELATION AND IMPLEMENTATION

The following preliminary adaptation of the concept to the VKF Range G is for demonstration purposes only, is limited in scope, and is not to be taken as final.

4.1 BASIC PHYSICAL PARAMETERS

To minimize scaling to actual reentry situations, it is generally preferred that tests in aeroballistics ranges be performed on the largest possible scale. Toward this end a base diameter of 5.08×10^{-2} m will be assumed for the projectile proposed herein. This is approximately the largest that can be accomodated by the 6.35×10^{-2} m bore of the Range G launcher in view of the fact that during launch the projectile is to be surrounded by a sabot which subsequently separates. The cylindrical portion of the projectile, and hence the diameter of the conductive shell, will be assumed to be one-half the base diameter, i.e., 2.54×10^{-2} m. The length of the shell will then be taken as four times its diameter, i.e., 1.016×10^{-1} m. This is a reasonable compromise between a desire on the one hand for a small length-to-diameter ratio to withstand launch loads, and a desire on the other hand for a large length-to-diameter ratio so as to be compatible with the previously developed theory.

The launch package as presently envisioned from the above is depicted in Fig. 20. As indicated, the magnetic forces are assumed to act at the midpoint of the copper shell. Also, as indicated, it is presumed that through use of appropriate flare angle, flare length, deployment of material, etc., the projectile's center of gravity will be placed a suitable distance ℓ_M behind and the center of aerodynamic pressure a suitable distance ℓ still further behind the shell's midpoint. For the purposes of this study, these distances or moment arms will be taken to be

$$\ell = 9.525 \times 10^{-3}\ \text{m} \tag{87}$$

and

$$\ell_M = 1.905 \times 10^{-2}\ \text{m}$$

Perhaps surprisingly, the influencing factor insofar as choice of guideway parameters is concerned derives from the sabot. This is because the first 30 m of postlaunch flight is through a so called "blast chamber" within which sabot separation and destruction occurs. Because it would otherwise interfere with this event, as well as sustain damage, the logical beginning of the guideway should be immediately downstream of the blast chamber exit. At this point, based on almost ten years of G-range history, a 5.08×10^{-2} m dispersion of the projectile away from the guideway centerline must be assumed. Upon adding to this the base radius of the projectile and an allowance for the conductors needed to carry guideway currents, the minimum allowable choice for the guideway dimension b (see Fig. 11) is 8.89×10^{-2} m. This value will be utilized herein. Next, from Fig. 8 it is seen that a good choice for the length ℓ_A of guideway transpositions is 17 times this value of b or, rounded off, 1.5 m.

Returning now to the projectile itself, the design velocity is taken to be 6,000 m/sec. The effective fundamental angular velocity of the spacewise magnetic field modulations then becomes

$$\omega = 2\pi V(2\ell_A)^{-1} = 12{,}560\ \text{radians/sec} \tag{88}$$

This, in conjunction with the correlation parameter of Fig. 6, enables determination of required shell area resistivity.

As seen in Fig. 6, a reasonable compromise insofar as concerns diamagnetic behavior of the conductive shell is where the eddy currents are 98-percent reactive and where $\S$ has a value of 0.22. At this point the correlation parameter has a value of 4.5, i.e.,

$$\mu_o \, a \, \omega (2n\varsigma)^{-1} = 4.5 \tag{89}$$

Now, from Ref. 8 (p. 299), the vector potential at polar coordinates r, θ attributable to a line current lying parallel to the z axis at r_o, θ_o can be expressed in terms of circular harmonics as (see Fig. 15)

$$A_z(r,\theta) = \frac{\mu_o I_z}{2\pi} \left[\ln r_o - \sum_{n=1}^{\infty} \frac{1}{n} (r/r_o)^n (\cos n\theta_o \cos n\theta + \sin n\theta_o \sin n\theta \right] \tag{90}$$

Also, as stated earlier, because the shell is of finite length, the net flow of current past its ends must be zero. Hence, for the postulated two-dimensional situation, any induced electric field attributable to the time derivative of the term "ln r_o" of Eq. (90) will be ineffective in producing eddy currents. All which exist must therefore be attributable to the time derivative of the indicated summation. Upon differentiation of the latter it becomes clear from inspection that if r_o is somewhat larger than r the n = 1 term dominates. Hence, by virtue of the fact that during flight the distance between the projectile axis and any of the line current segments of Figs. 1 or 3 is to be maintained relatively large* as compared to all $r \leq a$, it is seen that the correlation parameter need only be considered for the value n = 1. Upon substituting this value for n along with the previously established values for a and ω into Eq. (89) and solving for area resistivity there results

$$\varsigma = 2.227 \times 10^{-5} \text{ ohms} \tag{91}$$

Assuming the shell to be oxygen-free, high conductivity copper with a volume resistivity of $\rho = 1.724 \times 10^{-8}$ ohm-m, the implied shell thickness is

$$w = \frac{\rho}{\varsigma} = 7.74 \times 10^{-4} \text{ m} \tag{92}$$

For previously stated reasons, the thickness of the end walls will be taken at twice this value.

All dimensions are now defined that are needed for calculating the mass and moment of inertia of that portion of the shell (with its

*From three to seven times greater.

Lexan® interior) which lies forward of the projectile's c_g. The total mass and moment of inertia of the projectile are simply twice the result plus an allowance for a nose piece. Upon using 8.89×10^3 and 1.19×10^3 kg/m^3 for the density of copper and Lexan, respectively, there results for the projectile totals

$$M = 1.65 \times 10^{-1} \text{ kg}$$

and

$$J = 3.0 \times 10^{-4} \text{ kg} - \text{m}^2 \tag{93}$$

4.2 GUIDEWAY CURRENTS

For the purpose of this preliminary correlation to the G range the following aerodynamic coefficients are believed to be adequate and will be utilized throughout

$$\begin{aligned} C_{DO} &= 0.3 \\ C_{L\alpha} &= 1.1 \\ C_{m\dot{\alpha}} &= -2.0 \end{aligned} \tag{94}$$

Only flights in air at atmospheric pressure and at one-half atmospheric pressure will be considered. For these, the corresponding densities are taken to be 1.1767 and 0.5883 kg/m^3, respectively.

4.2.1 Current Magnitude

For the particular dimensions, shielding ratio, and area resistivity established above, is is found through use of Figs. 14 and 18 that

$$K_M = -8.0 \times 10^{-7} I_p^2$$

and

$$K_{MD} = -3.3 \times 10^{-10} I_D^2 \tag{95}$$

Upon insertion of proper current levels the resulting values of K_M and K_{MD}, in conjunction with values of the other parameters as have now been established, form the input data for the computer programs mentioned in Sect. 3.2.1. Dispersion (ψ) of the model about the range centerline and its angle of attack (α) as functions of downstream position as well as roots of the characteristic equation of Eqs. (79) and (80) can be computed.

Being primarily influenced by the current rating of the Tunnel "F" generators (Ref. 7) the authors have chosen 10^5 amp as being an appropriate I_D and I_P magnitude for demonstration of the concept. For such magnitudes Eq. (95) yields

$$K_M = -8 \times 10^3 \text{ N/m} \tag{96}$$

and

$$K_{MD} = -3.3 \text{ N - sec/m}$$

Initial conditions for the computed examples to be presented, i.e., ψ_o, α_o, and γ_o, are in all cases taken to be 5.08×10^{-2} m and 1×10^{-2} and 1×10^{-3} radians, respectively. Results for an atmospheric case in the existing range length of 300 m are depicted in Fig. 21 while Fig. 22 demonstrates the effect of reducing density to that for one-half of atmospheric. The behavior of ψ and α as depicted in the figures is in agreement with the desired effect, and the roots are in accord with expectations based on the theory of controls.

In Figs. 23 and 24 the velocity is reduced to 4,500 m/sec with an attendant shift in shielding ratio and accordingly a change in magnetic postional force constant to

$$K_M = 6.154 \text{ N/m} \tag{97}$$

K_{MD} is not significantly altered since its magniture is not dependent on velocity through the transposed (or modulated) field. All other variables remain as in the previous two examples, and Fig. 23 depicts the atmospheric and Fig. 24 the one-half atmospheric case. Again, results are gratifying and guidance is demonstrated.

The effect of varying the levels of I_D and I_P can be seen in Figs. 25 and 26 where an atmospheric and a one-half atmospheric case similar to those of Figs. 21 and 22 have been computed except using an increased I_D of 1.25×10^5 amp. It is apparent that the reduction in

error from the initial value for both y and α is greatest with this modification. Reasons for presenting the other examples in which I_D and I_P are the same will become clear in a following section.

Figures 21 through 26 exhibit significant reduction of initial error with any of the above mentioned sets of parameters, i.e., use of these sets of parameters results in guided flight. It should be emphasized here that these results are in marked conflict with any unguided case where for the assumed initial conditions y would have attained a value of 0.35m at a distance of 300 m downrange.

It should be noted here that the distance between excursions across the range centerline is a minimum of 45 m which compares to a 1.5-m transposition length. Therefore, as desired, eddy currents induced by the nontransposed field have a frequency more than 20 times lower than those resulting from velocity through the transposed field and are $\geq$ 98-percent real, as desired.

A final point that should be made is that the range length is also an important parameter. Note that if this were increased, with all other parameters remaining fixed, the initial error would be further reduced. To illustrate, if the error is reduced to one-fifth its original value in a 300-m range it would be reduced to a twenty-fifth of its original value in a 600-m range. Hence, application to longer ranges is encouraging from this viewpoint.

4.2.2 Implementation

Although not specifically stated, the establishment in Section 4.1 of the guideway dimension b (see Fig. 2) as 8.87×10^{-2} m includes an allowance for conductors of diameter 2.54×10^{-2} m to carry the guideway currents. This diameter, in conjunction with the b dimension and a guideway length of 300 m are the basis of the calculated inductance and resistance values that are used in the following development.

Because of the transposition all tendencies for mutal inductance between the I_P and I_D currents of Fig. 1 cancel when overall guideway length is considered. Hence, with reference to Figs. 1, 2, and 16, the energy stored inductively in the basic guideway field of the I_D currents alone can be written as

$$\mathcal{U}_{BF(ind)} = 4[\tfrac{1}{2}(L_{self} - 2L_{mut\ 1-2} + L_{mut\ 1-3})I_D^2] \qquad (98)$$

where $L_{self\ 1}$ is the self inductance of each of the conductors and $L_{mut\ 1-2}$ and $L_{mut\ 1-3}$ is the mutual inductance between diagonal and adjacent conductors, respectively. Based on working formulae 3 and 7 of Grover (Ref. 14), approximate values of self and mutual inductance for the aforementioned dimensions are

$$L_{self\ 1} = 6.01 \times 10^{-4}\ h$$

$$L_{mut\ 1-2} = 4.48 \times 10^{-4}\ h$$

$$L_{mut\ 1-3} = 4.27 \times 10^{-4}\ h \tag{99}$$

Upon substitution into Eq. (98), there results for inductive energy in the I_D field

$$\mathcal{W}_{BF(ind)} = 2.64 \times 10^{-4}\ I_D^2 \tag{100}$$

Although consideration of transpositions would result in a slightly higher value, the effective self and mutual inductances of the conductors for the I_P currents will be taken to be equal to those for I_D. Using nomenclature of Fig. 11, then the inductive energy of the transposed field is

$$\mathcal{W}_{TF(ind)} = 2.64 \times 10^{-4}\ I_P^2 \tag{101}$$

Total inductive guideway energy is then

$$\mathcal{W}_{GW(ind)} = \mathcal{W}_{BF(ind)} + \mathcal{W}_{TF(ind)} = 2.64 \times 10^{-4}(I_D^2 + I_P^2) \tag{102}$$

For I_D and I_P of 10^5 amp as used in 4.2.1 above the inductive energy in the guideway field would be

$$\mathcal{W}_{GW(ind)} = 5.28 \times 10^6\ J \tag{103}$$

This field energy level coupled with current levels of 10^5 amp and the fact that the guideway need only be energized for approximately 0.1 sec* suggests the utilization of the nearby flywheel/inductor energy store power supply for the VKF Tunnel F (Ref. 7). Approximately 4×10^8 J is available from its flywheel-driven, acyclic generators at 10^6 amp and 90 v, or at 5×10^5 amp and 180 v; or from its storage inductor,

*The time required for a projectile to travel the guideway length, plus contingency time.

10^8 J is available at 10^6 amp up to 2×10^4 v. However, unless sectionalization is utilized as will be discussed below, or unless conductors are utilized at cryogenic temperatures, and space requirements for thermal insulation discourages this, overall guideway resistance will not allow either approach. If it is of copper at room temperature, resistance of a single conductor of 2.54×10^{-2} m diameter and 300-m length is

$$\text{Res} = \frac{(300\ \text{m})(1.71 \times 10^{-8}\ \text{ohm} - \text{m})}{(\pi/4)(2.54 \times 10^{-2}\ \text{m})^2}$$

$$= 1.012 \times 10^{-2}\ \text{ohm} \tag{104}$$

The current that can be driven through two such conductors in series (one go and one return) at maximum generator voltage of 180 v is thus

$$I_P \approx I_D = \frac{180}{2(1.012 \times 10^{-2})} = 8{,}893\ \text{amp} \tag{105}$$

This is inadequate by an order of magnitude. Moreover, if one resorts to utilization of the storage inductor (assuming its current could be commutated through the guideway with reasonable efficiency) the energy to joulean heating of the eight guideway conductors by a 10^5 amp, 10^{-1} sec pulse through each would be

$$\mathcal{E}_{GW(real)} = 4(I_D^2 + I_P^2)(\text{Res})(\Delta t)$$

$$= 4[(10^5)^2 + (10^5)^2](1.012 \times 10^{-2})(10^{-1})$$

$$= 8 \times 10^7\ \text{J} \tag{106}$$

This is approximately the full rating of the storage inductor. Considering that vast amounts of energy must inescapably be lost in commutating current through the guideway and that the delivered current pulse would be a rapidly decaying exponential, this approach is unsatisfactory. It is noteworthy, however, that calculations show the desired pulse would lead to a guideway temperature rise of only 20°C.

One viable alternative would be to procure a large flywheel-driven generator whose energy, voltage, and current ratings would be matched to the guideway. From Eqs. (101) and (106) it appears that a total flywheel energy on the order of the 6.84×10^8 joule total for Tunnel F would be adequate. As mentioned above, an attractive

possibility for Range G which would allow utilization of the Tunnel F power supply is offered through guideway sectionalization. Each section would be powered independently of all others, and then only for the period needed for the projectile to pass. This might be achieved by explosively or perhaps pneumatically actuated switches which would appropriately connect and disconnect each section to two large, range-length conductors* that would be energized by the Tunnel F generators. Minimal switch developmental effort should be required because of the low operating voltage (180 v) and because the guideway inductance to resistance ratio is relatively low.

As still another alternative, relatively small flywheel-driven generators could be stationed at intervals along the wayside for powering each guideway section at the appropriate time. Or, alternatively, banks of energy storage capacitors could be utilized. It is to be expected, however, that the rotating machinery approach would be the most economical, more trouble free, and with an expected life that would be significantly longer.

Returning again to Figs. 1 and 3, attention is invited to the fact that if I_D and I_P are equal in magnitude, the basic guideway field is canceled by alternate transpositions and is doubled in value by the ones between. This suggests the possibility of utilizing currents (and their conductors or coils) only at alternate intervals as shown in Fig. 27. To make this point clear is the reason for computing flight paths in Sec. 4.2.1 for equal I_D and I_P despite the fact that improved results were achieved with increased I_D. This means an increased level for the basic, or average (nonmodulated field) is desired. Hopefully, it can be seen that essentially this same biasing effect can be achieved by making the z spacing between the coils of Fig. 27 less than the z dimension of the coils themselves. An obvious bonus feature of such spaced coils would be that, while in the intervals between coils, the projectile would be free of shock interactions and there would be no obstructions insofar as wayside photography is concerned.

*One go and one return conductor, each having an area on the order of 0.1 m^2.

5.0 CONCLUDING REMARKS

An electromagnetic-guideway/guided-projectile system concept that is believed suited to the VKF Range G, and perhaps numerous other aeroballistic ranges, has been presented and developed from a theoretical viewpoint. Basis of the system is guided, aerodynamic flight via motion-induced, electrodynamic interactions between wayside magnetic fields that form a guideway, and conductive material that is deployed in the projectile structure. The geometry of the fields is such that induction decays to zero with proximity to the guideway axis so that interference with aerodynamic flow or ablation near a projectile's stagnation point should be minimal. Aside from being devoid of sliding surface contact as is used in mechanical guideways, a possible attractive feature of the system is periods of essentially free flight, with no obstructions to interfere with wayside photography.

Quite naturally, system theory, and hence the concept itself, has been developed on the most elementary basis possible. For example, the concept as presented utilizes conductive material in the form of a cylindrical shell that is placed principally about the projectile's forebody. It should be possible, and from an aerodynamic viewpoint perhaps desirable, to achieve the necessary electrodynamic interaction with the guideway if a shell of conical or other shape were used. However, the electrodynamic theory would be most difficult to develop as the problem would no longer be two-dimensional. Fortunately, with the cylinder it has been possible to develop most of that needed by two independent means, the briefest of which has been presented. Certain idealizations and simplifying assumptions have, however, been made during the course of the development which apply to both. For this reason, experiments are underway that are intended to confirm theory insofar as concerns electrodynamic interactions. A report on the results is planned for the near future. No experimentation as regards aerodynamics is planned as adequate wind tunnel data should be available for this purpose.

For the particular case of Range G the possibility of energizing a guideway from the nearby Tunnel F generators is optimistically offered, provided that the guideway is sectionalized and that each section be powered only during the time the projectile is passing through, plus contingency. Possible alternate methods of guideway energization for this and other ranges have also been offered. However, in retrospect, it is possible that stronger fields with correspondingly stiffer flight control may be desired in lieu of these

values used in the Range G examples of Section 4.2.1. One reason is that ablating and/or eroding nose test specimens may initially have (or tend to develop) asymmetry and cause the projectile to become stubborn. Another is that greater downrange accuracy may be needed for capture. This could, of course, be improved by a smaller initial error. Such reduction additionally would allow a smaller guideway dimension b, and hence, from Figs. 14 and 18, greater magnetic force coefficients for given currents. Also, with sectionalization, there is the possibility of utilizing greater currents from the Tunnel F power supply which would lead to still greater force coefficients.

Still another reason for stiffer control is to achieve a reduction in the maximum angle of attack assumed by the projectile. Quite obviously this would be achievable with lowered initial error. But a reduction could also be achieved by virtue of the fact that greater magnetic forces would permit lesser reliance on the development of aerodynamic forces. In turn, lower magnetic moment and moment arms would be required. To visualize the trend, consider the case of zero ℓ_M where the magnetic forces would attempt to correct the projectiles course, but with zero change in angle of attack. Finally, it should be pointed out that the need for stiffer control becomes less urgent with increased range length as more time is available for recovery from initial errors.

In conclusion, it is recognized that numerous variations and ramifications of the concept presented are obviously possible, most of which are left to the reader's imagination. Opportunity is taken, however, to emphasize the fact that a more efficient approach is possible for situations where space and launch accelerations will permit superconducting magnets on the projectile. In the meantime, subsequent to the experimental verifications promised above, it appears that construction of a scaled-down, developmental version of the present concept would be in order. This could most easily be accomplished in the presently inactive VKF Tunnel J (Ref. 15) where proper power is available for the guideway.

REFERENCES

1. Clemens, P. L. "The von Kármán Gas Dynamics Facility 1000-ft Hypervelocity Range - Description, Capabilities, and Early Test Results." AEDC-TR-66-197 (AD801906), November 1966.

2. Powell, J. R. and Danby, G. T. "High Speed Transport by Magnetically Suspended Trains." ASME publication 66-RR-5, Winter Annual Meeting, New York, New York, November 1966.

3. Reitz, J. R., Borcherts, R. H., Davis, L. C., Hunt, T. K., and Wilkie, D. F. "Preliminary Design Studies of Magnetic Suspensions for High Speed Ground Transportation." Federal Railroad Administration Report FRA-TR-73-27, March 1973.

4. Coffey, H. T., Chilton, F., and Hoppie, L. O. "The Feasibility of Magnetically Levitating High Speed Ground Vehicles." Federal Railroad Administration Report FRA-TR-72-39, February 1972.

5. Guderjahn, C. A., Wipf, S. L., and Fink, H. J. "Magnetic Suspension and Guidance for High Speed Rockets by Superconducting Magnets." Journal of Applied Physics, Vol. 40, No. 5, April 1969, pp. 2133-40.

6. Erickson, E. E. "A Superconducting Magnet Dewar Missile for Launching in Ballistic Ranges." AEDC-TR-76-3, March 1976.

7. Patterson, J. N. "Inductive Power Supply for a 100-in. Hotshot Wind Tunnel." AEDC-TR-66-260 (AD649376), March 1967.

8. Smythe, W. R. Static and Dynamic Electricity. Third Edition, McGraw-Hill Book Company, New York, 1968.

9. Corson, D. R. and Lorrain, P. Introduction to Electromagnetic Fields and Waves. W. H. Freeman and Company, San Francisco, 1962.

10. Halliday, D. and Resnick, R. Physics for Students of Science and Engineering - Part II. Second Edition, John Wiley and Sons, Inc., New York, 1962.

11. Jackson, J. D. Classical Electrodynamics. John Wiley and Sons, Inc., New York, 1962.

12. Haigue, B. The Principles of Electromagnetism. Dover Publications, Inc., New York 1962.

13. Goldman, S. Transformation Calculus and Electrical Transients. Prentice-Hall, Inc., Englewood Cliffs, N. J., 1949.

14. Grover, F. W. Inductance Calculations. Dover Publications, Inc., New York, 1946.

15. Norman, W. and Walker, R. R., III. "Status of Research on Magnetohydrodynamic Augmentation of a Shock Tunnel." AEDC-TR-66-25 (AD482453), May 1966.

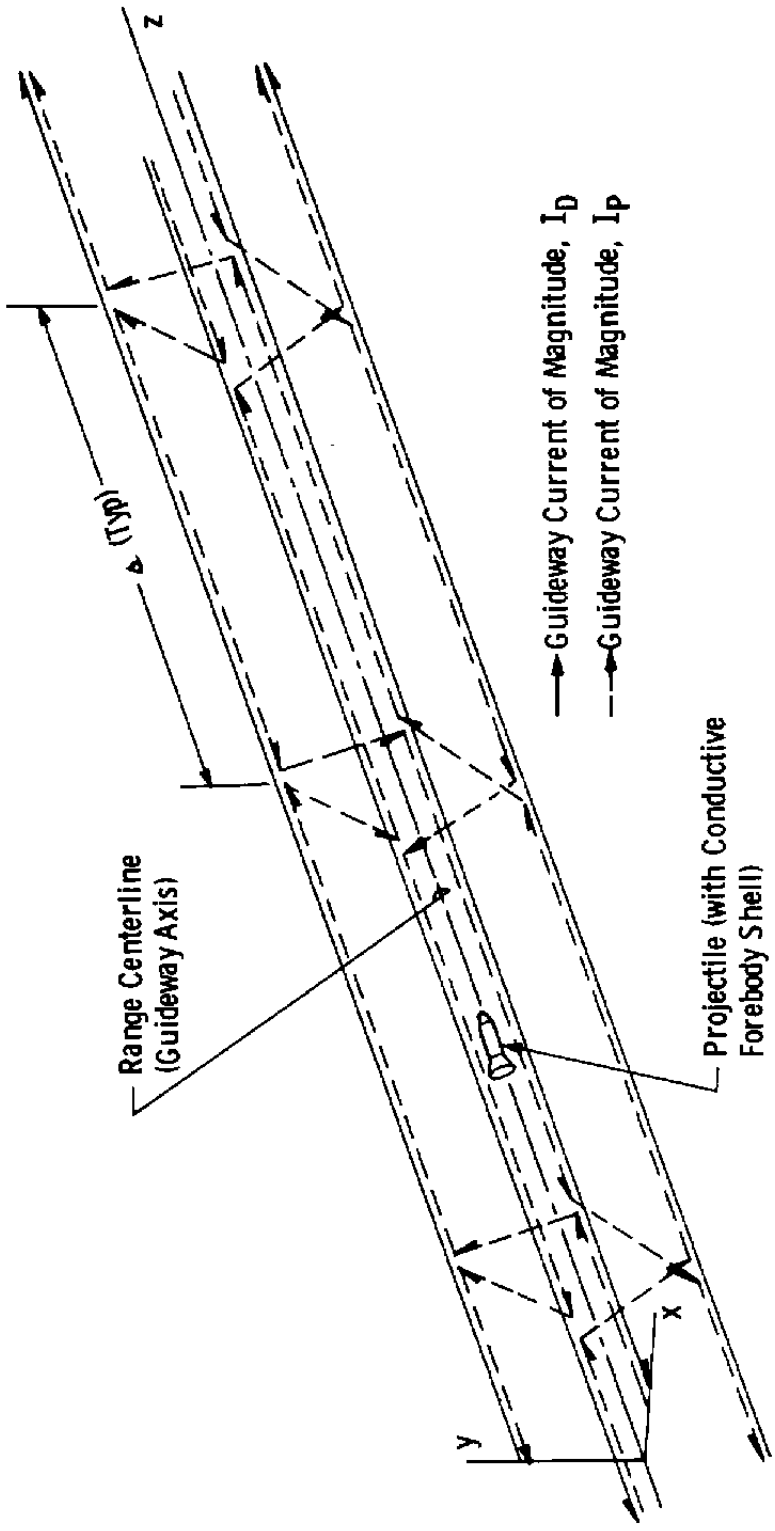

Figure 1. System concept.

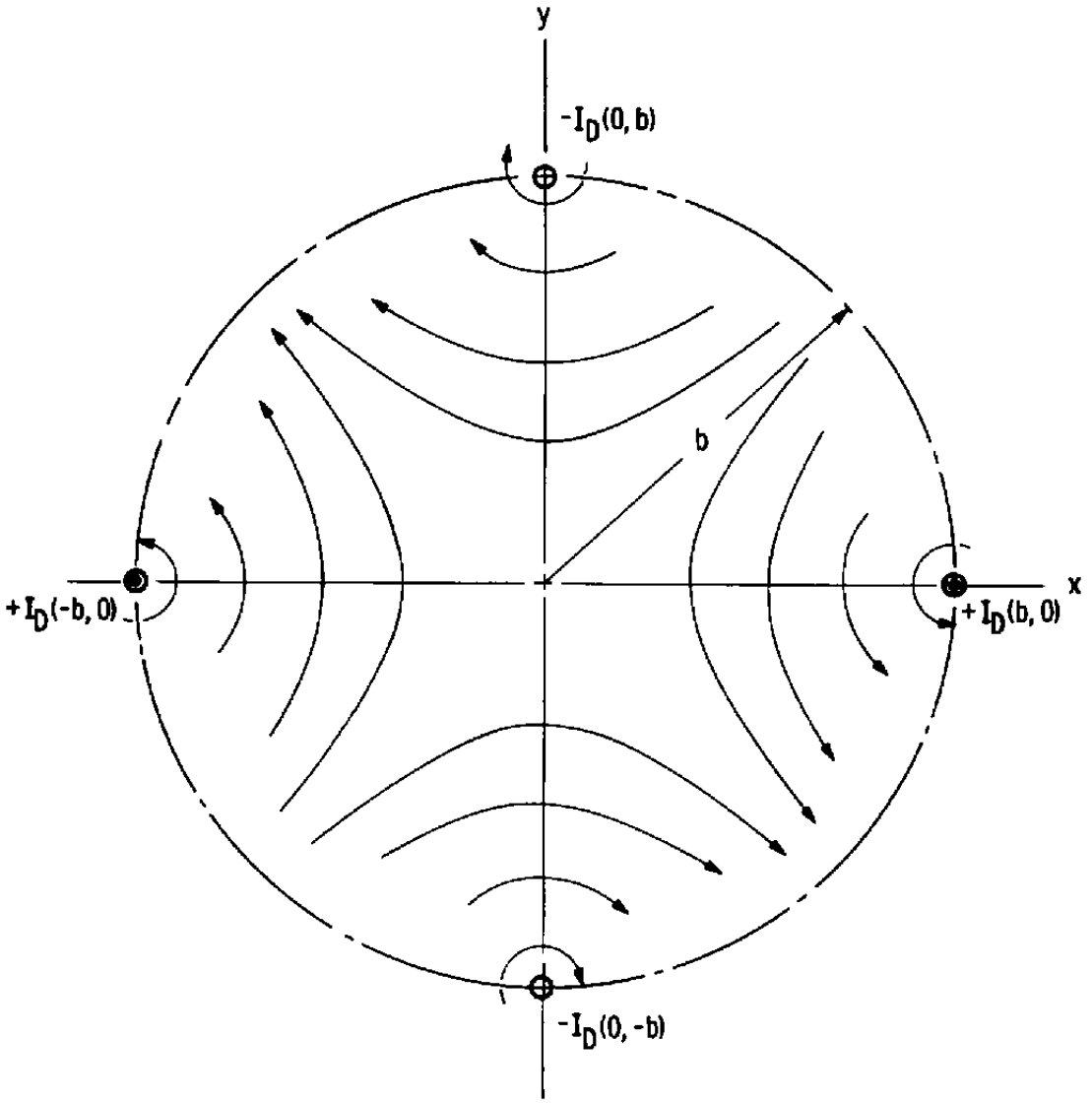

Figure 2. Null-flux field of I_D currents.

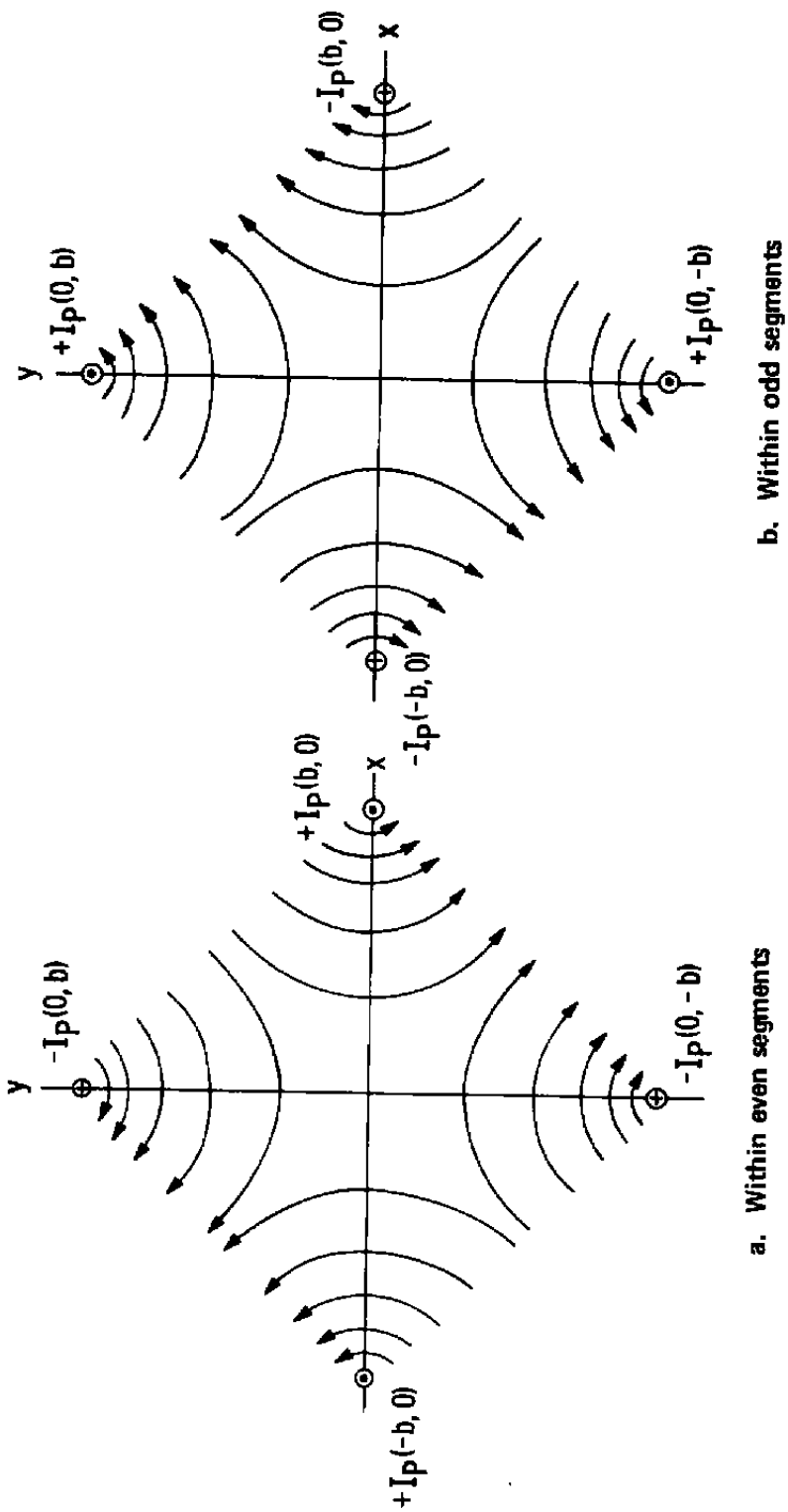

a. Within even segments

b. Within odd segments

Figure 3. Null-flux field of I_p currents.

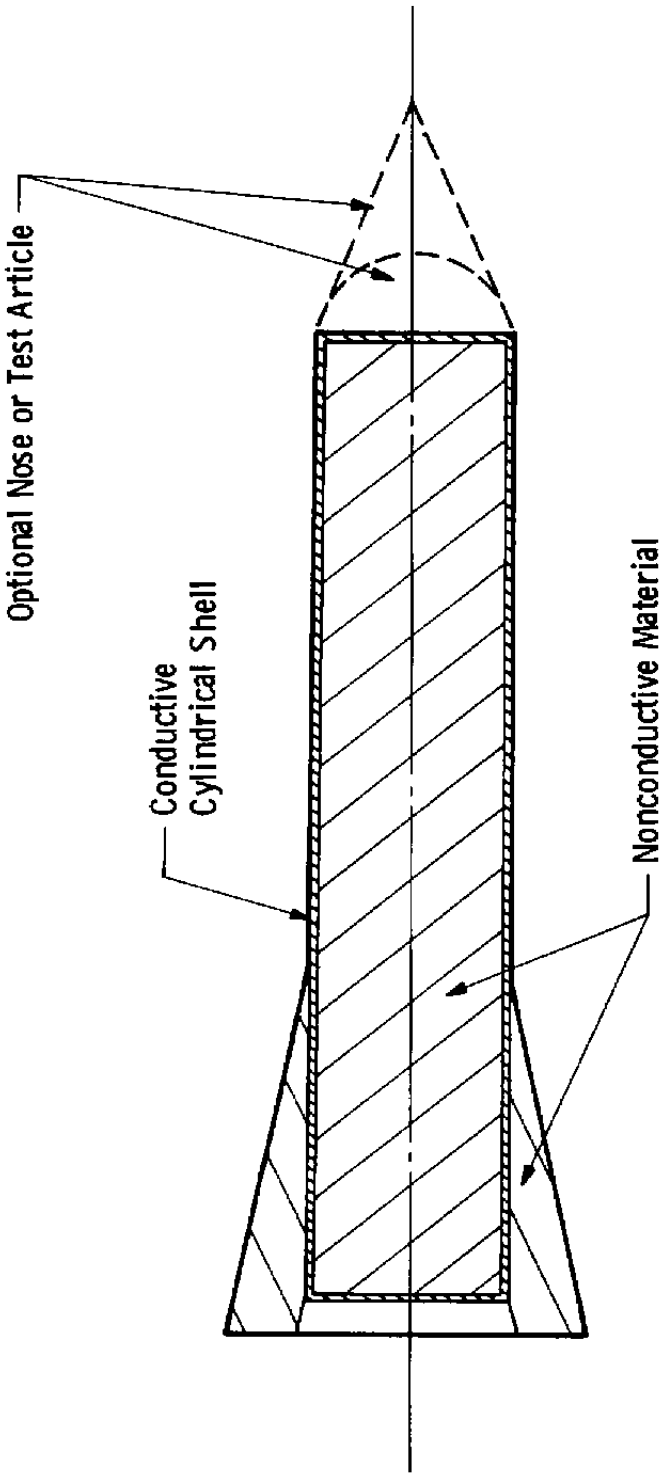

Figure 4. Projectile configuration for feasibility study.

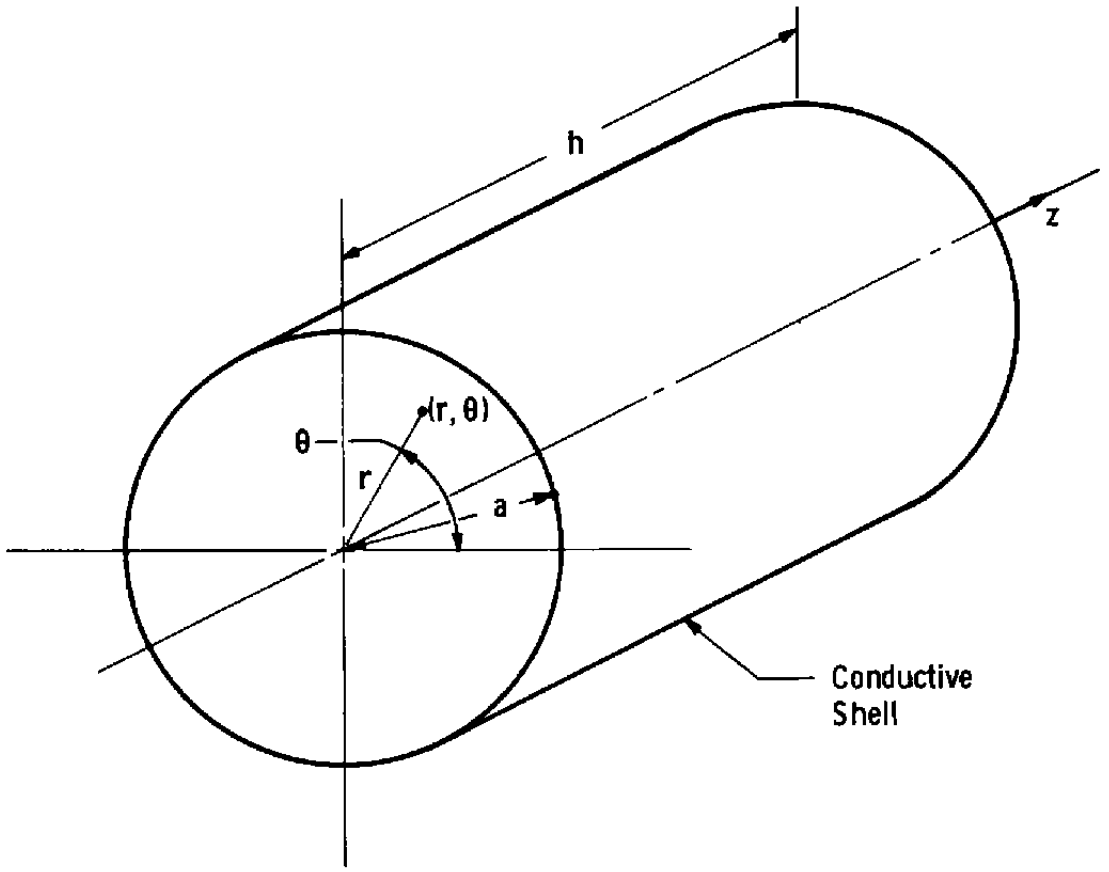

Figure 5. Nomenclature for study of diamagnetic and dissipative behavior.

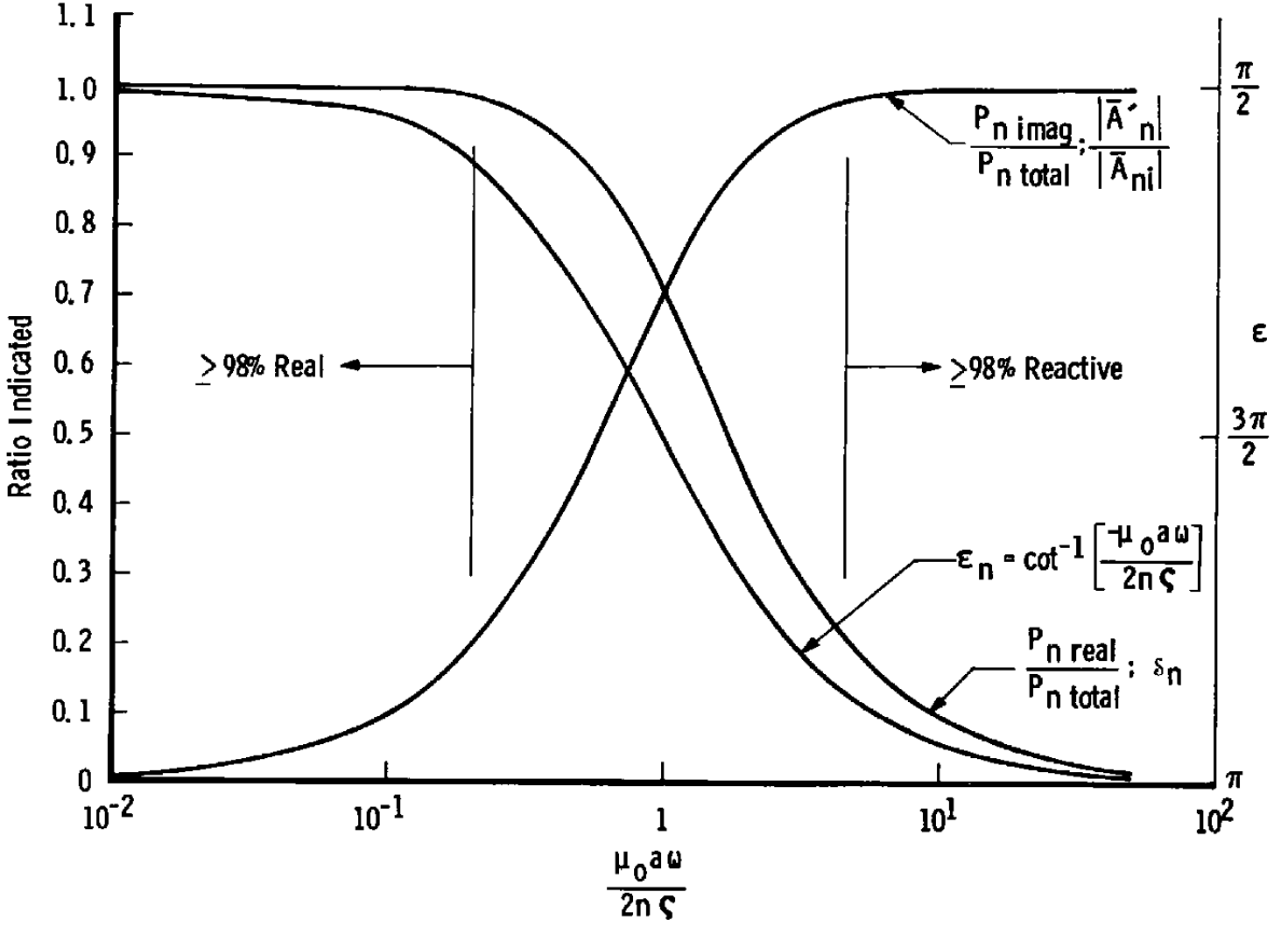

Figure 6. Power, shielding, and vector potential relationships.

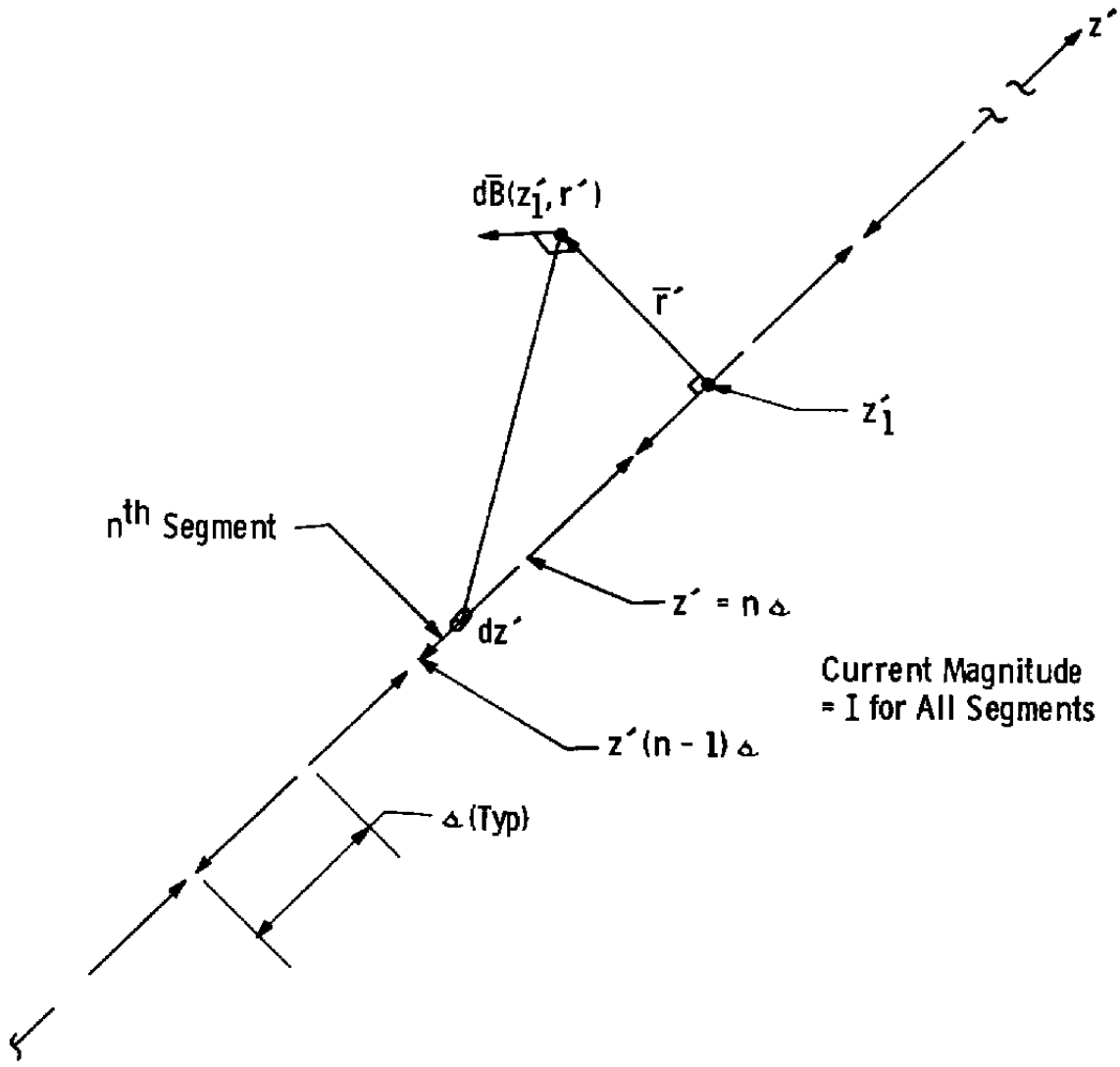

Figure 7. Transposed line current segments.

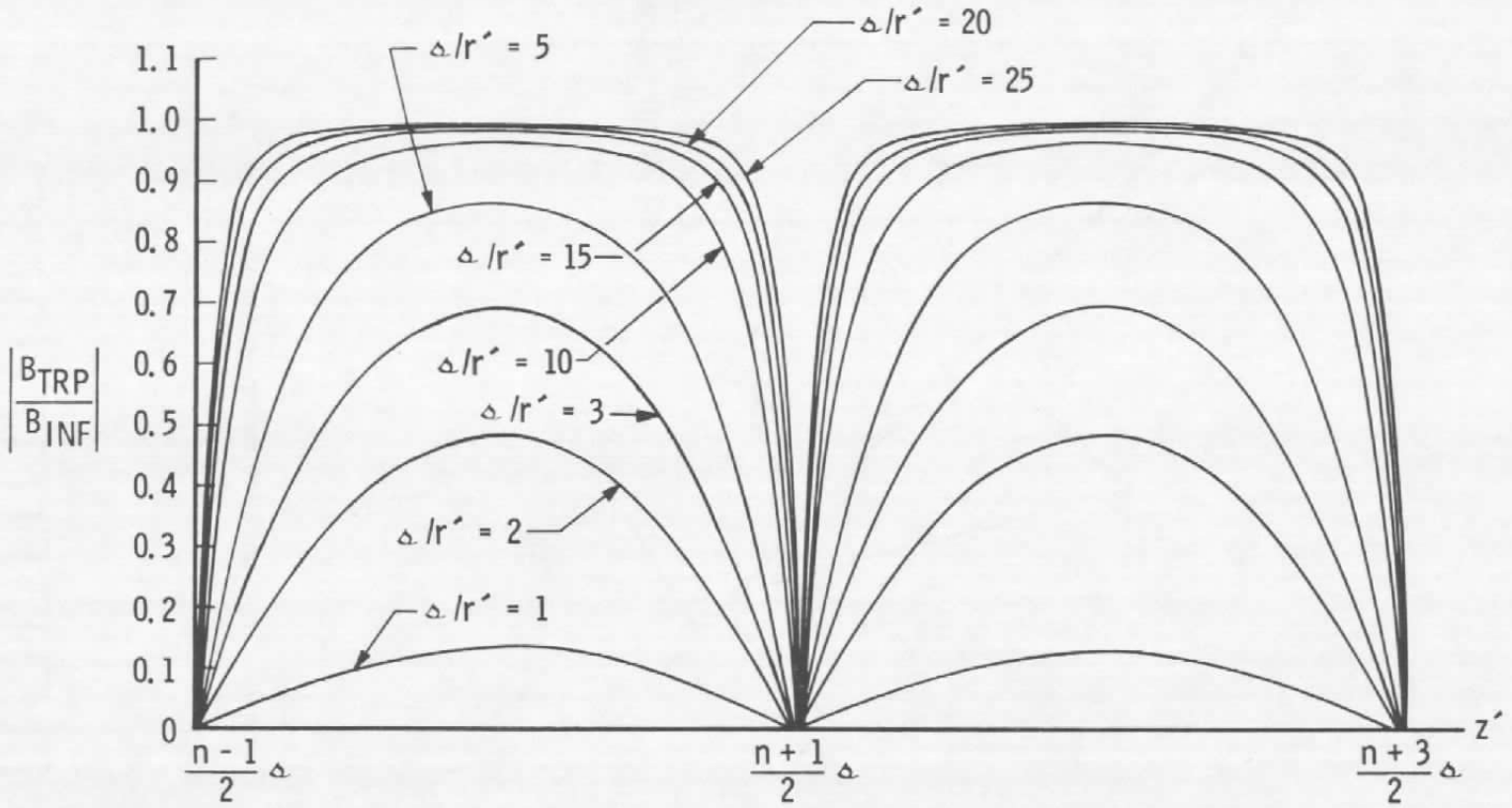

Figure 8. Magnetic field of line current versus field of transposed current segments.

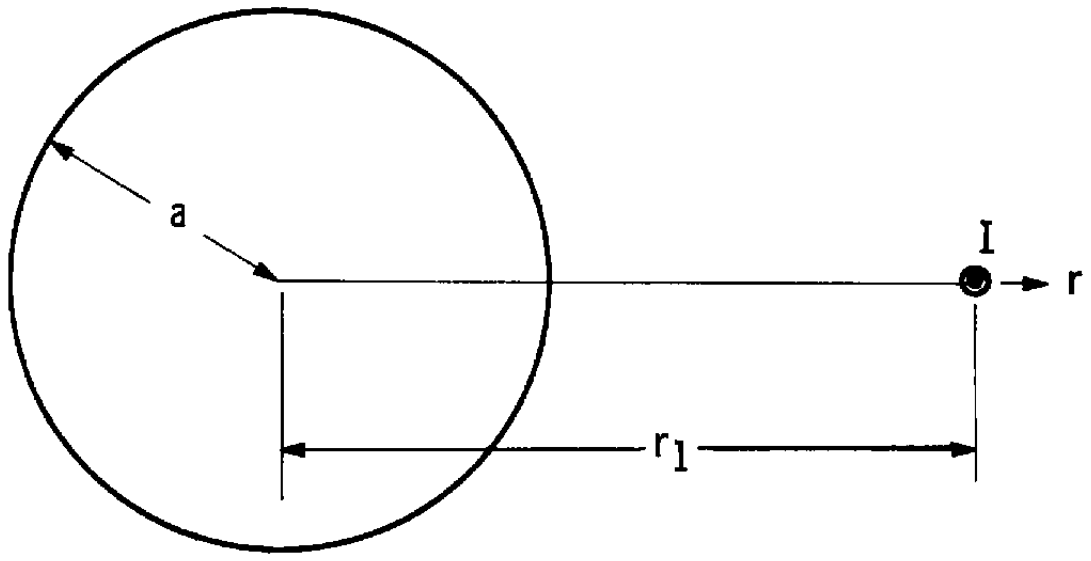

a. Magnetic cylinder and line current

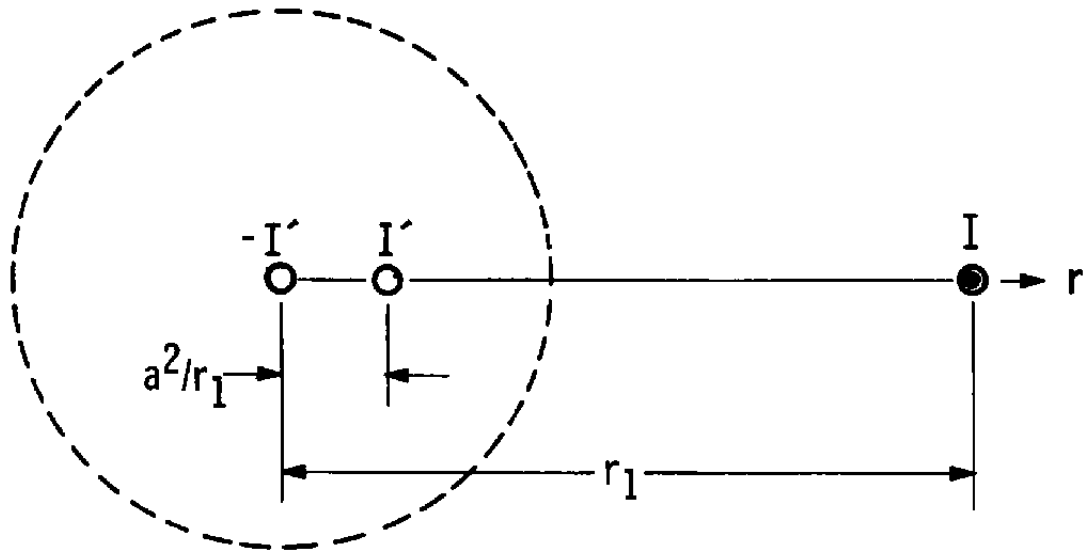

b. Image currents for equivalent fields exterior to cylinder

Figure 9. Magnetic cylinder in presence of a line of current.

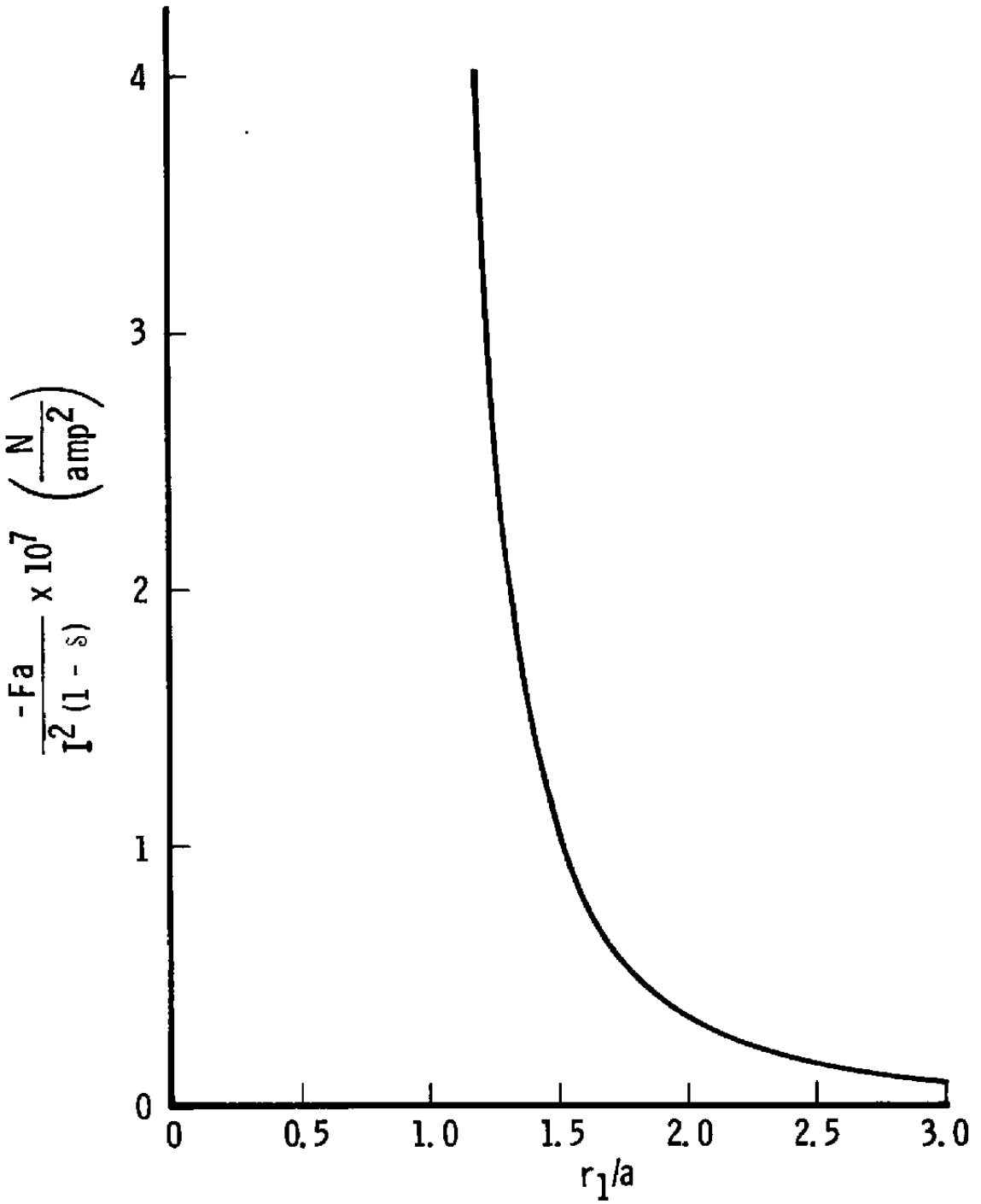

Figure 10. Force exerted on a diamagnetic cylinder by a parallel line current.

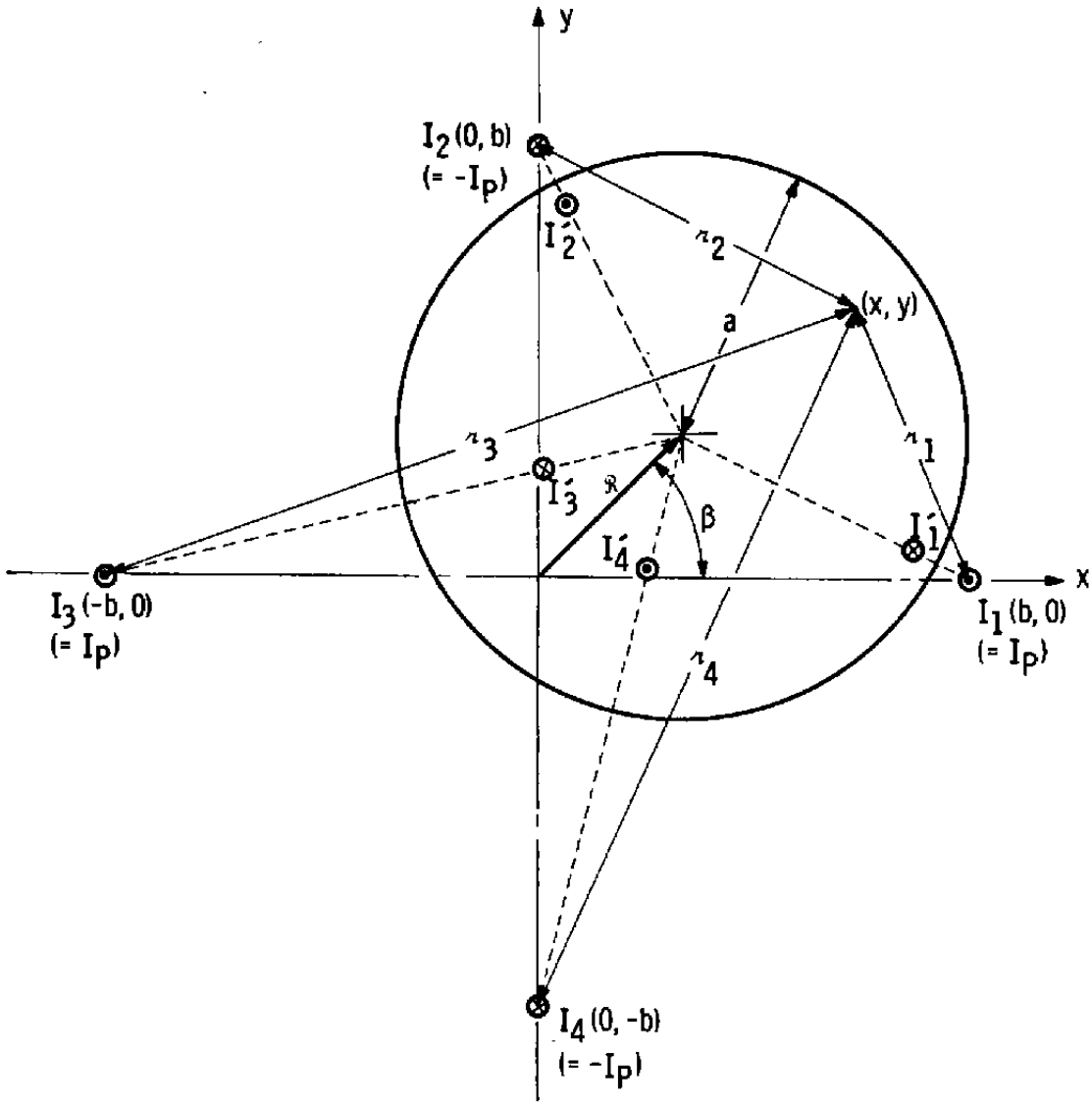

Figure 11. Nomenclature for positional force calculations.

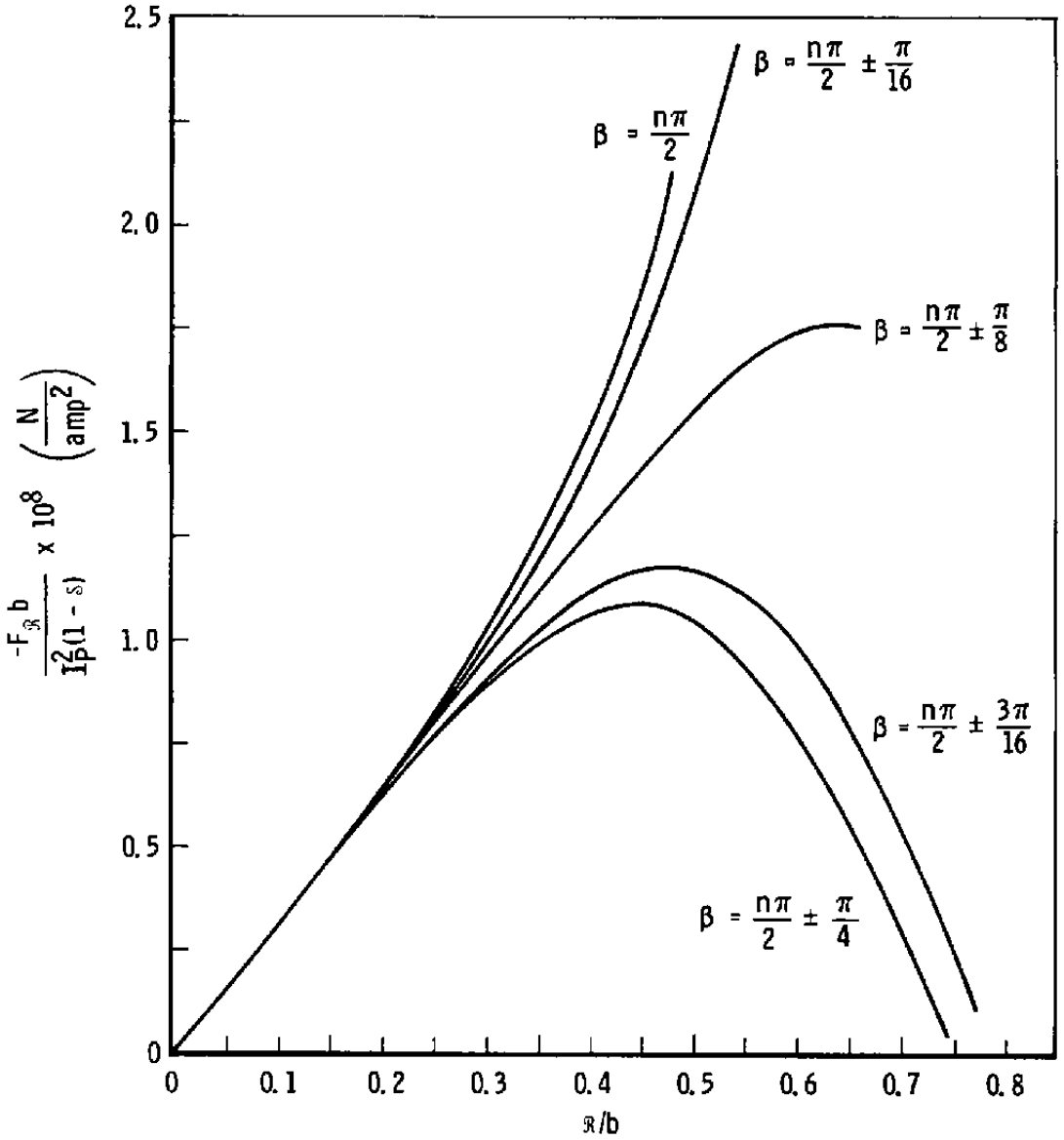

a. a/b = 0.1

Figure 12. Radial positional forces.

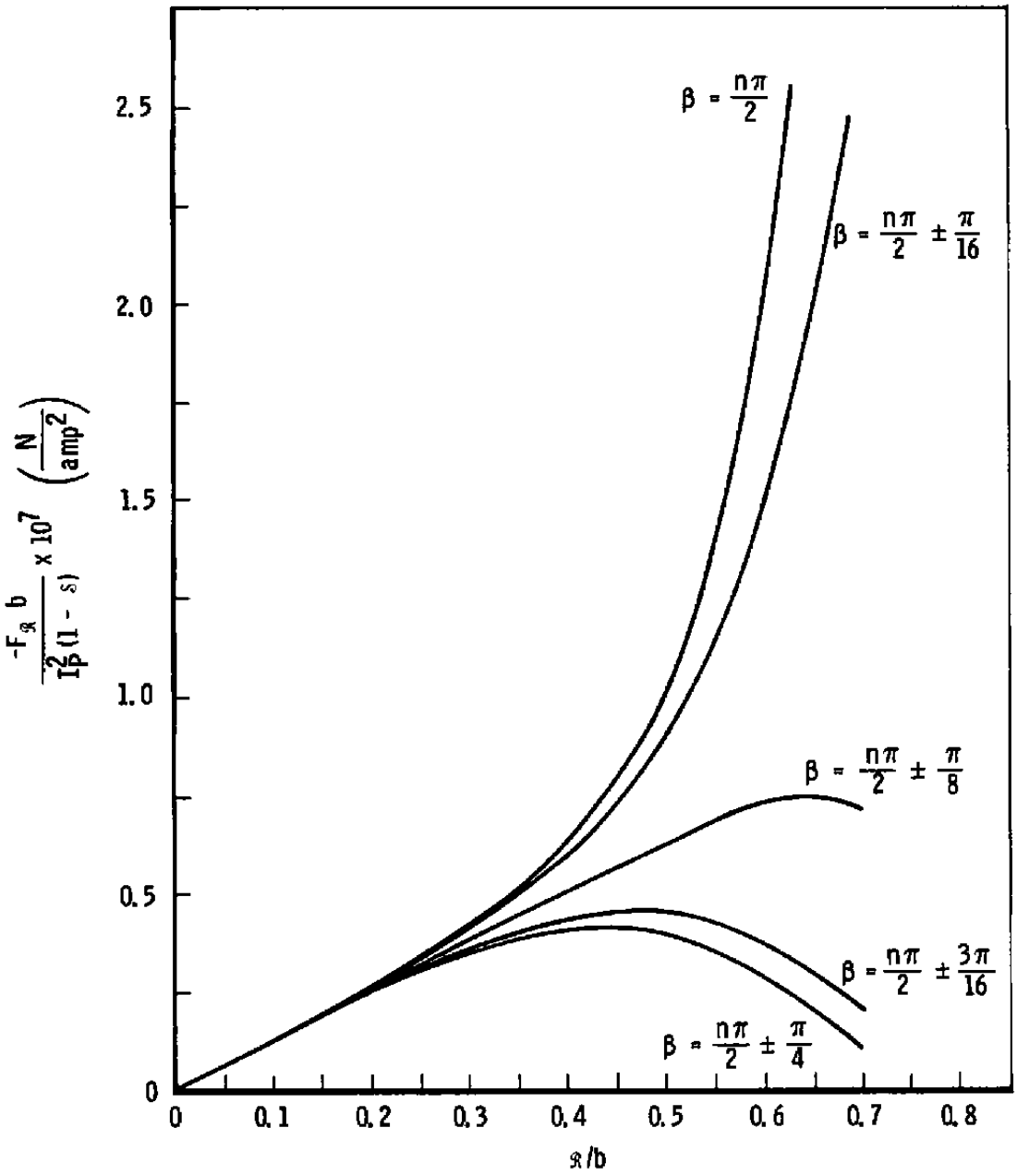

b. a/b = 0.2

Figure 12. Continued.

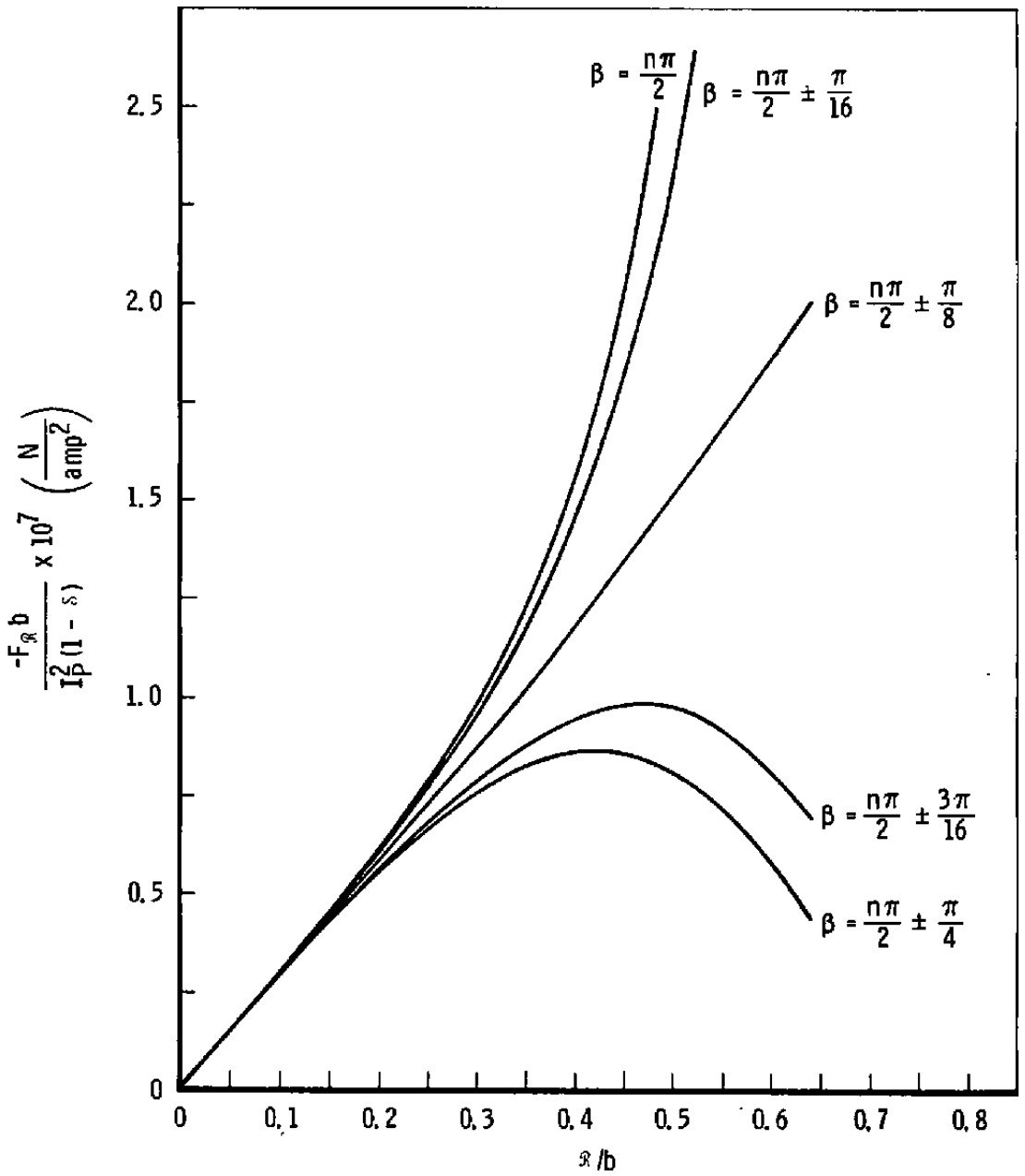

c. a/b = 0.3

Figure 12. Continued.

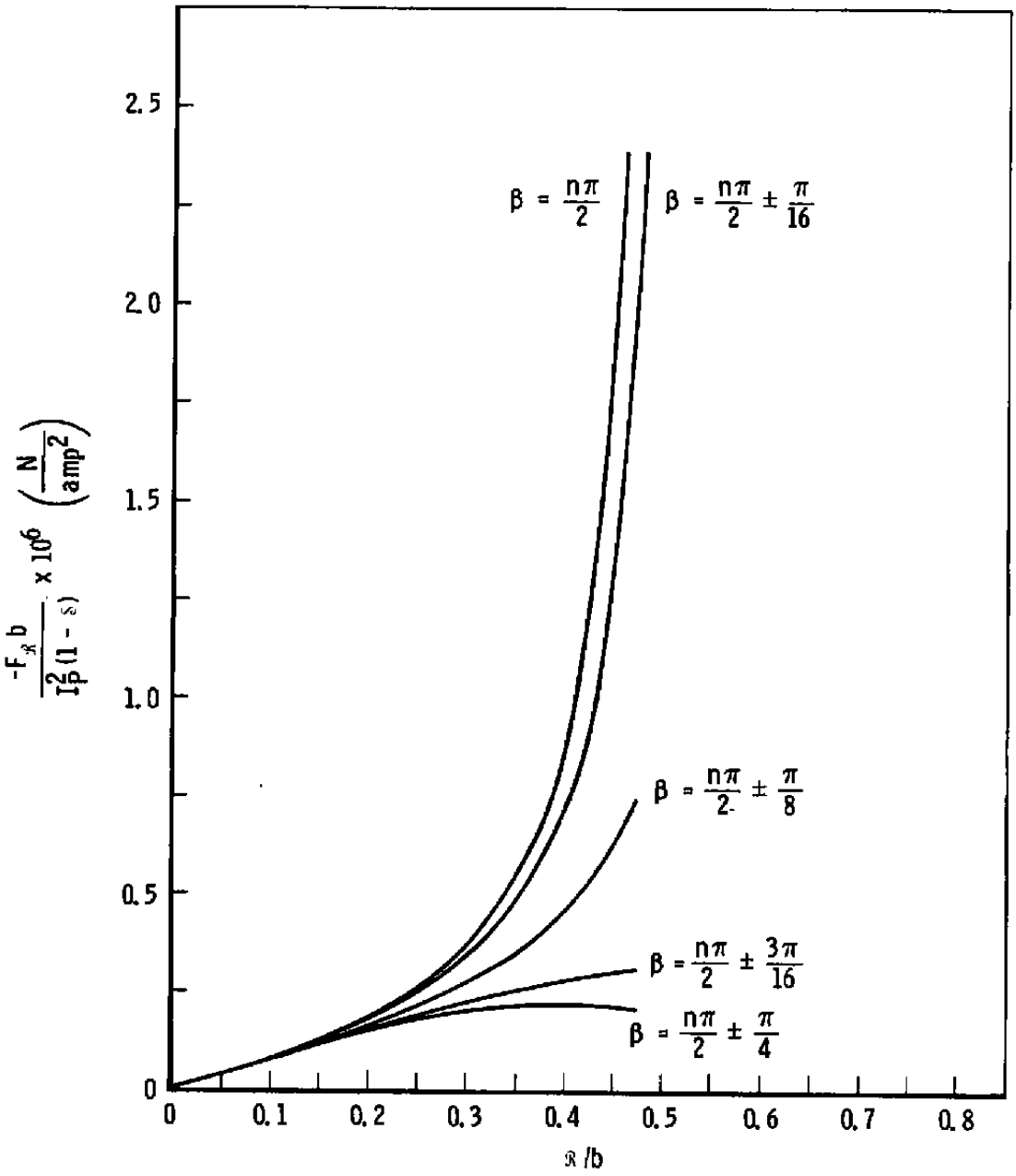

d. a/b = 0.5

Figure 12. Continued.

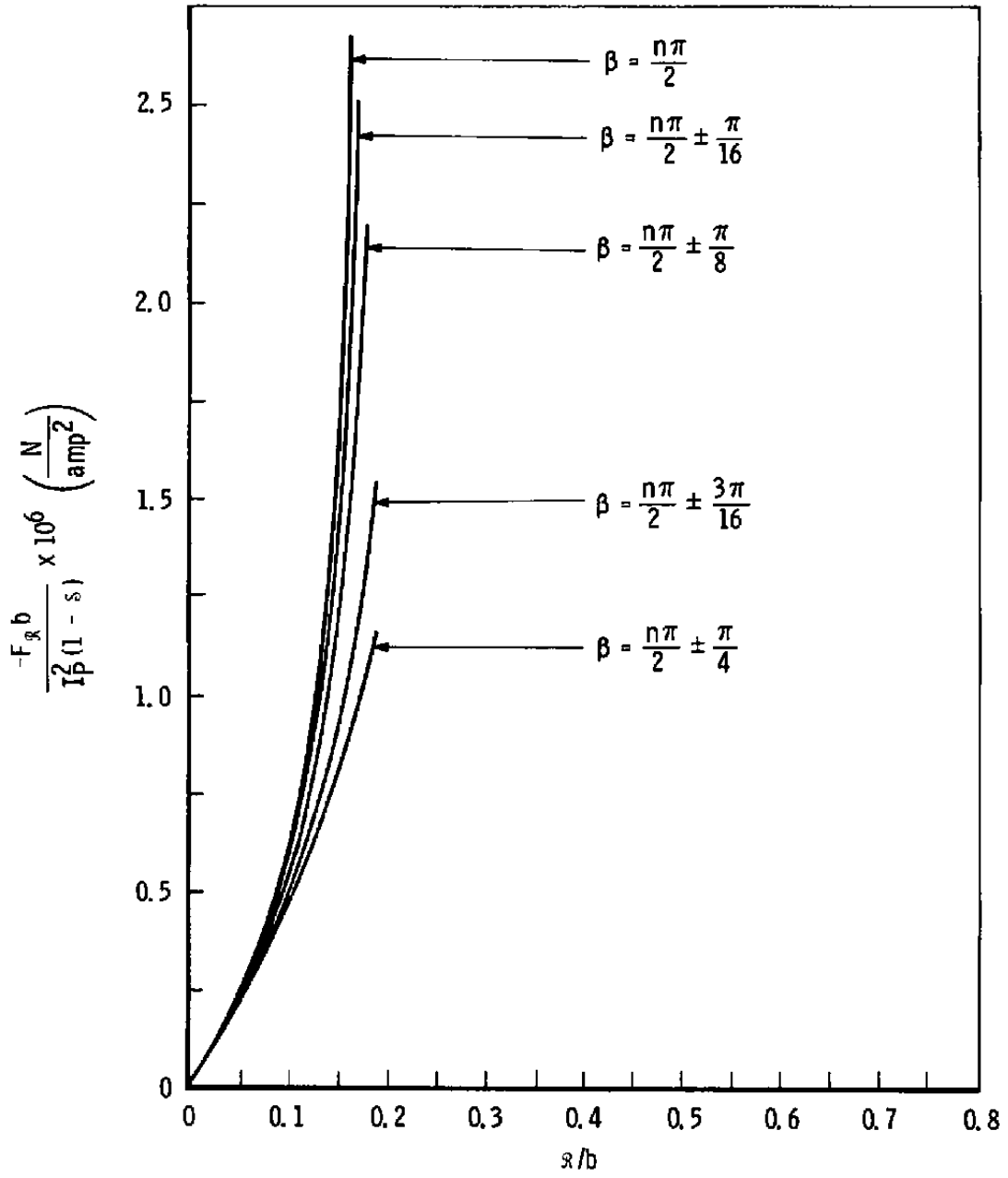

e. a/b = 0.8

Figure 12. Concluded.

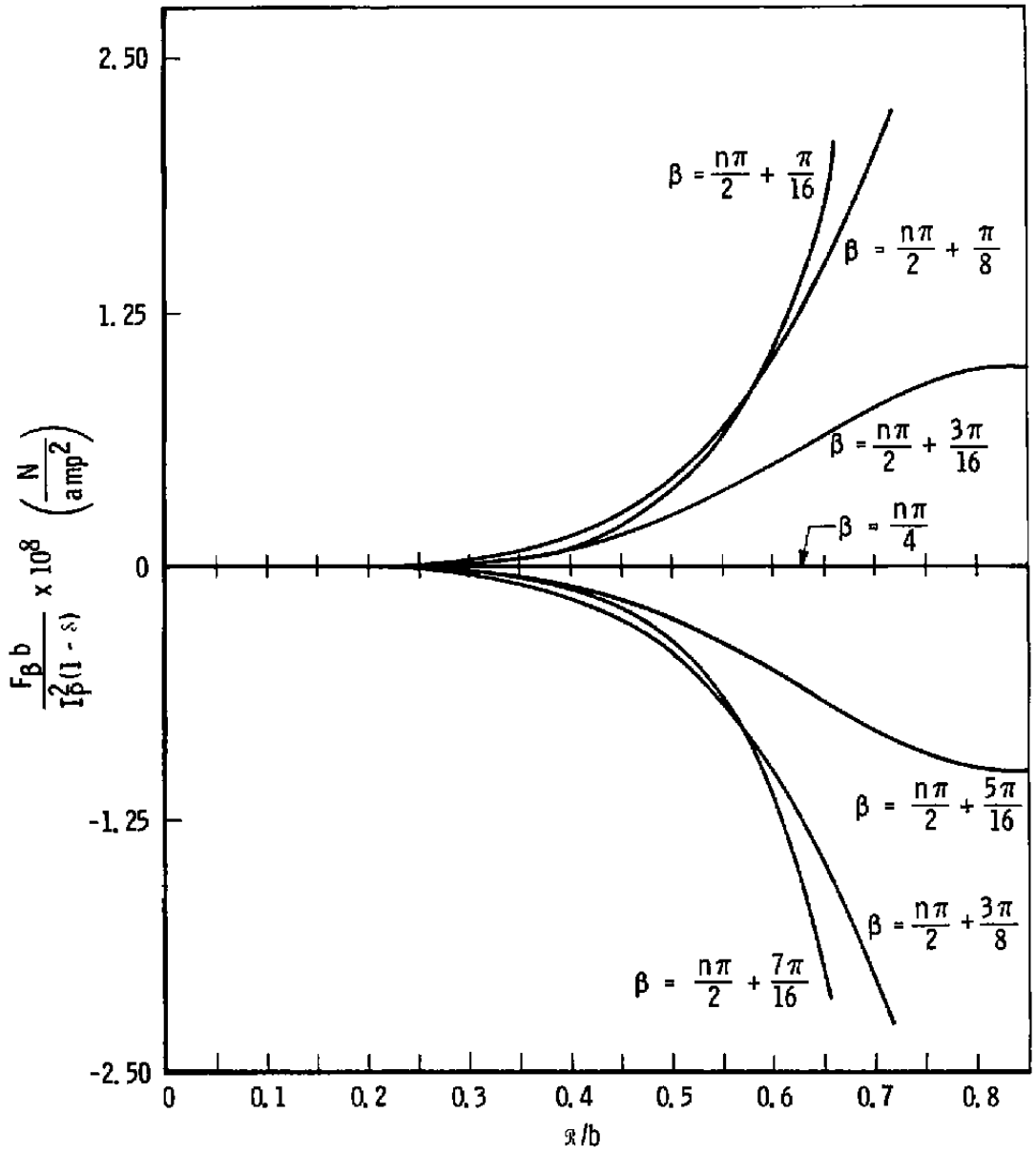

a. a/b = 0.1

Figure 13. Angular positional forces.

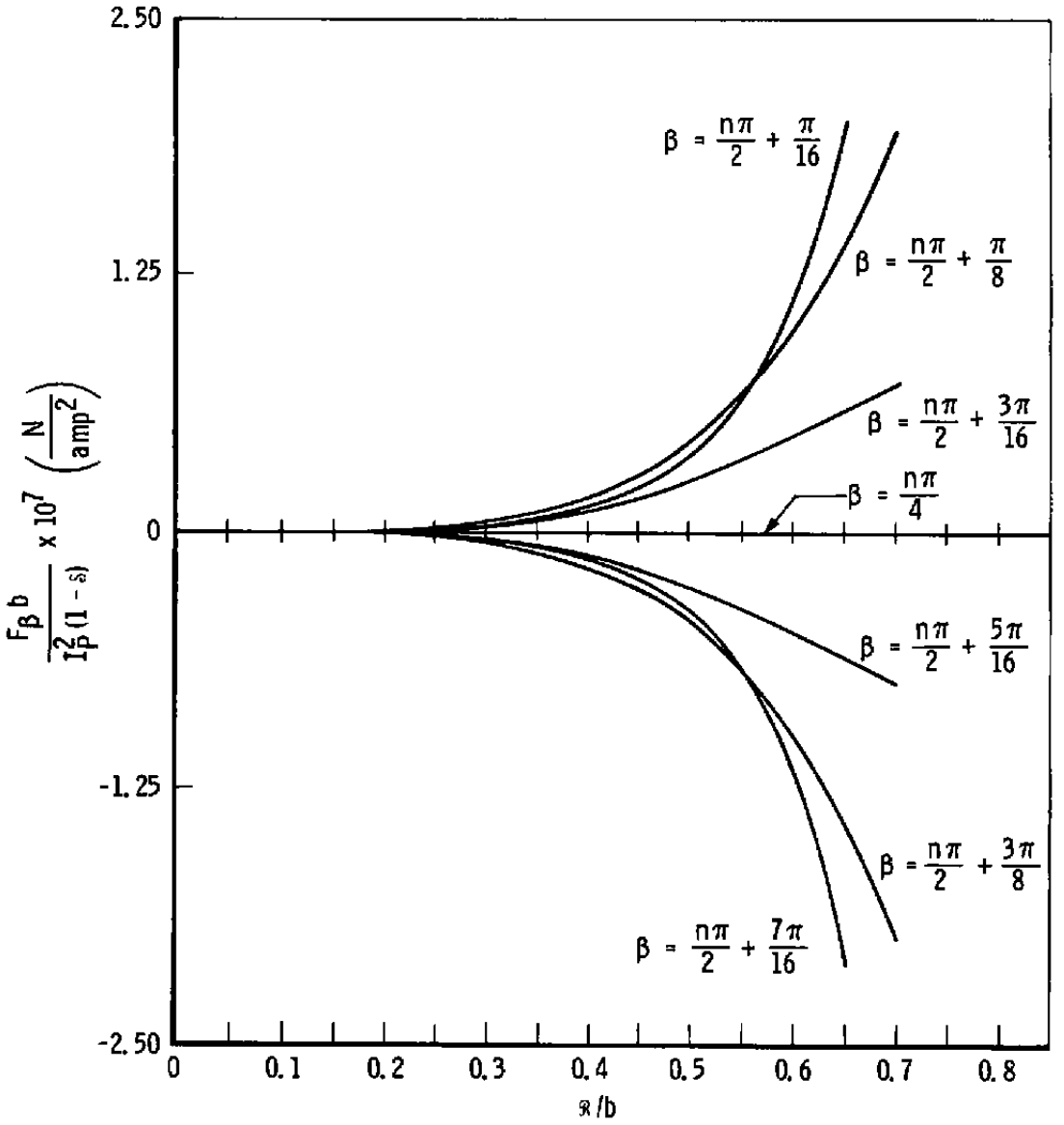

b. a/b = 0.2

Figure 13. Continued.

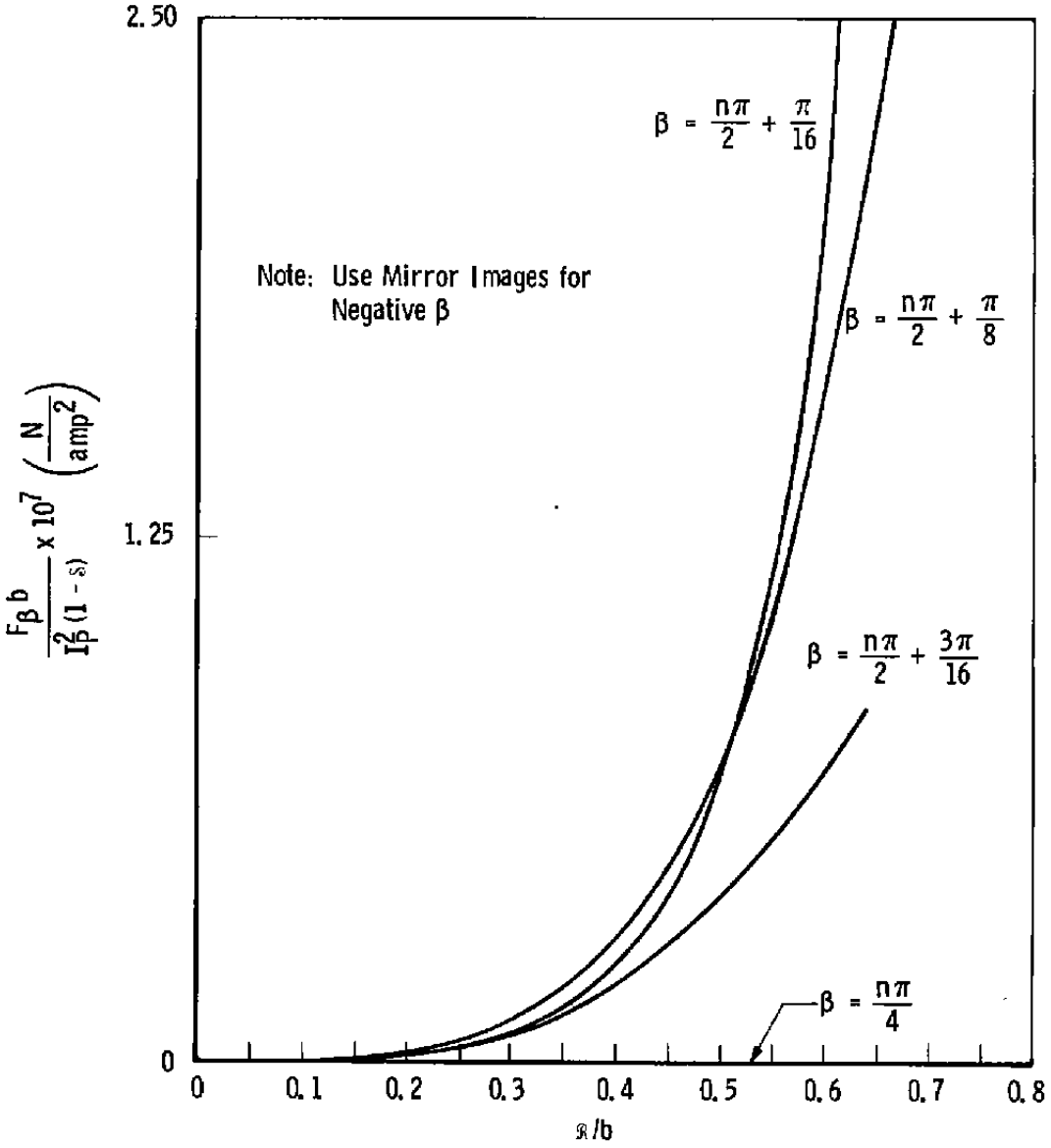

c. a/b = 0.3

Figure 13. Continued.

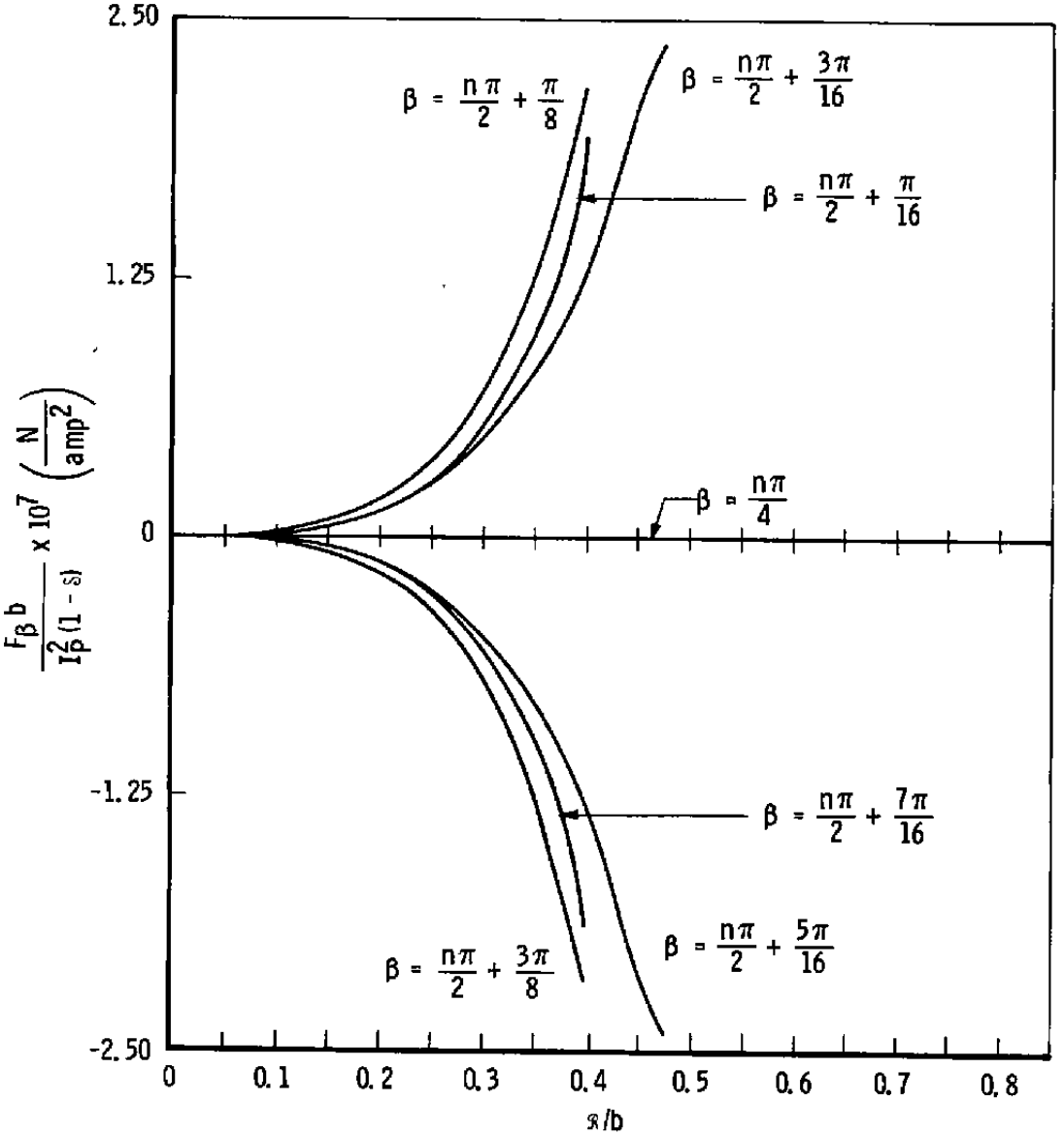

d. a/b = 0.5

Figure 13. Continued.

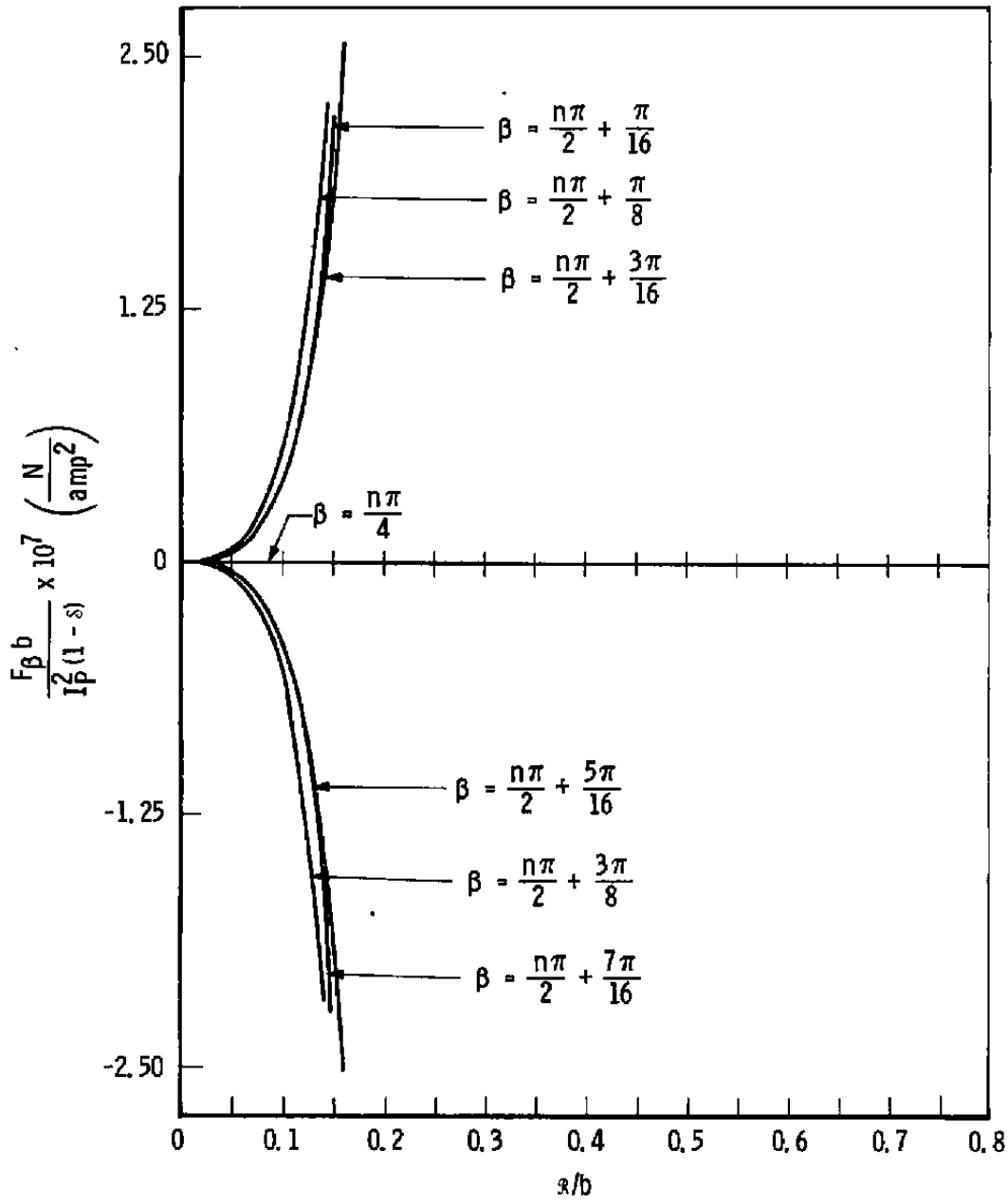

e. a/b = 0.8

Figure 13. Concluded.

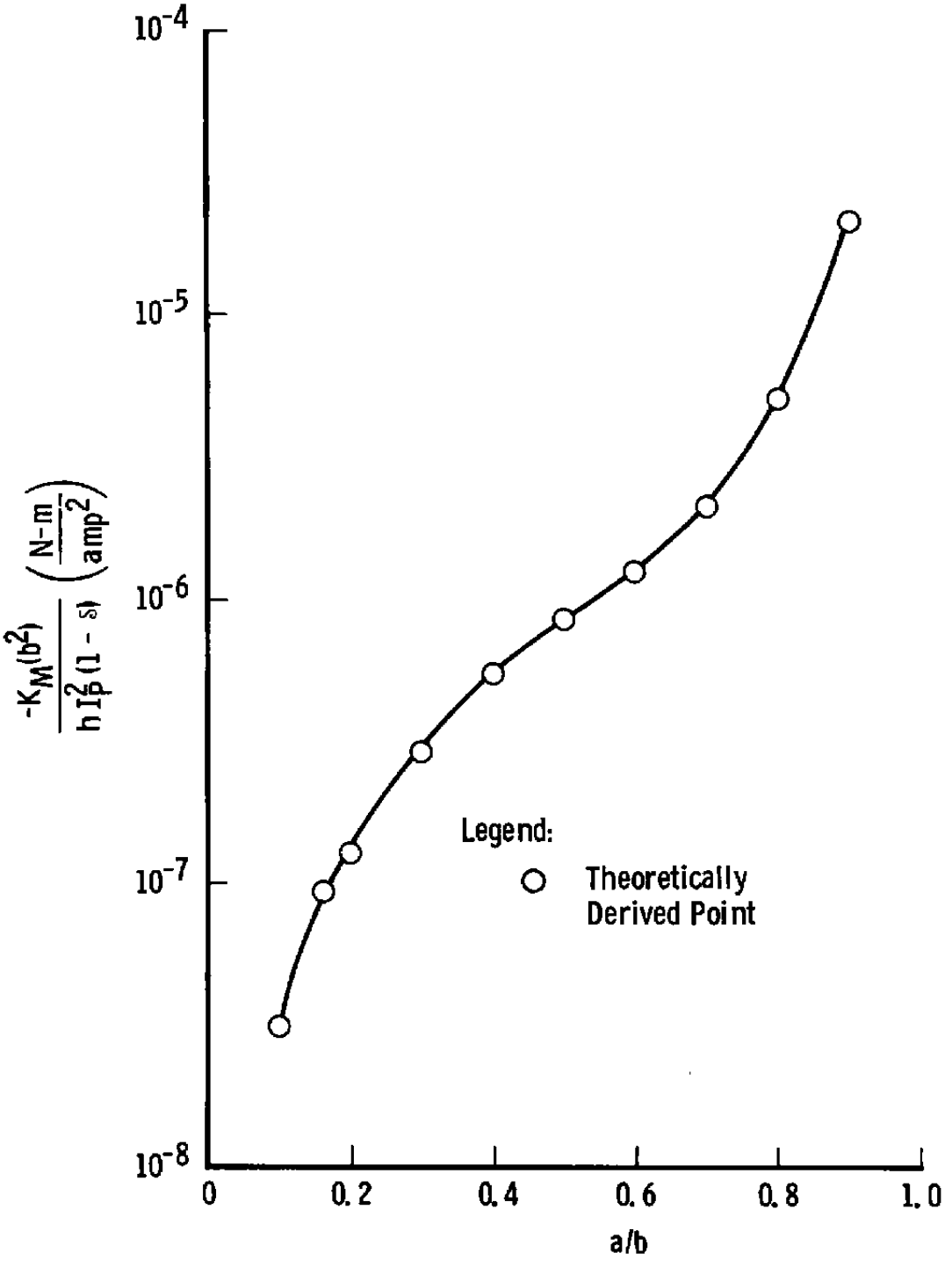

Figure 14. Magnetic positional force coefficients (summary).

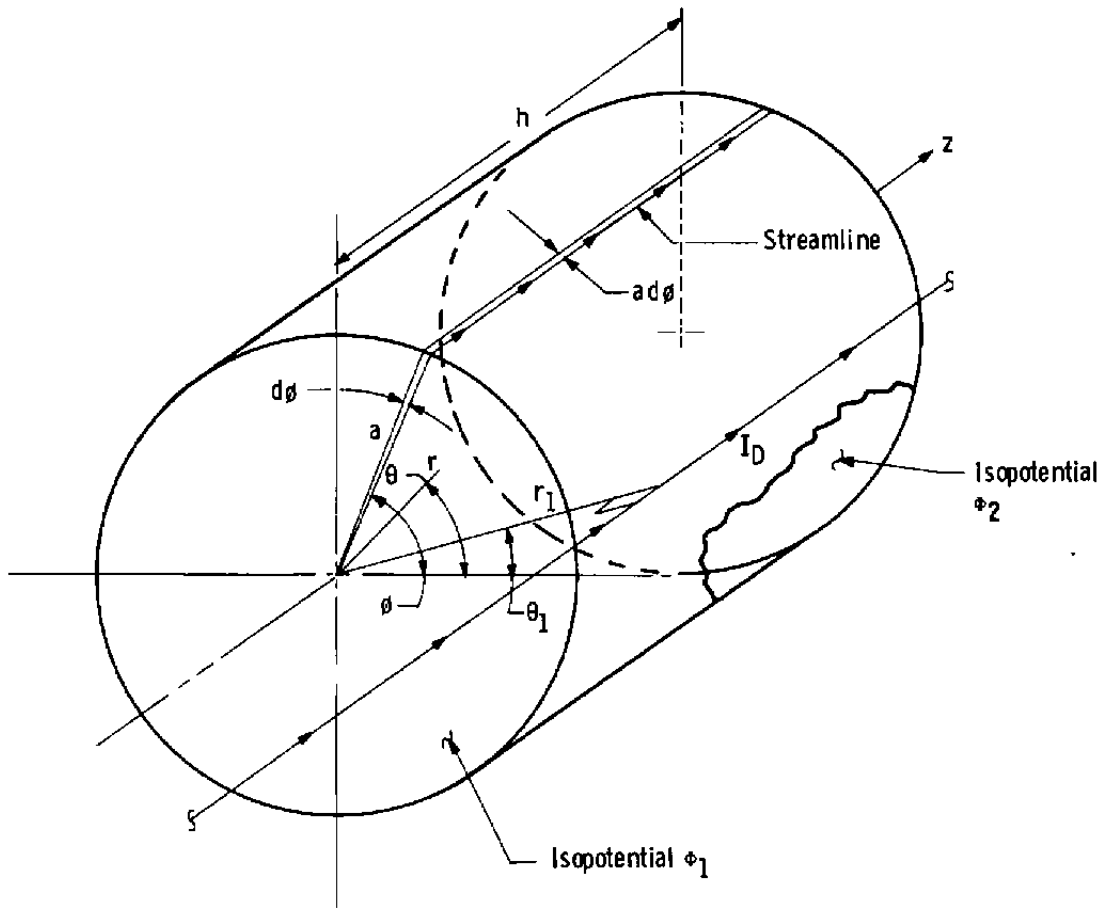

Figure 15. Cylindrical shell and line current.

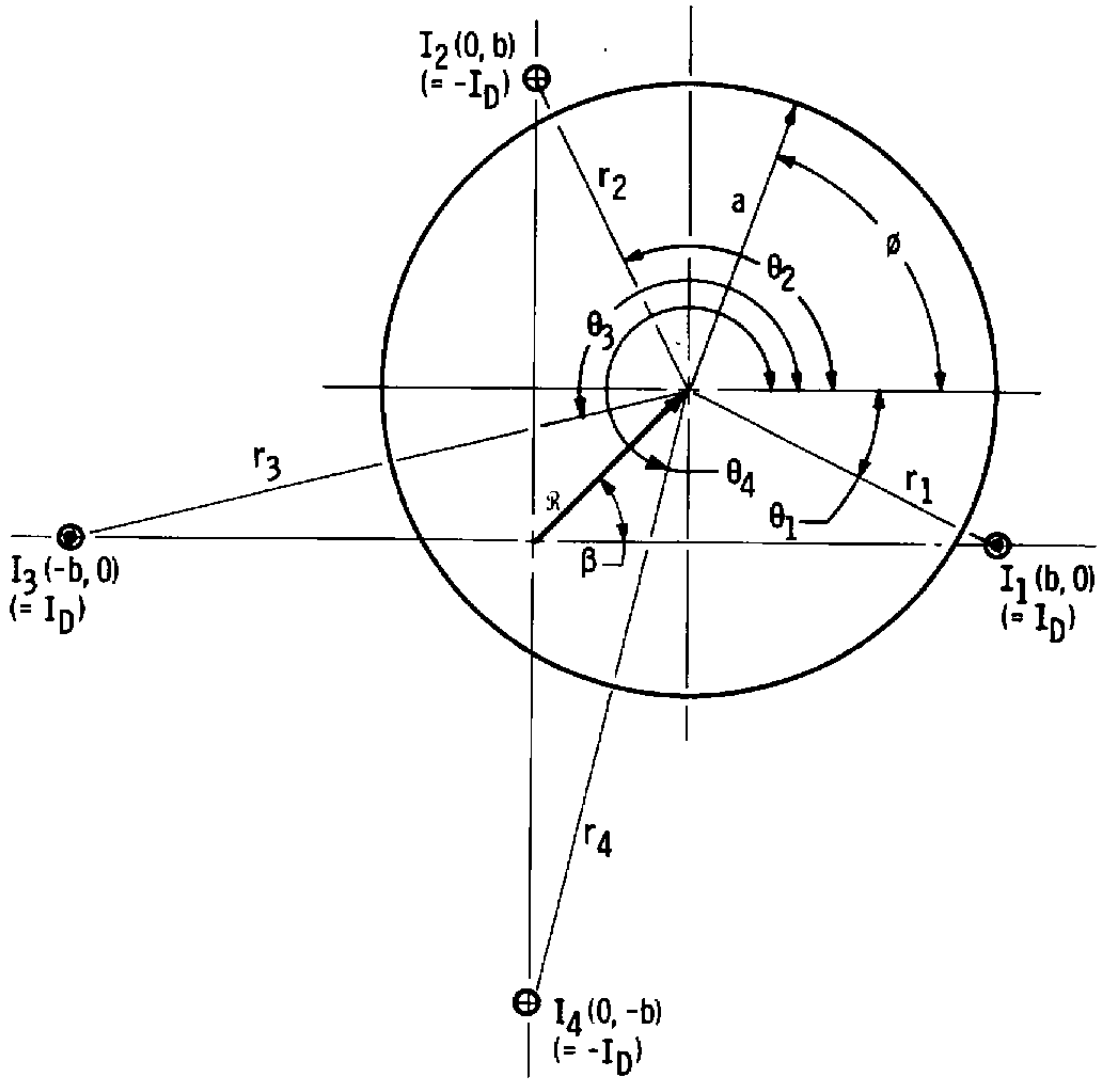

Figure 16. Nomenclature for determination of damping forces.

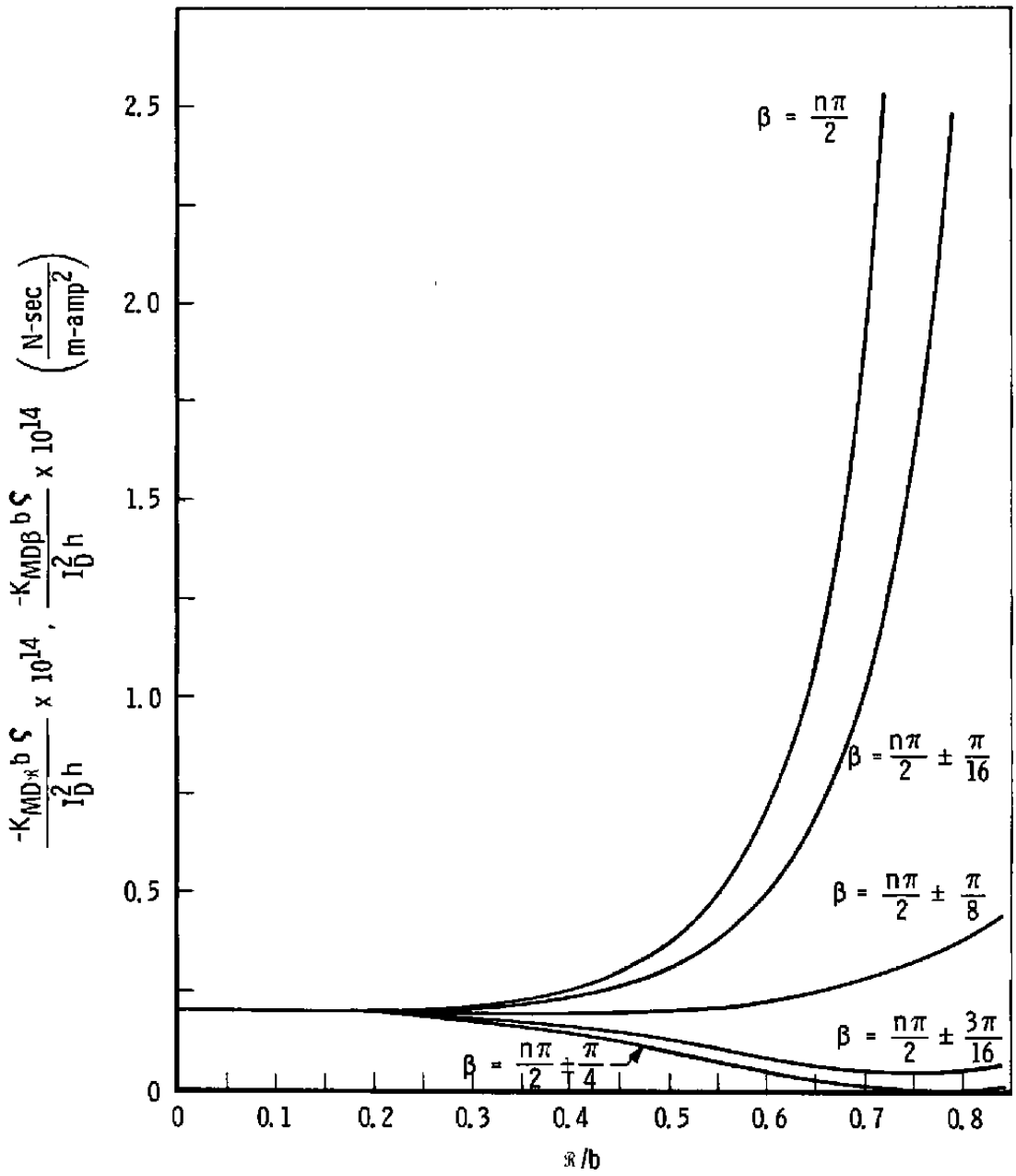

a. a/b = 0.1

Figure 17. Magnetic damping coefficients.

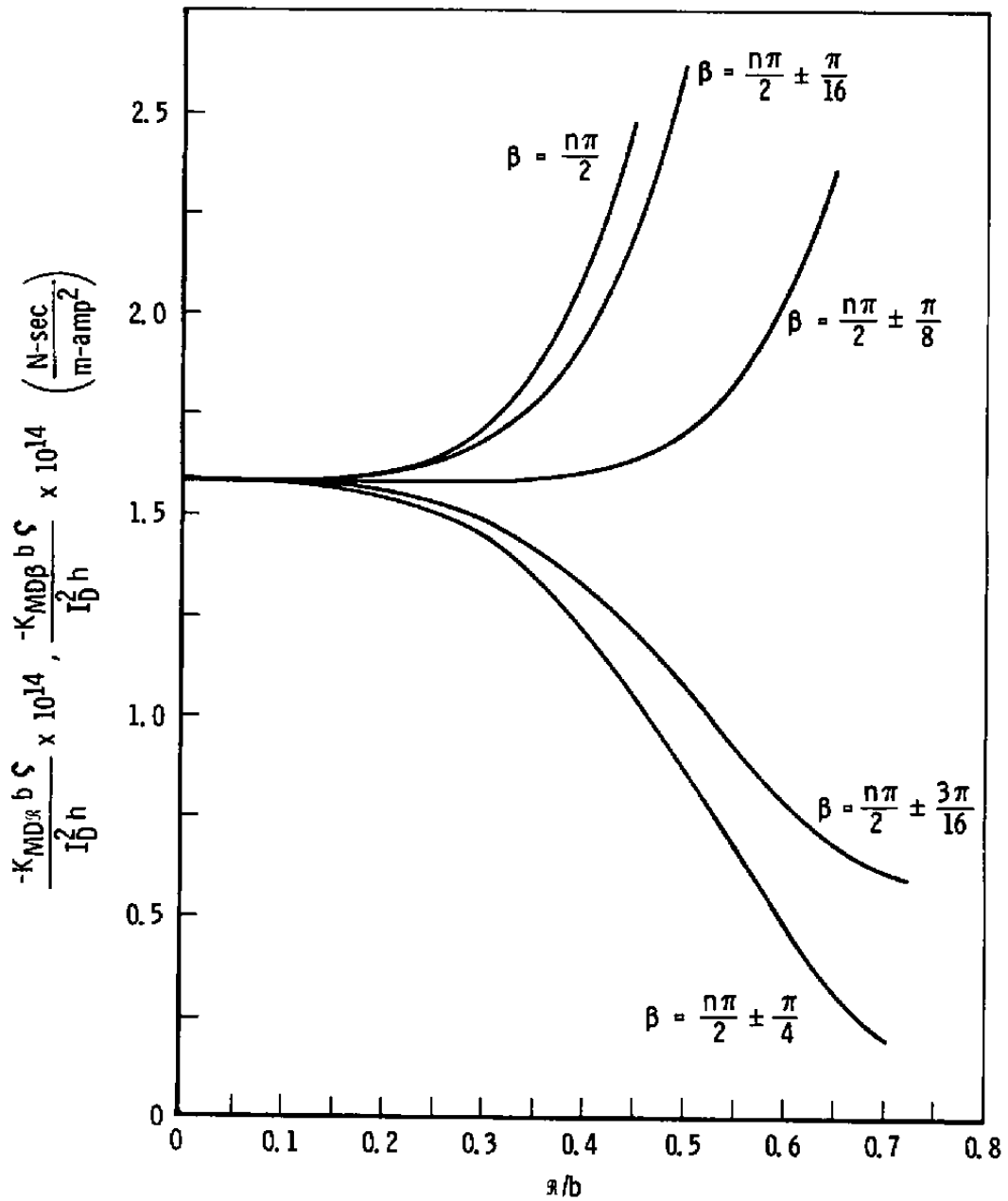

b. a/b = 0.2

Figure 17. Continued.

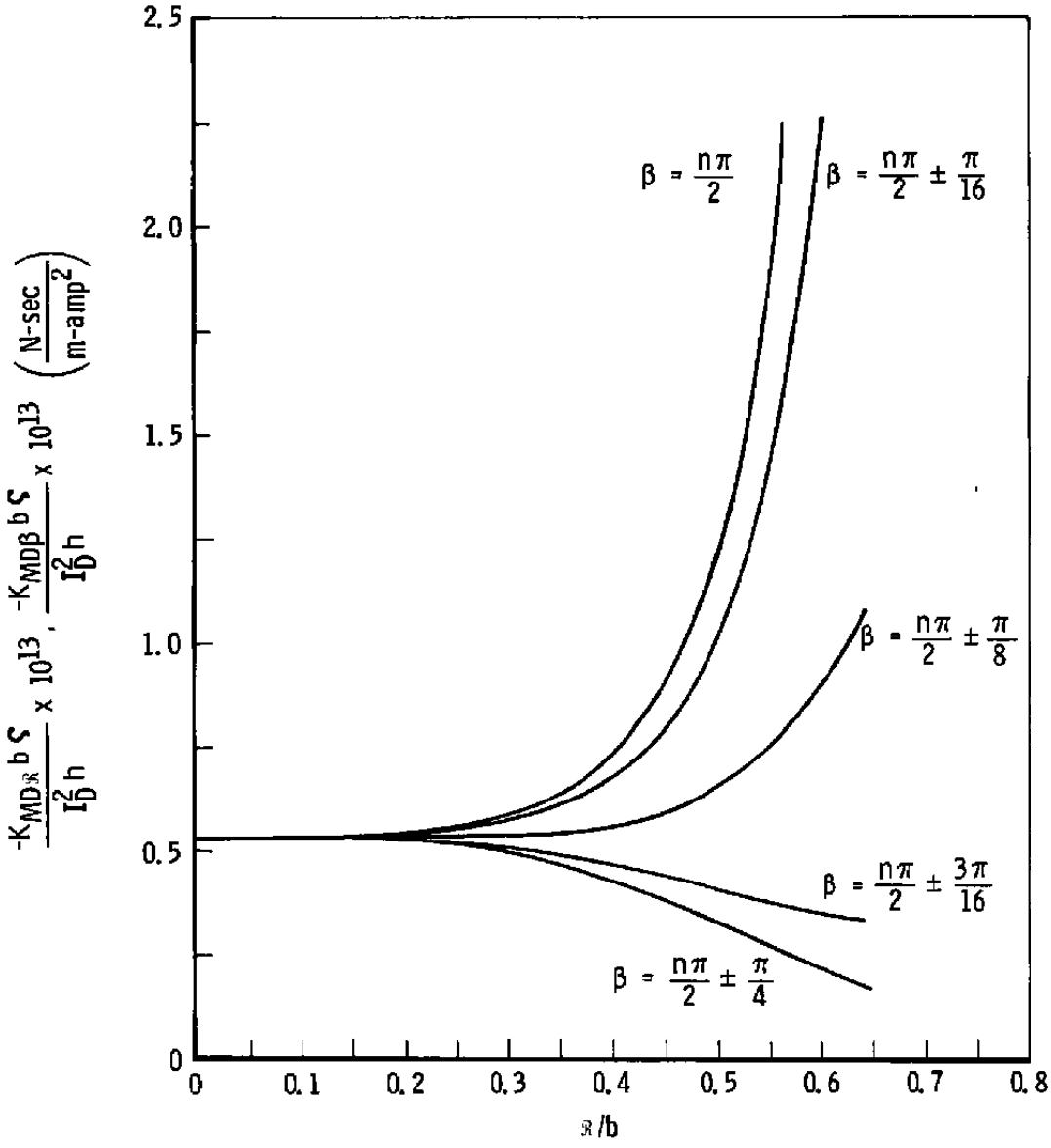

c. a/b = 0.3

Figure 17. Continued.

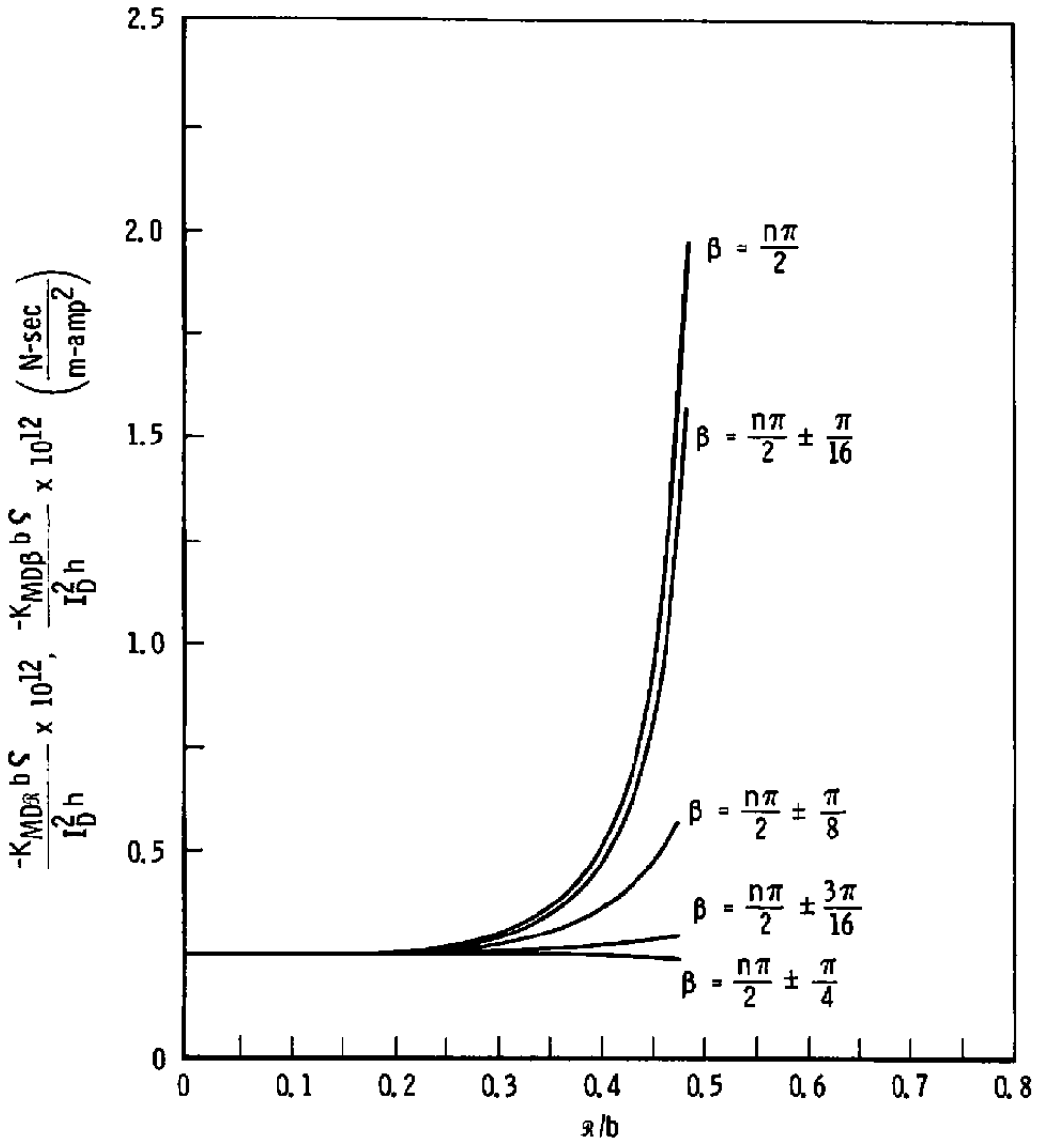

d. a/b = 0.5

Figure 17. Continued.

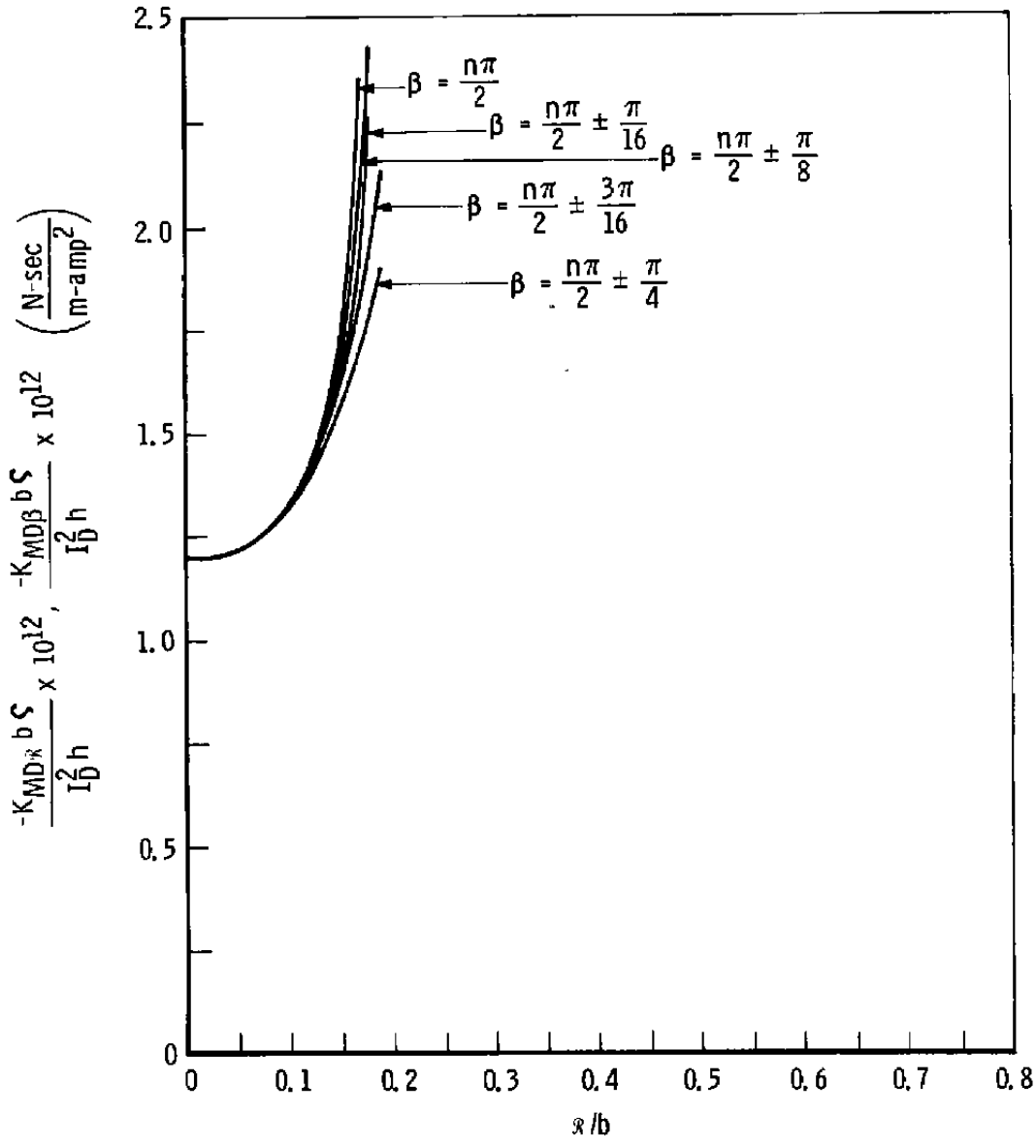

e. a/b = 0.8

Figure 17. Concluded.

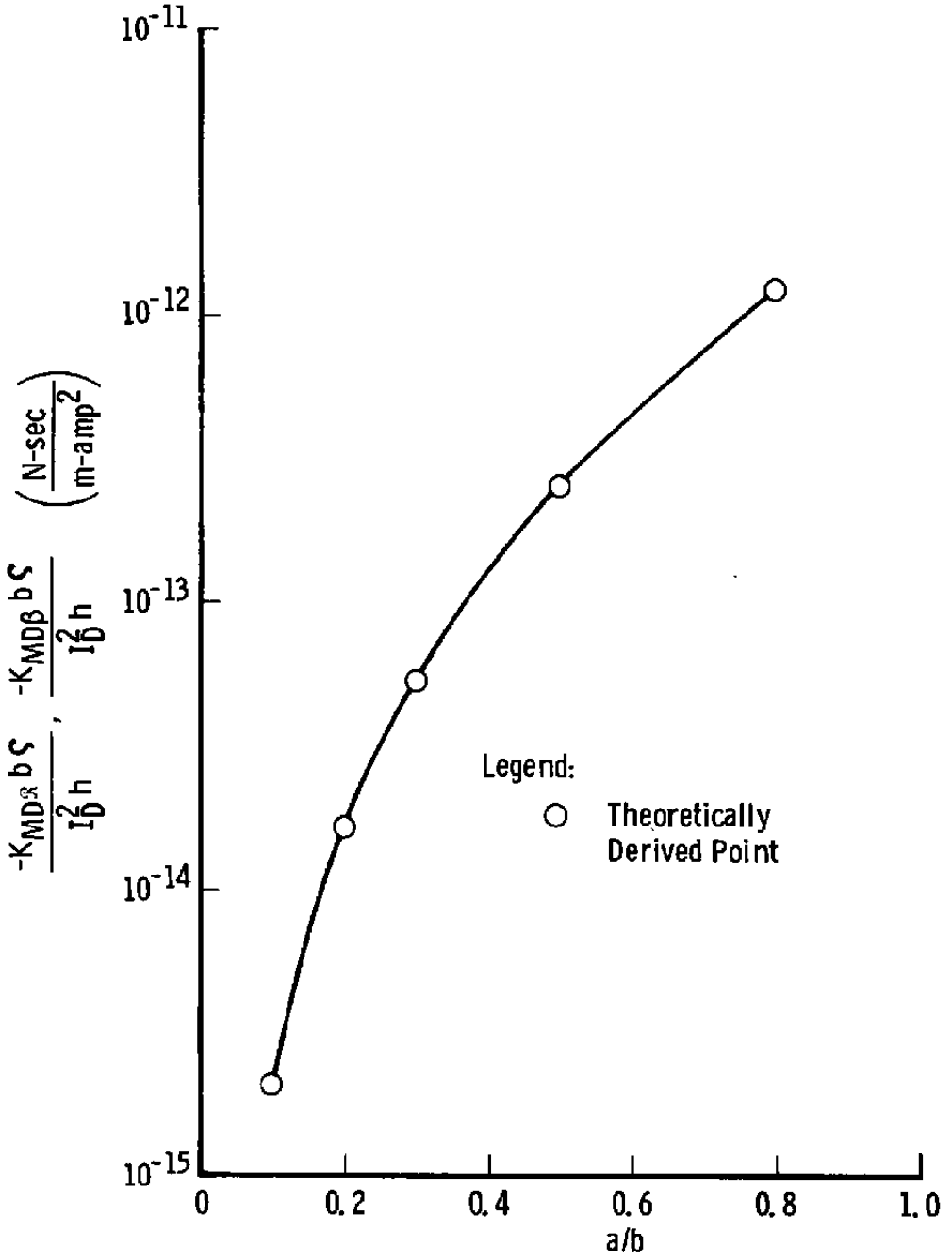

Figure 18. Magnetic damping coefficient (summary).

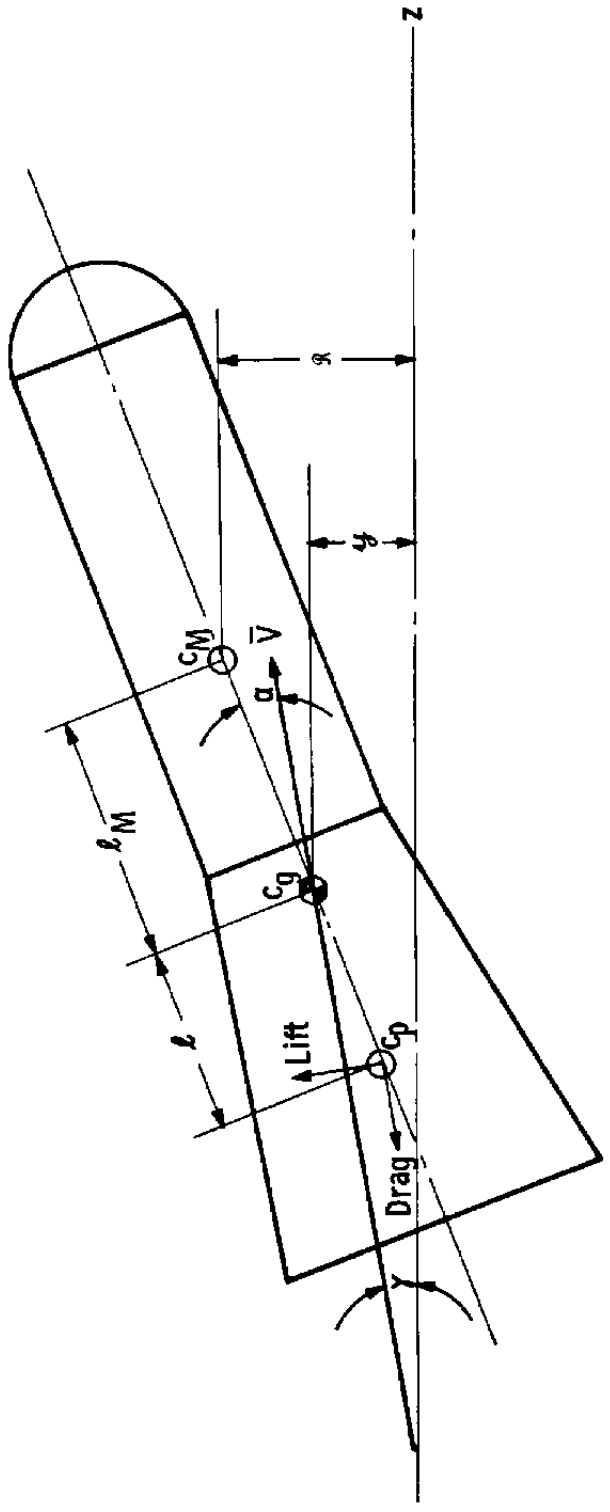

Figure 19. Flight nomenclature.

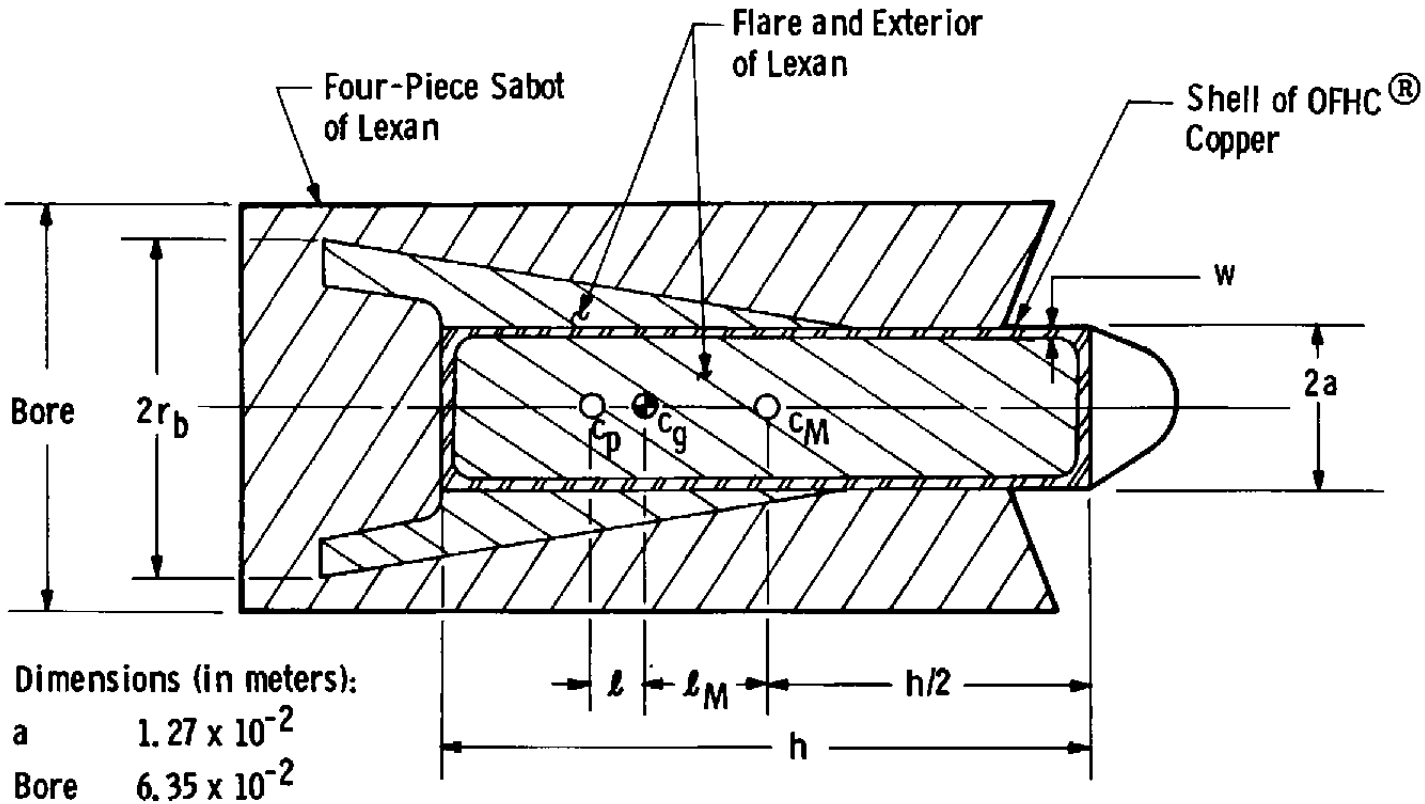

Dimensions (in meters):

a	1.27×10^{-2}
Bore	6.35×10^{-2}
h	1.016×10^{-1}
ℓ	9.525×10^{-3}
ℓ_M	1.905×10^{-2}
r_b	2.54×10^{-2}
w	See Text

Figure 20. Launch package.

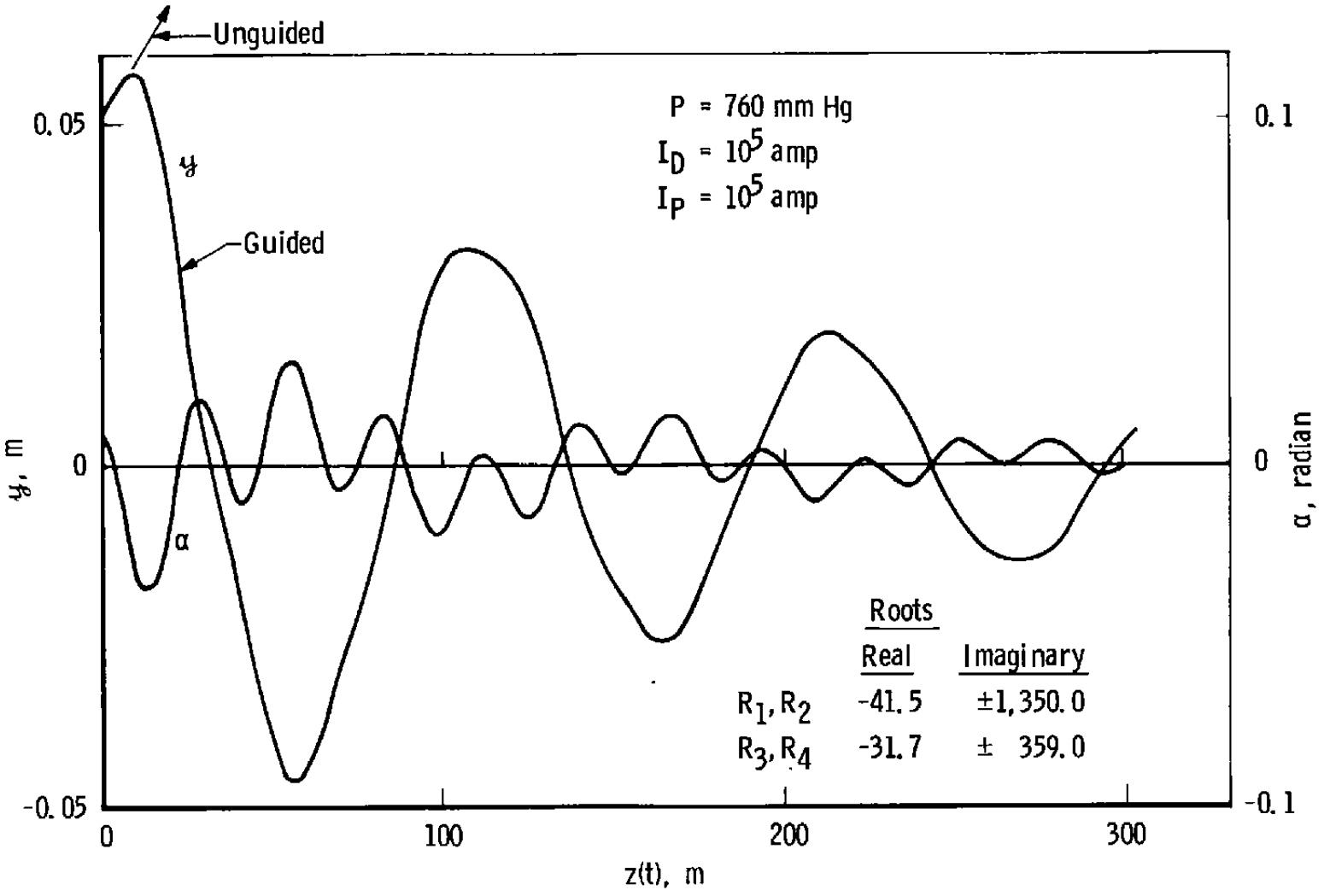

Figure 21. Computed flight path (6,000 m/sec, 1 atm).

AEDC-TR-76-149

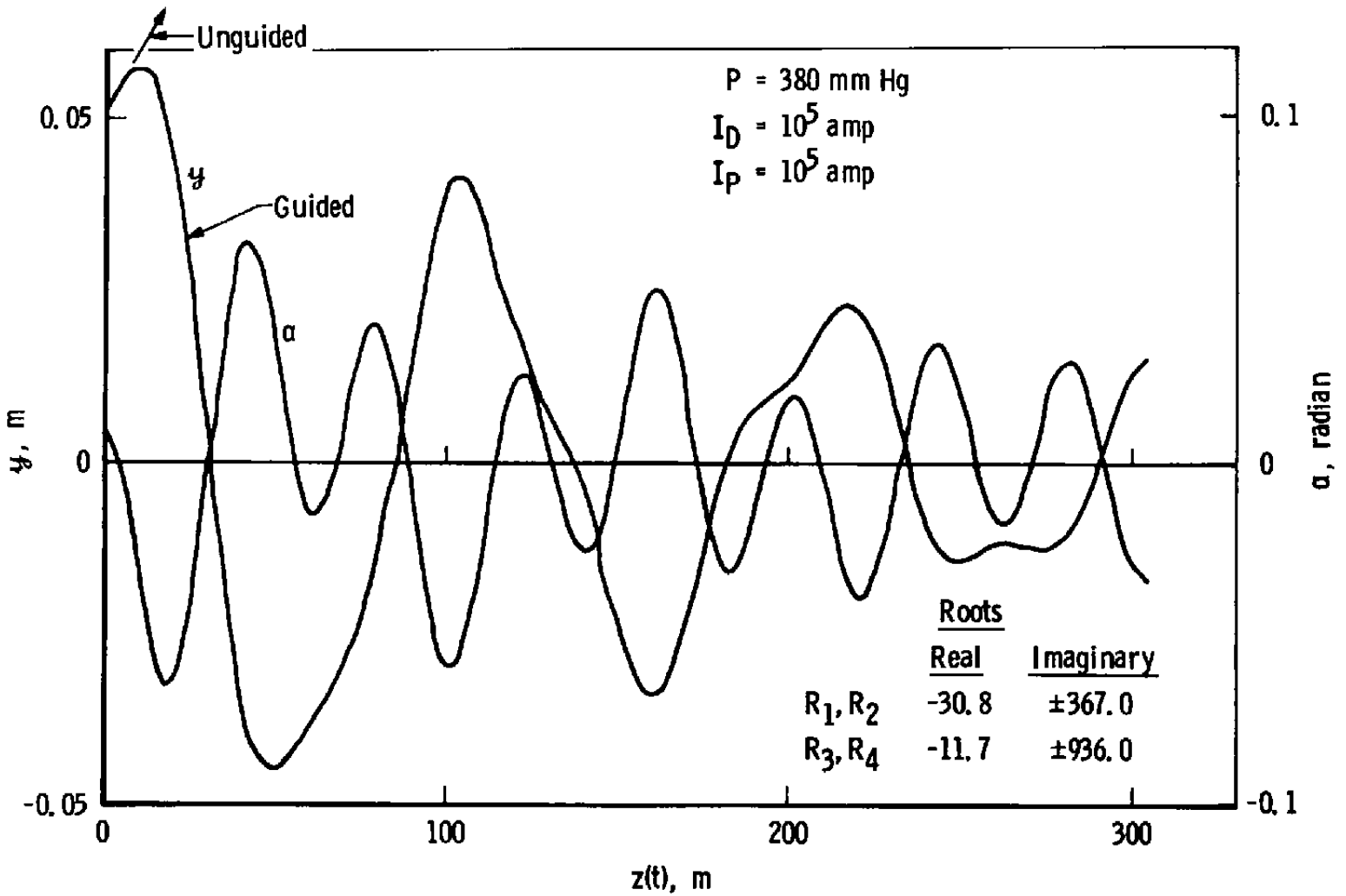

Figure 22. Computed flight path (6,000 m/sec, ½ atm).

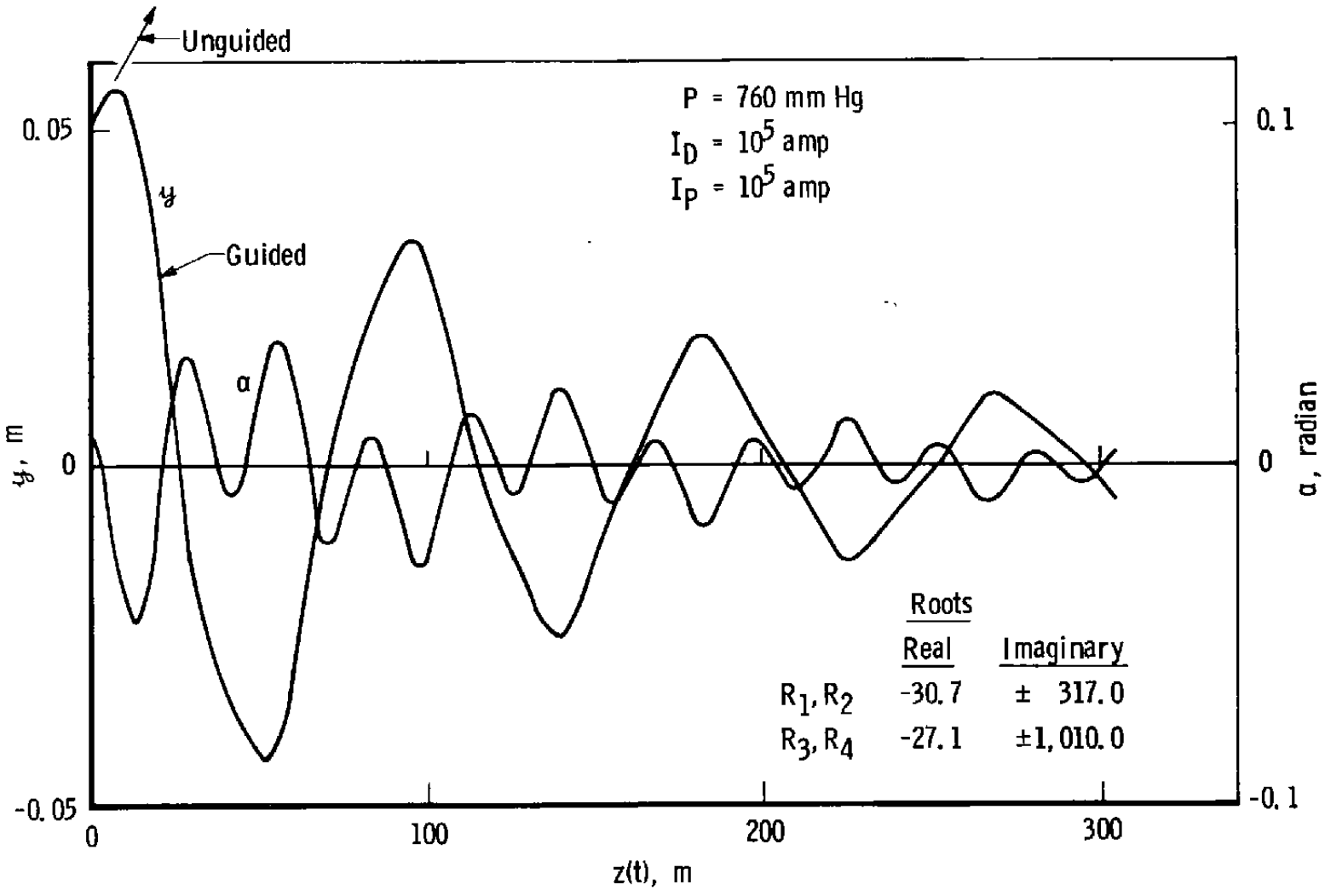

Figure 23. Computed flight path (4,500 m/sec, 1 atm).

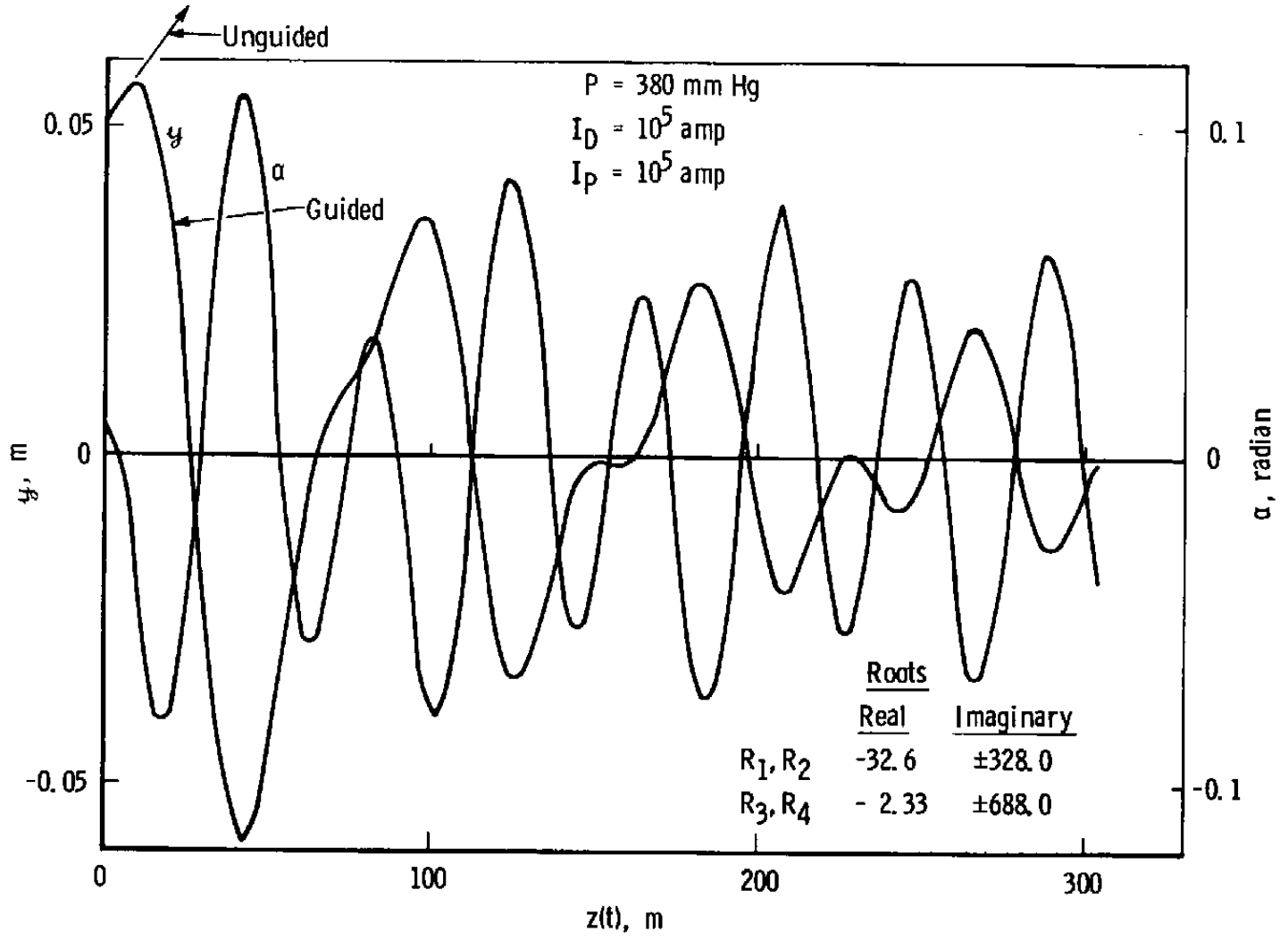

Figure 24. Computed flight path (4,500 m/sec, ½ atm).

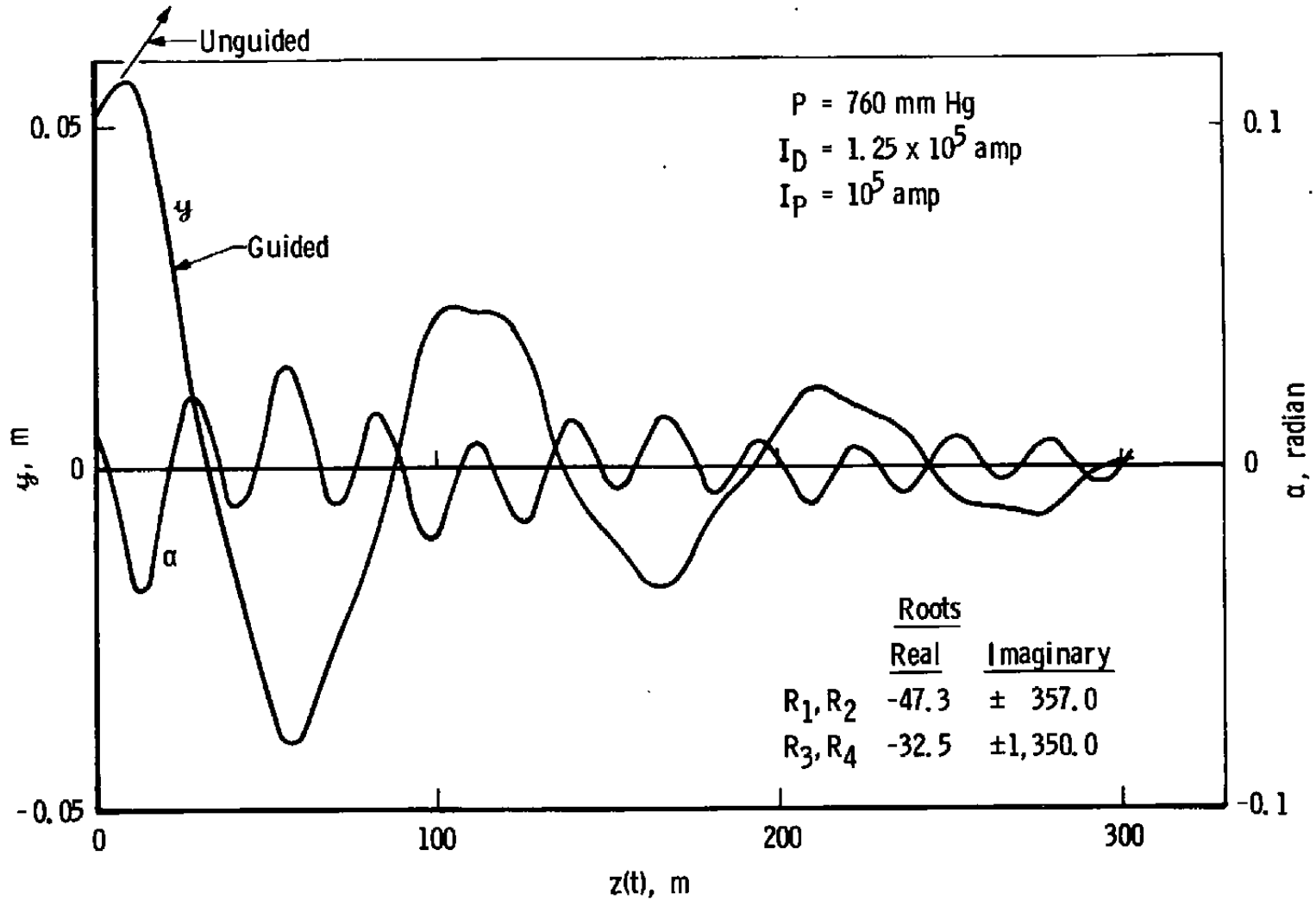

Figure 25. Computed flight path with increased I_D (6,000 m/sec, 1 atm).

AEDC-TR-76-149

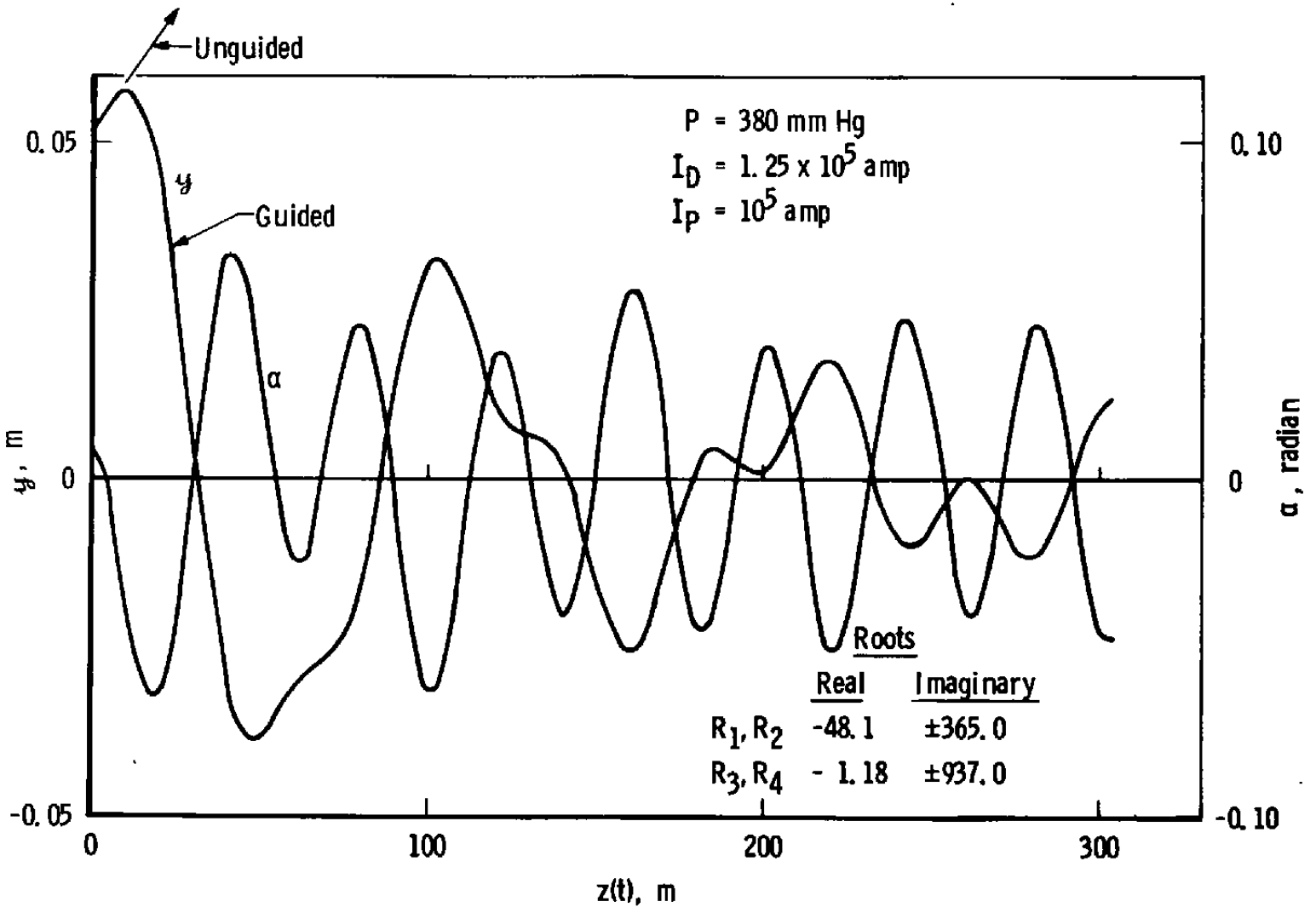

Figure 26. Computed flight path with increased I_D (6,000 m/sec, ½ atm).

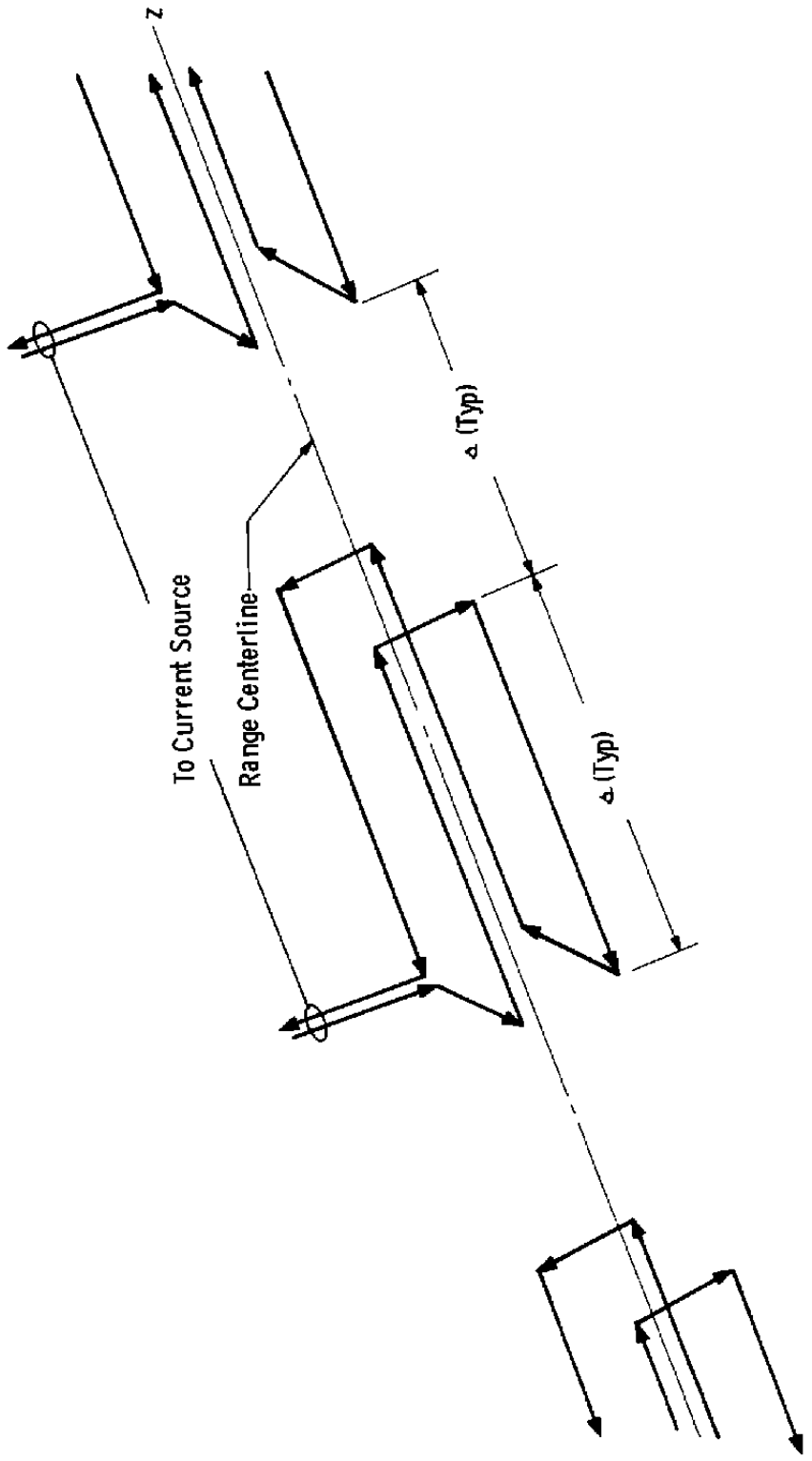

Figure 27. Alternate arrangement of guideway currents.

APPENDIX A
COMPUTER PROGRAMS

```
C  ********************************************************************
C  **                                                                **
C  **              PROGRAM FOR B-SEGMENTED/B-INFINITE                **
C  **                                                                **
C  ********************************************************************
C
C
C
C
C
C
C
C  M SPECIFIES THE NUMBER OF SEGMENTS CONSIDERED (SHOULD BE ODD)
C
      M=9
C
C  SEG IS THE LENGTH OF ONE SEGMENT
C
      SEG=2.0
      DO 1 L=1,5
      AL=L
C
C  B IS THE DISTANCE OF THE POINT OF INTEREST FROM THE Z-AXIS
C
      B=SEG/AL
C
C  THIS DO LOOP STEPS THE POINT OF INTEREST ALONG THE Z-AXIS
C
      DO 1 I=1,41
      E=I    -1
      S=(M-1)/2
C
C  Z IS THE Z-COMPONENT OF THE LOCATION OF THE POINT OF INTEREST
C
      Z=(S+.05*E)*SEG
      RATIO=0.0
      DO 2 N=1,M
      A=N
      C=Z- A*SEG
      D=Z-(A-1.0)*SEG
      R=.5*(-1.)**N*(C/SQRT   (C**2+B**2)-  D/SQRT  (D**2+B**2))
2     RATIO=RATIO + R
      WRITE(6,10)M,SEG,B,Z,RATIO
1     CONTINUE
10    FORMAT(1H0,3HM =,I3   /1H ,16HSEGMENT LENGTH =,E10.4/1H ,3HB =,
     1E10.4/1H ,3HZ =,E10.4/1H ,24HB-SEGMENTED/B-INFINITE =,E15.6)
      STOP
      END
/*
```

```
C  ********************************************************************
C  **                                                                **
C  **                  PROGRAM FOR POSITIONAL FORCES                 **
C  **                                                                **
C  ********************************************************************
C
C
C
C
C
C
      DIMENSION X(4),Y(4),R(4),XC(4),YC(4),A(4),RDX(4),ADX(4),DERVX(4),
     1RDY(4),ADY(4),DERVY(4),FPIX(4),FPIY(4)   ,DANGLE(100),BIGR(100)   ,
     2BX(4),BY(4),SMRSQD(4)
      PI=3.1415926535
      DANGLE(1)=-PI/16.
      BIGR(1)=-.05*.0254
      ARAD=0.2*.0254
      BRAD=1.0*.0254
C
C  (XC(N),YC(N)) INDICATES POSITION OF NTH LINE CURRENT
C  BRAD(BORE RADIUS), ARAD(MODEL RADIUS)
C
      PRINT 25, BRAD , ARAD
   25 FORMAT('0       BORE RADIUS ', E20.12, '  MODEL RADIUS ',E20.12)
      XC(1)=BRAD
      XC(2)=0.0
      XC(3)=-BRAD
      XC(4)=0.0
      YC(1)=0.0
      YC(2)=BRAD
      YC(3)=0.0
      YC(4)=-BRAD
      DO 500 L=2,3
      DO 500 K=2,14
      BIGR(K)=BIGR(K-1)+.05*.0254
      DANGLE(L)=DANGLE(L-1)+PI/16.
C
C  S(BETA) DEFINES THE MODEL POSITION
C  (X(N),Y(N)) INDICATES POSITION OF NTH IMAGE CURRENT
C
      S=BIGR(K)
      BETA=DANGLE(L)
      B=S**2-2.*S*BRAD*COS(BETA)+BRAD**2
      X(1)=S*COS(BETA)+(ARAD**2*(BRAD-S*COS (BETA)))/B
      Y(1)=S*SIN(BETA)-(ARAD**2*S*SIN(BETA))/B
      C=S**2+BRAD**2-2.*S*BRAD*SIN(BETA)
      X(2)=S*COS(BETA)-(ARAD**2*S*COS(BETA))/C
C
C
C                        (PROGRAM CONTINUED ON NEXT PAGE)
```

```
      Y(2)=S*SIN(BETA)+(ARAD**2*(BRAD-S*SIN(BETA)))/C
      D=S**2+BRAD**2+2.*S*BRAD*COS(BETA)
      X(3)=S*COS(BETA)-(ARAD**2*(BRAD+S*COS(BETA)))/D
      Y(3)=S*SIN(BETA)-(ARAD**2*S*SIN(BETA))/D
      E=S**2+BRAD**2+2.*S*BRAD*SIN(BETA)
      X(4)=S*COS(BETA)-(ARAD**2*S*COS(BETA))/E
      Y(4)=S*SIN(BETA)-(ARAD**2*(BRAD+S*SIN(BETA)))/E
C
C  M IS THE NUMBER OF LINE CURRENTS PRESENT (E.G. 4 IN THE CASE OF A
C  QUADRUPOLE FIELD)
C
      M=4
      DO 10 J=1,M
      DO 1 I=1,M
      SMRSQD(I)=(XC(J)-X(I ))**2+(YC(J)-Y(I))**2
      BX(I)=(-1.)**(I-1)*(YC(J)-Y(I))/SMRSQD(I)  *2.E-7
    1 BY(I)=(-1.)**(I-1)*(XC(J)-X(I))/SMRSQD(I)  *2.E-7
      IF(M-1) 200,200,300
C
C  BX(N)--X COMPONENT OF H PER I
C  BY(N)--Y COMPONENT OF H PER I
C
  300 DO 2 I=2,M
      BX(I)=BX(I)+BX(I-1)
    2 BY(I)=BY(I)+BY(I-1)
  200 CONTINUE
      FPIX(J)= BY(M)  *(-1.)**(J+1)
   10 FPIY(J)=BX(M )  *(-1.)**(J+1)
      IF(M-1) 51,51,50
C
C  FPIXT IS THE X COMPONENT OF FORCE PER I SQUARED FOR A 1 METER LONG MODEL
C  FPIYT IS THE Y COMPONENT OF FORCE PER I SQUARED FOR A 1 METER LONG MODEL
C
   51 FPIXT=-FPIX(1)
      FPIYT=-FPIY(1)
      GO TO 52
   50 FPIXT=-FPIX(1)-FPIX(2)-FPIX(3)-FPIX(4)
      FPIYT=-FPIY(1)-FPIY(2)-FPIY(3)-FPIY(4)
   52 CONTINUE
      FR=FPIXT*COS(BETA)+FPIYT*SIN(BETA)
      FBETA=-FPIXT*SIN(BETA)+FPIYT*COS(BETA)
      PRINT 100, S, BETA, FPIXT, FPIYT, FR, FBETA
  100 FORMAT(1H0,1HR,1X,E10.4,2X,4HBETA,1X,E10.4,2X,2HFX,E10.4,2X,
     22HFY,E10.4,2X,2HFR  ,1X,E10.4,2X,5HFBETA,1X,E10.4)
  500 CONTINUE
      STOP
      END
/*
```

```
C  ********************************************************************
C  **                                                                **
C  **                  PROGRAM FOR DAMPING CONSTANTS                 **
C  **                                                                **
C  ********************************************************************
C
C
C
C
C
C
      DIMENSION _DONT(4),DONUT(4),ANGLE(4),SMLR(4),THETA(4),BANGLE(4),
     2          A(4,365),B(4,365),  C(4),D(4),E(4),EC(4),F(4),G(4,365),
     3H(4,365),GT(365),HT(365),SQIR(365),BIGR(99),PWRR(365),PWRB(365),
     4SQIB(365),DANGLE(40),PHI(365)   ,DOT(4),SSRSQD(4)
      PI=3.1415926535
C
C  ARAD IS THE MODEL RADIUS, BRAD IS THE GUIDEWAY BORE RADIUS
C  S(=BIGR) AND BETA(=DANGLE) DEFINES THE MODEL POSITION
C  M INDICATES THE NUMBER OF LINE CURRENTS PRESENT
C
      BRAD=3.5355*.0254
      ARAD=(0.5-(.049/2.))*.0254
      PRINT 35, ARAD,BRAD
   35 FORMAT ('0        MODEL RADIUS ', E20.12, '  BORE RADIUS ', E20.12)
      BIGR(1)=-(BRAD/10.)
      DANGLE(1)=-PI/16.
      DO 500 J=2,8
      DO 500 K=2,10
      BIGR(K)=BIGR(K-1)-BIGR(1)
      DANGLE(J)=DANGLE(J-1)+PI/16.
      S=BIGR(K)
      BETA=DANGLE(J)
      M=4
C
C SIMPSON INTEGRATION--N BEING THE NUMBER OF INTERVALS
C
      DO 1 N=1,360
      IF (N-1) 50,50,51
   50 PHI(1)=0.
      GO TO 52
   51 PHI(N)=PHI(N-1)+2.*PI/360.
   52 CONTINUE
    1 CONTINUE
      DO 55 N=1,360
      DO 2 I=1,M
      DOT(I)=I-1
      DONT(I)=DOT(I)/2.
C
C
C                        (PROGRAM CONTINUED ON NEXT PAGE)
```

```
      DONUT(I)=DONT(I )*PI
      ANGLE(I)=DONUT(I)-BETA
      SMLR(I)=SQRT(BRAD**2 +S**2-2.*S*BRAD*COS(ANGLE(I)))
      THETA(I)=DONUT(I)+ASIN(S/SMLR(I)*SIN(ANGLE(I)))
      BANGLE(I)=    (PHI(N)-THETA(I))
      SSRSQD(I)=ARAD**2+SMLR(I)**2  -2.*ARAD*SMLR(I)*COS(BANGLE(I))
      A(I,N)=2.E-7*(ARAD*SMLR(I)*COS(BANGLE(I))-ARAD**2)/
     2(SMLR(I)*SSRSQD(I))
      B(I,N)= -2.E-7*(ARAD*SIN(BANGLE(I)) *SMLR(I) /SSRSQD(I))
      C(I)=(S-BRAD*COS(ANGLE(I)))/SMLR(I)
      D(I)=-BRAD*SIN(ANGLE(I)) /SMLR(I)
      EC(I)=1./SQRT(SMLR(I)**2-S**2*SIN(ANGLE(I))**2)
      E(I)=EC(I)*(SIN(ANGLE(I))          -S*SIN(ANGLE(I))*(S-BRAD*
     2COS(ANGLE(I))) /SMLR(I)**2)
      F(I)=-EC(I)*(  COS(ANGLE(I))          -S*BRAD*SIN(ANGLE(I))**2
     2/SMLR(I)**2)
      G(I,N)=A(I,N)*C(I)+  B(I,N)*E(I)
  2   H(I,N)=A(I,N)*D(I)+  B(I,N)*F(I)
C
C G=CURRENT DUE TO RADIAL VELOCITY*SIGMA/INDUCING CURRENT
C H=CURRENT DUE TOANGULAR VELOCITY*SIGMA/INDUCING CURRENT
C
      IF(M-2) 3,4,5
  3   GT(N)=G(1,N)
      HT(N)=H(1,N)
      GO TO 8
  4   GT(N) =G(1,N)-G(2,N)
      HT(N)=H(1,N)-H(2,N)
      GO TO 8
  5   IF(M-4)  6,7,7
  6   GT(N)=G(1,N)-G(2,N)+G(3,N)
      HT(N)=H(1,N)-H(2,N)+H(3,N)
      GO TO 8
  7   GT(N)=G(1,N)-G(2,N)+G(3,N)-G(4,N)
      HT(N)=H(1,N)-H(2,N)+H(3,N)-H(4,N)
  8   CONTINUE
      SQIR(N)=GT(N)**2
  55  SQIB(N)=HT(N)**2
      Q=2.*PI/360. *ARAD
      PWRR(1)=Q/3.*SQIR(1)
      PWRB(1)=Q/3.*SQIB(1)
      PWRR(360)=Q/3.*SQIR(360)
      PWRB(360)=Q/3.*SQIB(360)
      DO 10 L=2,359
      IF((-1)**L) 11,11,12
  11  PWRR(L)=4.*Q/3.*SQIR(L)
      PWRB(L)=4.*Q/3.*SQIB(L)
      GO TO 10
  12  PWRR(L)=2.*Q/3.*SQIR(L)
      PWRB(L)=2.*Q/3.*SQIB(L)
  10  CONTINUE
C
C  KMDR(S(BETA)) = PWRR
C
C
C                          (PROGRAM CONTINUED ON NEXT PAGE)
```

```
C  KMDB(S(BETA)) = PWRB
C
      DO 20 L=2,360
      PWRR(L)=PWRR(L-1)+PWRR(L)
   20 PWRB(L)=PWRB(L-1)+PWRB(L)
      PRINT 100,S, BETA, PWRR(360),PWRB(360)
  100 FORMAT(1H0,1HR,1X,E10.4,2X,4HBETA,1X,E10.4,2X,4HKMDR,E10.4,
     2 2X,7HKMDBETA,E10.4)
  500 CONTINUE
      STOP
      END
```

```
C  ********************************************************************
C  **                                                                **
C  **                    PROGRAM FOR GUIDED FLIGHT                   **
C  **                                                                **
C  ********************************************************************
C
C
C
C
C
C
      REAL I,I0,KM,KMD,L,LM,LENGTH,M                                    GUIDE
      COMPLEX BCOF,ROOT,YT,ALPHA,UCOF,R1,R2,R3,R4                       GUIDE
      DIMENSION ACOF(4),BCOF(5),CCOF(5),C(8),D(8),ROOT(4),YCOF(4)       GUIDE
      DIMENSION DCOF(5),ECOF(5)                                         GUIDE
      DIMENSION BN(11),COF(11)                                          GUIDE
      DO 200 N=1,4                                                      GUIDE
      ACOF(N)=0.0                                                       GUIDE
      YCOF(N)=0.0                                                       GUIDE
      BCOF(N)=0.0                                                       GUIDE
      BN(N)=0.0                                                         GUIDE
      COF(N)=0.0                                                        GUIDE
  200 ROOT(N)=0.0                                                       GUIDE
      DO 201 N=1,5                                                      GUIDE
  201 CCOF(N)=0.0                                                       GUIDE
      YT=0.0                                                            GUIDE
      ALPHA=0.0                                                         GUIDE
      R1=0.0                                                            GUIDE
      R2=0.0                                                            GUIDE
      R3=0.0                                                            GUIDE
      R4=0.0                                                            GUIDE
      KOUNT=0                                                           GUIDE
   10 KOUNT=KOUNT+1                                                     GUIDE
C
C   VARIABLES TO BE USED
C P(PRESSURE),SB(REFERENCE AREA), L(SEPARATION BETWEEN CP AND CG),
C  CMQ-CLA-CDO(AERODYNAMIC COEFFICIENTS), RB(BASE RADIUS), IO(ROTATIONAL
C  INERTIA),  KM-KMD(MAGNETIC COEFFICIENTS),  LM(SEPARATION BETWEEN
C  CG AND CM), VO(INITIAL VELOCITY), YO(INITIAL ERRROR), AO(INITIAL ANGLE
C  OF ATTACK), GAMMAO(ANGLE BETWEEN Z-AXIS AND V), M (MASS OF PROJECTILE),
C  U(RATE OF CHANGE OF ANGLE OF ATTACK),INVL(Z-AXIS POSITION INTERVAL),
C  DT(TIME INTERVAL CORRESPONDING TO INVL), LENGTH (RANGE LENGTH)
C
      READ(5,110)P,SB,L,CLA,CDO,CMQ,RB,I0                               GUIDE
      READ(5,110)KM,KMD,LM,V0,Y0,A0,GAMA0,M                             GUIDE
      READ(5,120)DT,INVL,LENGTH,U                                       GUIDE
      IF(P.EQ.0.0) GO TO 1091                                           GUIDE
      WRITE(6,170)                                                      GUIDE
C
C
C                       (PROGRAM CONTINUED ON NEXT PAGE)
```

```
      WRITE(6,130) P,SB,L,CLA,CDO,CMQ,RB,I0                                  GUIDE
      WRITE(6,140)  KM,KMD,LM,V0,Y0,A0,GAMA0,M,DT,LENGTH,U                  GUIDE
      ICNT=1                                                                 GUIDE
      IPNT=1                                                                 GUIDE
      V=V0                                                                   GUIDE
      I=I0                                                                   GUIDE
      T=0.0                                                                  GUIDE
      X=0.0                                                                  GUIDE
      RHO=0.0022831*515.379*P/760.0                                          GUIDE
      Q=RHO*V**2/2.0                                                         GUIDE
      YOPR=V*GAMA0                                                           GUIDE
      C(1)=Q*SB*L*(CLA+CDO)                                                  GUIDE
      C(2)=(+(CMQ*Q*SB*2.0*RB*RB/V))                                         GUIDE
      C(3)=KM*LM                                                             GUIDE
      C(4)=KMD*LM                                                            GUIDE
      C(5)=Q*SB*CLA                                                          GUIDE
      C(6)=KM                                                                GUIDE
      C(7)=(+(Q*SB*CDO/V))                                                   GUIDE
      C(8)=KMD                                                               GUIDE
      D(1)=(C(3)*LM+C(4)*V)/I                                                GUIDE
      D(2)=V*(C(2)+C(4)*LM)/I                                                GUIDE
      D(3)=C(3)*V/I                                                          GUIDE
      D(4)=V*(C(1)-C(3)*LM)/I                                                GUIDE
      D(5)=-((C(6)*LM)/(M*V))+((C(7)-C(8))/M)
      D(6)=C(8)*LM/M                                                         GUIDE
      D(7)=C(6)/M                                                            GUIDE
      D(8)=(C(5)+C(6)*LM)/M                                                  GUIDE
C
CCC      THE ARRAY CCOF CONTAINS THE COEFFICIENTS OF THE CHARACTERISTIC
C        EQUATIONS FOR BOTH DISPERSION AND THE ANGLE OF ATTACK.
C
      CCOF(1)=V+D(6)
      CCOF(2)=-D(2)+D(5)*V+D(8)                                              GUIDE
      CCOF(3)=D(4)-D(5)*D(2)-D(7)*V-D(6)*D(1)                                GUIDE
      CCOF(4)=D(5)*D(4)+D(7)*D(2)-D(6)*D(3)-D(8)*D(1)                        GUIDE
      CCOF(5)=-D(8)*D(3)-D(7)*D(4)                                           GUIDE
      DO 20 K=1,5                                                            GUIDE
   20 DCOF(K)=CMPLX(CCOF(K)/CCOF(1),0.0)                                     GUIDE
      CALL QANDC(1,DCOF(2),DCOF(3),DCOF(4),DCOF(5),R1,R2,R3,R4)              GUIDE
      ROOT(1)=R1                                                             GUIDE
      ROOT(2)=R2                                                             GUIDE
      ROOT(3)=R3                                                             GUIDE
      ROOT(4)=R4                                                             GUIDE
  203 WRITE(6,202)R1,R2,R3,R4                                                GUIDE
  202 FORMAT('0R1=  ',2E12.3,'0R2=  ',2E12.3,'0 R3=  ',2E12.3,'0 R4=  ',GUIDE
     *2E12.3)
  204 CONTINUE                                                               GUIDE
      WRITE(6,150)                                                           GUIDE
      YODPR=D(7)*Y0+D(8)*A0-D(5)*YOPR+D(6)*U                                 GUIDE
C
CCC      THE ARRAY YCOF CONTAINS THE COEFFICIENTS OF THE NUMERATOR OF THE
C        LAPLACE EQUATION FOR DISPERSION.
      YCOF(1)=(V+D(6))*Y0                                                    GUIDE
C
CCC
C                        (PROGRAM CONTINUED ON NEXT PAGE)
```

```
      YCOF(2)=(-D(2)*D(8)+V*D(5))*Y0+(V+D(6))*YOPR                      GUIDE
      YCOF(3)=(D(4)-D(2)*D(5)-D(6)*D(1))*Y0+D(8)*V*A0+(-D(2)+D(8))*YOPR+GUIDE
     *D(6)*YOOPR+D(6)*V*U                                               GUIDE
      YCOF(4)=(D(4)*D(5)-D(8)*D(1))*Y0+(- D(8)*D(2)-D(4)*D(6))*A0+D(4)*YGUIDE
     *OPR+D(8)*YOOPR+D(8)*V*U                                           GUIDE
C
C        THE ARRAY ACOF CONTAINS THE COEFFICIENTS OF THE NUMERATOR OF THE
C        LAPLACE EQUATION FOR THE ANGLE OF ATTACK.
C
      ACOF(1)=(V+D(6))*A0                                                GUIDE
      ACOF(2)=(D(5)*V-D(2))*A0-D(7)*Y0+D(5)*YOPR+YOOPR+V*U               GUIDE
      ACOF(3)=(-D(5)*D(2)-D(1)*D(6)-D(7)*V)*A0+D(3)*Y0+D(1)*YOPR+D(5)*YOGUIDE
     *OPR-D(7)*YOPR+D(5)*V*U                                            GUIDE
      ACOF(4)=(-(-D(3)*D(5)-D(1)*D(7))*Y0-(-D(2)*D(7)+D(3)*D(6))*A0+D(3)GUIDE
     **YOPR-D(7)*YOOPR-D(7)*V*U)                                        GUIDE
      DO 99 J=1,4                                                       GUIDE
      YCOF(J)=YCOF(J)/CCOF(1)                                           GUIDE
   99 ACOF(J)=ACOF(J)/CCOF(1)                                           GUIDE
  100 CALL VERT(YCOF,ROOT,T,YT)                                         GUIDE
      CALL VERT(ACOF,ROOT,T,ALPHA)                                      GUIDE
      IF(ICNT.NE.IPNT) GO TO 105                                        GUIDE
      WRITE(6,160) T,X,V,YT,ALPHA,GAMA0                                 GUIDE
  104 IPNT=IPNT+INVL                                                    GUIDE
  105 CONTINUE                                                          GUIDE
       ICNT=ICNT+1                                                      GUIDE
      T=T+DT                                                            GUIDE
      IF(T.GT.0.10) GO TO 106                                           GUIDE
      X=V*T                                                             GUIDE
      IF(X-LENGTH)100,100,107                                           GUIDE
  106 WRITE(6,190)                                                      GUIDE
      GO TO 108                                                         GUIDE
  107 WRITE(6,190)                                                      GUIDE
  108 CONTINUE                                                          GUIDE
      GO TO 10                                                          GUIDE
 1091 CONTINUE                                                          GUIDE
  110 FORMAT(8E10.3)                                                    GUIDE
  120 FORMAT(E10.3,I3,2E10.3)                                           GUIDE
  130 FORMAT(1H0,9HP       = ,E10.4,6H MM HG/1H ,9HS8      = ,E10.4,10H SQGUIDE
     * METERS/1H ,9HL       = ,E10.4,7H METERS/1H ,9HCLA     = ,E10.4,10H GUIDE
     *1/RADIANS/1H ,9HCDO     = ,E10.4/1H ,9HCMQ     = ,E10.4/1H ,9HRB    GUIDE
     * = ,E10.4,7H METERS/1H ,9HI       = ,E10.4,20H KILOGRAMS-METERS**2)GUIDE
  140 FORMAT(1H ,9HKM      = ,E10.4,14H NEWTONS/METER/1H ,9HKMD     = ,E10GUIDE
     *.4,21H NEWTON-SECONDS/METER/1H ,9HLM      = ,E10.4,7H METERS/1H ,9HGUIDE
     *V0      = ,E10.4,14H METERS/SECOND/1H ,9HY0      = ,E10.4,7H METERS/GUIDE
     *1H ,9HALPHA0 = ,E10.4,8H RADIANS/1H ,9HGAMMA0 = ,E10.4,7HRADIANS/1GUIDE
     *H ,9HMASS    = ,E10.4,10H KILOGRAMS/1H ,9HDT      = ,E10.4,8H SECONDGUIDE
     *S/1H ,9HLENGTH = ,E10.4,7H METERS/1H ,9HU       = ,E10.4,15H RADIANGUIDE
     *S/SECOND)                                                         GUIDE
  150 FORMAT(1H0,5X,4HTIME,9X,8HDISTANCE,7X,8HVELOCITY,20X,1HY,25X,5HALPGUIDE
     *HA,19X,5HGAMMA/1H ,4X,7HSECONDS,8X,6HMETERS,7X,10HMETERS/SEC,16X,6GUIDE
     *HMETERS,22X,7HRADIANS,17X,7HRADIANS)                              GUIDE
  160 FORMAT(1H ,(8E15.6))                                              GUIDE
  170 FORMAT(1H1,37X,8HTUNNEL G/1H ,29X,24HELECTROMAGNETIC GUIDANCE/1H0,GUIDE
C
C
C                        (PROGRAM CONTINUED ON NEXT PAGE)
```

```
   *24HTHE INPUT PARAMETERS ARE)                                          GUIDE
 180 FORMAT('0 MAX TIME REACHED  ')                                       GUIDE
 190 FORMAT('0 MODEL HAS REACHED TUNNEL LIMITS  ')                        GUIDE
     END                                                                  GUIDE
     SUBROUTINE QANDC(N,B,C,D,E,X1,X2,X3,X4)                              QANDC
     IMPLICIT COMPLEX*8(A-G,O-Z)                                          QANDC
     COMPLEX*8I                                                           QANDC
     I=(0.,1.)                                                            QANDC
     IF(N .EQ. 0)GO TO 10                                                 QANDC
     A=((4.00*C*E-(B**2*E)-D**2)/2.0)                                     QANDC
     A1=(C*(B*D-4.00*E)/6.00)                                             QANDC
     A2=-((C**3)/27.00)                                                   QANDC
     A=A+A1+A2                                                            QANDC
     BB= CSQRT((A**2)+((B*D-4.00*E-((C**2)/3.00))**3)/27.00)              QANDC
     A=-A                                                                 QANDC
     CALL CUBRT(A,BB,R)                                                   QANDC
     PSTAR=B*D-4.00*E-C*C/3.00                                            QANDC
     R1=-PSTAR/(3.00*R)                                                   QANDC
     R=(R+R1+(C/3.00))                                                    QANDC
     P= CSQRT((B**2/4.00)-C+R)                                            QANDC
     PQ= CSQRT(0.2500*R**2-E)                                             QANDC
     AB2=.500*B*R-D                                                       QANDC
     PPQ2=2.00*P*PQ                                                       QANDC
     IF( CABS(AB2-PPQ2) .GT.  CABS(AB2+PPQ2))PQ=-PQ                       QANDC
     PP=( CABS(P))                                                        QANDC
     A1=(1.0,0.0)                                                         QANDC
     B1=(B/2.00)+P                                                        QANDC
     C1=(R/2.00)+PQ                                                       QANDC
     X1=(-B1+ CSQRT(B1**2-4.00*A1*C1))/(2.00*A1)                          QANDC
     X2=(-B1- CSQRT(B1**2-4.00*A1*C1))/(2.00*A1)                          QANDC
     B1=(B/2.00)-P                                                        QANDC
     C1=(R/2.00)-PQ                                                       QANDC
     X3=(-B1+ CSQRT(B1**2-4.00*A1*C1))/(2.00*A1)                          QANDC
     X4=(-B1- CSQRT(B1**2-4.00*A1*C1))/(2.00*A1)                          QANDC
     RETURN                                                               QANDC
  10 CONTINUE                                                             QANDC
     P=C-(B**2/3.00)                                                      QANDC
     Q=D-(B*C/3.00)+((2.00*B**3)/27.00)                                   QANDC
     Z1=-(Q/2.00)+( CSQRT((Q**2/4.00)+(P**3/27.00)))                      QANDC
     Z2=-(Q/2.00)-( CSQRT((Q**2/4.00)+(P**3/27.00)))                      QANDC
     IF( CABS(Z1).GE. CABS(Z2))Z=Z1                                       QANDC
     IF( CABS(Z2).GE. CABS(Z1))Z=Z2                                       QANDC
     IF( CABS(Z) .EQ. 0.0)X1=-(B/3.00)                                    QANDC
     IF( CABS(Z) .EQ. 0.0)X2=-(B/3.00)                                    QANDC
     IF( CABS(Z) .EQ. 0.0)X3=-(B/3.00)                                    QANDC
     IF( CABS(Z) .EQ. 0.0)RETURN                                          QANDC
     BBB=(0.00,0.00)                                                      QANDC
     CALL CUBRT(Z,BBB,R1)                                                 QANDC
     R=-(P/(3.00*R1))                                                     QANDC
     W1=-(.500)+((3.00**.5)/2.00)*I                                       QANDC
     W2=-(.500)-((3.00**.5)/2.00)*I                                       QANDC
     X1=-(B/3.00)+R1+R                                                    QANDC
     X2=-(B/3.00)+W1*R1+W2*R                                              QANDC
C
C
C                    (PROGRAM CONTINUED ON NEXT PAGE)
```

```
      X3=-(B/3.00)+W2*R1+W1*R                                          QANDC
      X4=0.00                                                          QANDC
      RETURN                                                           QANDC
      END                                                              QANDC
      SUBROUTINE CUBRT(AA,BB,RR)                                       QANDC
      IMPLICIT COMPLEX*8(A-G,O-Z)                                      QANDC
      REAL*4H,H1A,H1B,HTH                                              QANDC
      REAL*4PI,SSSS                                                    QANDC
      COMPLEX*8I                                                       QANDC
  990 CONTINUE                                                         QANDC
      I=(0.,1.)                                                        QANDC
      II=1                                                             QANDC
      Z1=AA+BB                                                         QANDC
      Z2=AA-BB                                                         QANDC
      IF( CABS(Z2) .GE.  CABS(Z1))A=Z2                                 QANDC
      IF( CABS(Z1) .GE.  CABS(Z2))A=Z1                                 QANDC
      B= CONJG(A)                                                      QANDC
      H1A=(A+B)/2.00                                                   QANDC
      H1B=-I*(A-B)/2.00                                                QANDC
      HTH= ATAN2(H1B,H1A)                                              QANDC
      H=(H1A**2+H1B**2)**.500                                          QANDC
      PI=3.14159265358979300                                           QANDC
      SSSS=3.00                                                        QANDC
      RR=(H**(1.00/3.00))*(  COS((HTH+(II-1)*2.00*PI)/SSSS)+I*(  SIN((HTQANDC
     1H+(II-1)*2.00*PI)/SSSS)))                                        QANDC
      END                                                              QANDC
      SUBROUTINE VERT(COF,ROOT,T,TF)
      COMPLEX ROOT,BCOF,TF,BN                                          GUIDE
      DIMENSION COF(4),BCOF(4),ROOT(4),BN(4)                           GUIDE
      DO 910 I=1,4                                                     GUIDE
  910 BN( I )=(COF(1)*ROOT(I)**3)+(COF(2)*ROOT(I)**2)+(COF(3)*ROOT(I))+CGUIDE
     $OF(4)                                                            GUIDE
      BCOF(1)=BN(1)/((ROOT(1)-ROOT(2))*(ROOT(1)-ROOT(3))*(ROOT(1)-ROOT(4GUIDE
     *)))                                                              GUIDE
      BCOF(2)=BN(2)/((ROOT(2)-ROOT(1))*(ROOT(2)-ROOT(3))*(ROOT(2)-ROOT(4GUIDE
     *)))                                                              GUIDE
      BCOF(3)=BN(3)/((ROOT(3)-ROOT(1))*(ROOT(3)-ROOT(2))*(ROOT(3)-ROOT(4GUIDE
     *)))                                                              GUIDE
      BCOF(4)=BN(4)/((ROOT(4)-ROOT(1))*(ROOT(4)-ROOT(2))*(ROOT(4)-ROOT(3GUIDE
     *)))                                                              GUIDE
      TF=BCOF(1)*CEXP(ROOT(1)*T)+BCOF(2)*CEXP(ROOT(2)*T)+BCOF(3)*CEXP  GUIDE
     *(ROOT(3)*T)+BCOF(4)*CEXP(ROOT(4)*T)                              GUIDE
      RETURN                                                           GUIDE
      END                                                              GUIDE
/*
```

NOMENCLATURE

$\bar{A}$	Magnetic vector potential, Wb/m
a	Radius of conductive shell or projectile forebody, m
a	Abbreviated coefficient (see Eqs. (79), (80), and (82))
$\bar{B}$	Magnetic induction, Wb/m^2
b	Distance from z axis to guideway line currents, m
b	Abbreviated coefficient (see Eqs. (79), (80), and (82))
C	Coefficient of circular harmonic
C_{DO}	Projectile's aerodynamic drag coefficient
$C_{L\alpha}$	Projectile's aerodynamic lift coefficient
$C_{m\dot{\alpha}}$	Projectile's aerodynamic damping coefficient
c_M	Effective center of magnetic forces
c_g	Projectile's center of mass
c_p	Effective center of aerodynamic pressure
c	Abbreviated coefficient (see Eqs. (79), (80), and (82))
D	Abbreviated coefficients (see Eqs. (76) through (81)
d	Abbreviated coefficient (see Eqs. (79), (80), and (82))
$\bar{E}$	Electric field, v/m
$\bar{F}$	Force per unit length, N/m
$\mathfrak{F}$	Function defined in Eq. (66)
f(s)	Laplace transform at function in terms of complex quantity
f(t)	Function in terms of time
$\mathfrak{G}$	Function defined in Eq. (67)
g	Abbreviated coefficient (see Eqs. (79), (80), and (82))
h	Length of conductive shell, m

$\bar{I}$	Electric current vector, amp
$\hat{i}$	Unit vector in x direction
$\bar{i}$	Area current density, amp/m
J	Projectile moment of inertia, kg-m^2
$\hat{j}$	Unit vector in y direction
K_M	Magnetic positional force constant, N/m
K_{MD}	Magnetic damping force constant, N-sec/m
K	Function defined in Eqs. (84) and (85)
$\hat{k}$	Unit vector in z direction
L_{self}	Self inductance of conductor, h
L_{mut}	Mutual inductance between conductors, h
ℓ	Moment arm for aerodynamic forces, m
ℓ_M	Moment arm for magnetic forces, m
M	Projectile's mass, kg
n	Number corresponding independently to the n^{th} circular harmonic, n^{th} line current, n^{th} current segment, n^{th} root, etc.
P	Eddy current power per unit length of shell, w/m
q	Dynamic pressure, N/m^2
R	Roots of characteristic equation determined by Eqs. (79) or (80)
$\mathcal{R}$	Radial position of projectile's axis with respect to guideway axis, m
$\hat{\mathcal{R}}$	Unit vector in direction of $\mathcal{R}$
r	Radial distance from axis of projectile or other reference to item or point of interest, m
r_b	Radius of projectile's base, m
$\hat{r}$	Unit vector in r direction
r_1	Distance from line current to item or point of interest, m
S_b	Base area of projectile, m^2

$\S$	Shielding ratio (see Eq. (10))
s	Complex variable
Δ	Guideway current segment length (see Fig. 1), m
t	Time, sec
$\bar{V}$	Velocity of projectile's c_g, m/sec
W	Energy of eddy currents dissipated per unit length of shell, J/m
$\mathfrak{W}$	Energy stored and/or dissipated in guideway, J
w	Thickness of copper shell (see Fig. 20), m
x	Cartesian coordinate, m
y	Cartesian coordinate, m
$\mathcal{Y}$	Dispersion of projectile's c_g from z axis, m
z	Cartesian and/or polar coordinate (coincident with the range and guideway axis), m
z'	Offset z axis (see Fig. 7), m
α	Angle of attack, rad
β	Angular position of shell referenced to x axis, rad
$\hat{\beta}$	Unit vector in β direction
γ	Angle between V and z axis, rad
δ	Phase angle of circular harmonic, rad
ϵ	Phase lag between inducing field and field of eddy currents, rad
θ	Angular position referenced to an x axis, rad
μ	Permeability, h/m
ρ	Volume resistivity, ohm-m; also density of working gas, kg/m^3
ς	Area resistivity, ohm
Φ	Potential of shell end surface, v
ϕ	Angular position referenced to an x axis, rad
ω	Angular frequency, rad/sec

SUBSCRIPTS

Numericals	Independently identifies line currents, abbreviated coefficients in Eq. (81), etc.
D	Damping field, currents, forces, etc.
BF	Basic guideway field (see Fig. 1)
GW	Guideway
i	Inducing field of guideway currents or other sources
M	Magnetic (positional)
MD	Magnetic damping
$M\mathcal{R}$	Radial M
$M\beta$	Angular M
$MD\mathcal{R}$	Radial MD
$MD\beta$	Angular MD
n	Independently refers to n^{th} circular harmonic, n^{th} line current, n^{th} segment, n^{th} root, etc.
n'	Associated with image of I_n
o	Independently refers to conditions of free space or initial flight conditions
P	Positional field, currents, forces, etc.
$\mathcal{R}$	Radial
$\mathcal{R}M$	Radial mechanical
$\mathcal{R}V$	Radial velocity
T	Total
TF	Transposed field (see Fig. 3)
z	Component in z direction
β	Angular component

SUPERSCRIPTS

'	Independently implies field of induced eddy currents, image current for equivalent exterior field, and an offset system of polar coordinates, or if centered over variable implies first-time derivative
''	Image current for equivalent interior field, or if centered over variable implies second-time derivative